ISSN: 3102-0372 (Online)

June 2025

Vol. 2, No. 1

Official Journal of

Nepal Society of Engineering Geology (NSEG)

Asian Journal of Engineering Geology

Vol. 2 No. 1, June 2025

Official Journal of Nepal Society of Engineering Geology

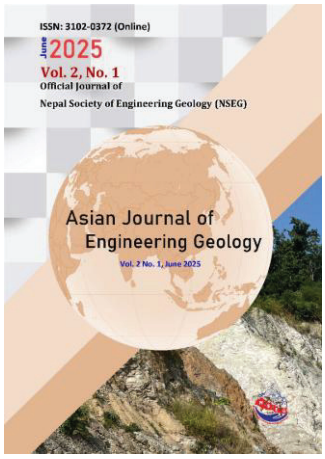

Asian Journal of Engineering Geology (AJEG)

Concept

The Asian Journal of Engineering Geology (**AJEG**), published by the Nepal Society of Engineering Geology (**NSEG**), is envisioned as a dedicated platform for advancing the understanding and application of engineering geology within the unique geological context of Asia, with a particular focus on the Himalayan region, while also welcoming contributions relevant to other parts of the world.

In recent years, research in engineering geology and related fields has seen significant progress. However, specialized publication platforms remain limited, especially in Asia, hindering the effective dissemination of research findings and knowledge sharing among engineering geologists. To address this gap, NSEG has launched the Asian Journal of Engineering Geology (AJEG), offering a professional and accessible forum for geoscientists, engineers, and environmentalists engaged in landslide studies, environmental geoscience, and engineering geological research.

AJEG aims to be a key resource for stakeholders seeking updated information on the geological challenges and engineering solutions relevant to seismically active and geologically complex regions like the Himalayas and beyond. The journal is committed to publishing original research, case studies, and technical notes that contribute to a deeper understanding of engineering geology in diverse terrains. Under the auspices of **NSEG**, **AJEG** places particular emphasis on:

- Slope stability and landslide hazard assessment
- Earthquake geology and seismic risk analysis
- Engineering geological aspects of infrastructure development
- Environmental and geotechnical investigations
- Integration of geological, geotechnical, and environmental knowledge for sustainable development

The journal actively promotes collaboration among researchers, engineers, and geologists from Asia and around the globe. By engaging regional experts and fostering interdisciplinary dialogue, **AJEG** seeks to address current and emerging challenges in engineering geology through shared knowledge and innovation.

In addition to peer-reviewed articles, **AJEG** will feature updates on conferences, research initiatives, and activities organized by the Nepal Society of Engineering Geology. This will position the journal not only as a scholarly publication but also as a hub for professional exchange and community building within the field of engineering geology in Nepal and across the region.

Aims and Scope

The Asian Journal of Engineering Geology (**AJEG**) serves as a common platform for the publication of integrated research covering all aspects of engineering geology. The journal welcomes original research articles, rapid reports on emerging engineering geology issues, case studies, and technical notes highlighting practical applications. Researchers and practitioners are encouraged to submit original, unpublished contributions. Subject areas include, but are not limited to, the following fields:

- Applied geomorphology
- Structural geology
- Applied geophysics and g
- Geochemistry
- Environmental geology
- Hydrogeology
- Land use planning
- Natural hazards
- Remote sensing techniques
- Soil and rock mechanics
- Applied geotechnical engineering
- Urban Engineering Geology
- Engineering Geology of marine and reservoir.
- Engineering geology in flash floods and tsunami
- Landslide hazard assessment and mapping
- GIS applications in engineering geology
- Landslide monitoring and landslide mitigation
- Engineering geology of the Himalayan slopes
- Rainfall-induced landslides
- Earthquake-induced landslides
- Anthropogenic controls on hazards
- Stability of dams and embankments
- Engineering geology of heritage areas, monitoring and mitigation
- Groundwater monitoring
- Seismic Hazard and Risk
- Disaster Risk Reduction and Management
- Engineering geology of Tunnels and bridges
- Foundations on slopes and plains

- Early warning of multi-hazard risk
- Landslide hazard management at community level
- Physical and numerical modeling in engineering geology
- High altitude engineering geological issues.
- Economics of natural hazards and related climate change
- Agricultural geology
- Snow avalanche
- Engineering geology and infrastructure development
- Snow cover in the Himalaya
- Environment friendly low cost infrastructure development
- Rural infrastructures and engineering geology
- Geotechnical engineering, modeling and ground improvement
- Nature-based solutions for disaster risk reduction

These topics suggest a multidisciplinary approach, encompassing various aspects of geology and engineering that have practical applications in fields such as environmental management, land planning, and geotechnical engineering.

Publication program

The Asian Journal of Engineering Geology (**AJEG**) publishes two issues each year. It is a peer-reviewed journal committed to disseminating the latest developments across various fields of engineering geology. **AJEG** is an open-access online journal, freely available to readers worldwide.

The Nepal Society of Engineering Geology promotes open access publishing to broaden the journal's global reach, enhance the visibility and impact of published research, and improve indexing across major search engines. Researchers and professionals from all relevant disciplines are invited to submit high-quality manuscripts presenting cutting-edge research or innovations in engineering geology and related areas. **AJEG** welcomes both individual and institutional submissions aligned with the journal's aims and scope.

Editorial Team

Associate Editor-in-Chief

Editorial Board Members

Editors for online handling

We invite researchers specializing in engineering geology to become part of the editorial board and contribute to our publication. If you are interested in joining, kindly send an email to nsegnepal@gmail.com.

Instructions to Contributors

All types of manuscripts, including original articles, rapid reports on recent engineering geology issues, case studies, and technical notes, submitted for publication will undergo peer review by at least two experts in the relevant field. The review process is double-blind, meaning the authors will not know the identity of the reviewers. In some cases, editors may also serve as reviewers.

Authors' Responsibilities

Only individuals who have made significant intellectual contributions to the content of the manuscript should be listed as authors. Authorship should be based on contributions to the conception and design of the study, active involvement in drafting or critically revising the manuscript, and participation in the final revision process.

The corresponding author is responsible for submitting the final version of the manuscript following the peer review process. Any external support, such as funding, equipment, or institutional assistance, must be clearly acknowledged in the Acknowledgment section.

In the Comments to the Editor section during submission, authors must disclose any prior or duplicate publication of the manuscript's content. All submissions to AJEG are subject to plagiarism screening, and the acceptable similarity index is limited to a maximum of 20%. Author should use given Template in the web site for preparation of manuscript.

Manuscript Preparation Overview

All submissions to the Asian Journal of Engineering Geology (AJEG) must be written in International English. Authors whose first language is not English are strongly encouraged to have their manuscripts reviewed by a native English speaker or to use a professional English editing service prior to submission. All references, including online sources, must be formatted according to the journal's referencing guidelines outlined in this document. Each submitted article must include an abstract that briefly summarizes the key content and findings of the study. The name, institutional address, and email address of the corresponding author must be clearly indicated on the title page.

Figures and tables should be embedded within the manuscript after the list of references. Original figures should be at least half the size of A4 paper in their longest dimension. Acceptable formats for figures and images are TIFF (TIF) with a resolution of 300–600 pixels per inch (ppi). Monochrome images should be saved in grayscale mode, while color images must be in RGB mode. Only single-layer images are accepted. Authors should make every effort to avoid jargon, clearly define all nonstandard abbreviations upon first use, and present the content in a clear, concise, and accessible manner.

Manuscript Preparation Guidelines for AJEG

Authors must use the official manuscript template available on the AJEG website for preparing their submissions.

Title Page

The **title page** should include the following details:

- **Title** of the article
- **Full name(s)** of all authors (first name, middle initial(s), and surname)
- **Affiliations** of the authors, including department or division, institution or organization, city, and country. Do not use abbreviations for affiliations.
- If multiple authors share the same affiliation, list all authors first, followed by the shared affiliation.
- **Email addresses** of all authors must be included.
- The **corresponding author** should be clearly identified with an asterisk (*).

Abstract and Keywords

The manuscript should begin with an **Abstract** of approximately **300 words**, clearly summarizing:

- The research problem
- The methods used
- Major findings
- Conclusions

Immediately following the abstract, list **up to five keywords or phrases** for indexing purposes as per the template provided.

Figures, Tables, and Symbols

- Special characters, mathematical symbols, and Greek letters not available on a standard keyboard must be created using the **Symbol** font.
- **Figures and tables** should be **embedded** at appropriate locations within the text **after the list of references**.
- After the manuscript is accepted, authors must also submit **figures as separate high-resolution files**.
- Figures should follow the formatting requirements outlined in the submission guidelines (e.g., TIFF format, 300–600 dpi, RGB/grayscale mode, single-layer).

Pagination, Line Numbering, and Equations

- Authors must insert both page numbers and continuous line numbers throughout the manuscript to facilitate the review process. Page numbers should appear in the footer of each page.
- Equations should be left-aligned, with reference numbers aligned to the right margin.
- For long equations, break the right side into approximately equal parts and align to the right. Place the equation number on the last line only.
- All equations must be numbered sequentially as they appear in the text.

Units

Use **SI units** throughout the manuscript. If alternative units are provided, they should appear in parentheses following the SI units.

Acknowledgments

Acknowledgments should be included before the list of References, and the title should read “Acknowledgments.” Author/s should obtain a permission to acknowledge from all those mentioned in the Acknowledgements.

References

In the list of references, provide complete information of each reference material. Cite a symposium paper only from published proceedings. Do not cite an article or book only accepted for publication but not published. Do not use ibid. Please avoid excessive referencing.

Unpublished data, unpublished abstracts and personal communications should not be included in the reference list. Footnotes are not acceptable.

AJEG prefers maximum 60 references per article. The journal follows the Harvard system for citation, with author name/s and year of publication in parentheses, such as one author: (Hungr 2003) or Hungr (2003), two authors: (Doe and Morris, 2009) or Doe and Morris (2009), and three authors or more: (Rahardjo et al., 2002) or Rahardjo et al. (2002).

APA-Style Reference Examples

Journal article

van Westen, C. J., Rengers, N., and Soeters, R. (2003). Use of geomorphological information in indirect landslide susceptibility assessment. Natural Hazards, 30, 399–419.

Multiple works by same author(s) in same year

Dahal, R. K., Hasegawa, S., Nonomura, A., Yamanaka, M., and Dhakal, S. (2008a). DEM-based deterministic landslide hazard analysis in the Lesser Himalaya of Nepal. Georisk: Assessment and Management of Risk for Engineered Systems and Geohazards, 2(3), 161–178.

Dahal, R. K., Hasegawa, S., Nonomura, A., Yamanaka, M., Dhakal, S., and Paudyal, P. (2008b). Predictive modelling of rainfall-induced landslide hazard in the Lesser Himalaya of Nepal based on weights-of-evidence. Geomorphology, 102(3–4), 496–510.

Journal article with DOI

Hasegawa, S., Dahal, R. K., Yamanaka, M., Bhandary, N. P., Yatabe, R., and Inagaki, H. (2009). Causes of large-scale landslides in the Lesser Himalaya of central Nepal. Environmental Geology, 57, 1423–1434. https://doi.org/10.1007/s00254-008-1420-z

Journal article in press

Dahal, R. K., and Hasegawa, S. (2008). Representative rainfall thresholds for landslides in the Nepal Himalaya. Geomorphology. https://doi.org/10.1016/j.geomorph.2008.01.014 (in press)

Maps and Pamphlets

Amatya, K. M., and Jnawali, B. M. (1994). Geological map of Nepal (Scale 1:1,000,000). Department of Mines and Geology, Kathmandu, Nepal.

Books (authored)

Dahal, R. K. (2006). Geology for technical students. Bhrikuti Academic Publication, Kathmandu.

Same author, multiple books same year

Krahn, J. (2004a). Seepage modeling with SEEP/W: An engineering methodology (1st ed.). Geo-Slope International Ltd., Alberta.

Krahn, J. (2004b). Stability modeling with SLOPE/W: An engineering methodology (1st ed.). Geo-Slope International Ltd., Calgary.

Edited Book

Wohletz, F., and Aaron, G. (Eds.). (1992). Sedimentology. California Press, CA.

Book Chapter

Ward, T. J., Li, R.-M., and Simons, D. B. (1981). Use of a mathematical model for estimating potential landslide sites in steep forested basin. In T. R. H. Davis and A. J. Pearce (Eds.), Erosion

and sediment transport in pacific rim steep lands (pp. 21–41). Institute of Hydrology, Wallingford, Oxon, UK.

Proceedings as a Book

Sassa, K. (1998). Recent urban landslide disasters in Japan and their mechanisms. In Proceedings of the 2nd International Conference on Environmental Management, Environmental Management (Vol. 1, pp. 47–58), Australia, 10–13 February. Elsevier, Amsterdam.

Proceedings with an editor, no publisher

Rahardjo, H., Leong, E. C., and Rezaur, R. B. (2002). Studies of rainfall-induced slope failures. In P. Paulus and H. Rahardjo (Eds.), Proceedings of the National Seminar, Slope 2002 (pp. 15–29). Bandung, 27 April 2002.

Proceedings without editor, with publisher

Doe, S.-T., and Morris, R. L. (1998). Rainfall-induced slope failures and damming of ravines. In Abstracts of international symposium on water-induced disasters. Tribhuvan University, Kathmandu, 4–9 June 1998.

Proceedings in CD/DVD format

Yatabe, R., Yagi, N., Yokota, K., and Bhandary, N. P. (2000). Influence of expansive chlorite on the strength of weathered Green Rock at Mikabu Belt of Japan. Proceedings of International Conference on Geotechnical and Geological Engineering, Melbourne, Australia, 19–24 November 2000 (CD format).

Publicly Available Unpublished Report

Wagner, A. (1983). The principal geological factors leading to landslides in the foothills of Nepal: A statistical study of 100 landslides – steps for mapping the risk of landslides. HELVETAS-Swiss Technical Cooperation and ITECO-Company for International Cooperation and Development.

Online Document

Hungr, O. (2003). Flow slides and flows in granular soils. In Proceedings of international workshop on occurrence and mechanisms of flows in natural slopes and earth fills (15 p.). http://www.unina2.it/flows2003/flows2003/articoli/Hungr-Flows.pdf (Accessed 15 January 2024)

Dissertation

Khanal, R. K. (1991). Historic landslides of Nepal during 1902–1990 A.D.: Extent and economic significance (M.Sc. dissertation). Central Department of Geology, Tribhuvan University, Nepal.

Standard

ASTM D3385-03. (2003). Standard test method for infiltration rate of soils in field using double-ring infiltrometer. ASTM International.

Review and Production Process

All manuscripts submitted to AJEG undergo peer review. Accepted materials are subject to copyediting to ensure clarity, consistency, and adherence to journal standards. Authors will receive galley proofs of their article prior to publication and are expected to respond promptly to any editorial queries. Proof corrections must be limited to typographical or printer's errors; substantial revisions or rewriting at the proof stage will not be permitted.

Page Charges

There is no page charge/s for papers submitted to the AJEG. The upper limit on length of a paper is approximately 35 manuscript pages, including tables and references. This limit may be exceeded at the discretion of the Editor-in-chief.

Online Submission

Please note that the online manuscript submission system is available through the journal's official website. This system is essential for preparing and submitting your manuscript electronically to the Asian Journal of Engineering Geology via its web-based peer-review platform.

Manuscripts should be submitted at https://ajeg.nseg.org.np . The submission portal also allows authors to track the progress of their manuscript throughout the peer-review and editorial process.

Author should use given Template in the web site for preparation of manuscript.

Research Article DOI: https://doi.org/10.64862/ajeg.2025.201.01 Open Access

Epigenetic Gorges and Their Treatments for Dam Safety: Case from Kundghat Dam, District Jamui, Bihar, India

Vinod Kumar Sharma[1*]

[1]Water Resources Department, Jalsansadhan Bhawan, Anisabad, Patna, Bihar, India

(*Corresponding E-mail: vksharma_gsi@yahoo.co.in)

Received: November 15, 2024, Accepted: June 05, 2025

Abstract: **A major engineering challenge was encountered during the construction of the Kundghat Dam in Bihar, India. During excavation for the dam's foundation, a buried river channel (paleo-channel) was discovered. The paleo-channel, or epigenetic gorge, was a deeply eroded trench in the bedrock filled with highly permeable materials and proved to be a significant geological surprise. This geological feature posed two major threats: first, potential leakage due to the porous nature of the paleo-channel material, and second, settlement within such deposits. To ensure the dam's long-term safety, a series of grouting techniques was implemented to reduce the permeability of the paleo-channel material. The remedial measures included row grouting, grout curtains, and Tube-à-Manchette (TAM) grouting, a specialized method that allows multiple, controlled injections into the same area to achieve thorough material consolidation. The use of these advanced grouting methods successfully stabilized the dam's foundation, mitigated the risks associated with the paleo-channel, and ensured the structural integrity of the Kundghat Dam.**

Keywords: ***Epigenetic gorges, Paleo-channel, Peninsular shield, Dam foundations, Dam safety.***

Introduction

Epigenetic gorges (or paleo channels) are formed when channels that have been laterally displaced incise down into the bedrock of the former valley. These Valley-filling events that promote epigenetic gorges may be localized or widespread. The term 'epigenetic' refers to the secondary nature of the bedrock gorges, which occur after the formation of the original gorge and are the result of lateral shifting of the channel by landslide debris, alluvial fans or widespread fluvial aggradations (Engeln von, 1942; Pant, 1975). Epigenetic gorges are valleys carved by a river that cut down through a new, often younger, layer of rock into an older, underlying geological structure. These gorges offer insights into the complex history of a landscape by showing how rivers can maintain their course despite changes in the geology below. This process is a result of the combined forces of erosion, the underlying geology, climate and tectonics. The paleo-channels or fossil valleys may also be the result of aggradations in response to climate change scenarios or fluctuating base-level situations. Epigenetic gorges have been well recognized in fluvial landscape regimes all around the world.

Paleochannels within dam foundations present substantial challenges due to their potential for increased permeability, which can lead to seepage and internal erosion. The paper presents a case of a paleo-channel in Kundghat dam foundation and its mitigation.

Kundghat dam project envisages construction of a 39.583m high earth dam across the Bahaur River, to impound a gross water storage of 8.76 million cubic meters at full reservoir level of 126.6 m for harnessing the available water resources of the Bahaur River up to the optimum. The project components also involve constructing a 5.88 km long main canal with a head discharge of 3.2 cusec. The main canal and its distribution system shall provide annual irrigation to 2035.47 ha catchment command area (CCA).

A 351 m Cut-off Trench (COT) along the dam axis with a grout curtain was designed as a principal measure for seepage control. The geological log of the COT reveals the presence of bedrock between 7 m and 14 m. However, the presence of a deep epigenetic gorge/paleo-channel between chainage 110 m and 165m was a geological surprise that poses a threat to the dam's safety. This feature is concealed and was not picked up during investigations.

Geological and geomorphic set-up of the site

Physiographical set-up of the area around the Kundghat dam site shows a diverse landscape of Jamui hills and east-west trending Burwa ridge, plateaus, erosion structures and river terraces. The Bahaur River near the dam axis flows towards a northwesterly direction, and after flowing about 400 m takes a northerly swing. In general, the area is characterized by distinct east-west trending hills comprising mainly quartzite with subordinate schists. The area exposes rocks of Chhotanagpur Gneissic Complex (CGC) wherein mainly quartzite with subordinate schists is exposed. The major distinctive litho-tectonic domains of the CGC in the area are the Rajgir– Munger metasedimentary Belt and Bihar Mica Belt. The metamorphic of Chotanagpur Mica Belt mainly comprises quartzites, mica schist and amphibolites (Lower to Middle Proterozoic), while

Munger Group comprise quartzite and phyllites (Middle Proterozoic) and granites, gneisses and migmatites, meta-dolerite and amphibolites and pegmatites (Upper Proterozoic). The Bihar Mica Belt encompasses mainly in Nawada, Jamui and Banka districts.

The Bahur River at the dam site flows from a southeasterly direction to a northwesterly direction, and the dam axis is N50°E-S50°W. The rocks exposed in the dam site area are quartzite with subordinate schists mainly on the right flank, which has a steeper slope, while on the left flank, River Borne Material (RBM) admixed with slope wash is present between the steep slope and the river course. The riverbed section is devoid of rock exposure; however, boulders and pebbles of quartzite with coarse to medium-grained sand occupy the river section.

The general trend of foliation in quartzite with subordinate schist partings trend N75^{0}W-S75^{0}E with sub-vertical dips (steep) in southwesterly direction in the right flank of the dam axis, whereas the dips are moderate (45^0-60^0) on the left flank of the dam axis. This variation may be attributed to regional folding in the rocks.

Tectonic uplift and climatic variability of epigenetic gorges

The presence of epigenetic gorges is an intriguing type of geological configuration with major implications for understanding the relationship between climate and tectonic activity. These deep, narrow gorges, carved by a river through a bedrock ridge that was buried by sediment, provide valuable insights into past landscape conditions.

Tectonic events, such as a localized uplift, can alter drainage patterns and create the conditions necessary for epigenetic gorge formation. The concept of antecedence is particularly relevant, where a river maintains its course as the landscape slowly rises around it due to tectonic forces. The river's ability to erode downward keeps pace with the uplift, resulting in a gorge. While not always a sign of ongoing tectonics, the presence and characteristics of these gorges can indicate past tectonic events. There are a few studies from the northwest and Central Himalaya where their formation mechanism and climate–tectonic significance have been highlighted (Pratt-Sitaula et al., 2007). Climate plays a crucial role in the gorge formation of gorges' aggradation and incision phases. Changes in precipitation or temperature can drastically affect a river's sediment load and discharge. For instance, a period of increased erosion due to a wetter climate can lead to the widespread deposition of sediment, burying the original valley. Conversely, a change to a drier climate might reduce sediment supply, enhancing the river's ability to incise and carve into the underlying bedrock.

The formation of epigenetic gorges and fossil valleys (the old, now-buried river channels) is a direct outcome of this climate-tectonic interaction. Studies in the Himalayas (Chakraborty et al., 2017) have shown that while the location of these gorges is often structurally controlled, the abandonment of the old river courses was a climatically induced event (Figure 1). The sediment filling the valleys can be dated to specific climatic periods, providing a timeline for these landscape changes. While not always directly indicative of ongoing tectonics, the presence of epigenetic gorges may be related to past tectonic events that caused uplift or altered drainage patterns. Climate change can significantly influence sediment production and transport in river systems.

Several mechanisms can lead to the formation of these intriguing landforms, viz., river capture, obstruction and diversion, such as landslide dams/paleo-landslides, and antecedence that refers to the existence of the river prior to the tectonic uplift episode, etc. The bedrock geometry affects the location and lateral mobility of an incising channel, whereas the original valley shape determines rates of bedrock incision (Ouimet et al., 2008).

In terms of the processes point of view, (i) before valley fill aggradation (in the present-day fossil valleys), the rivers were sediment-limited, and thus the ambient stream power was used to incise the channel (Fig.1). This probably happened because. (ii) The rivers did not migrate laterally to their present course (epigenetic gorge), as observed in cases of landslide-dam river courses (Ray and Srivastava, 2010). Landslide dams are also one of the major causes to change the river courses and to facilitate the formation of epigenetic valleys.

Geological challenges of epigenetic gorges in dams

The challenges associated with epigenetic gorges in the context of storage dams relate to their geological and hydraulic implications, potentially affecting dam safety and reservoir management. These channels can pose significant implications for dam construction and stability, including structural Integrity, water leakage and sediment management, etc., which may impact the lifespan of the dam and its reservoir. It is, therefore, imperative to conduct thorough geological assessments to identify such channels and evaluate their impact on the safety of dams.

Most epigenetic gorges documented in the literature occur about landslide dams, including examples from the northwest Himalaya along the Indus River (Hewitt, 1998), Central Nepal along trans-Himalayan rivers (Korup et al., 2006; Pratt-Sitaula et al., 2007).

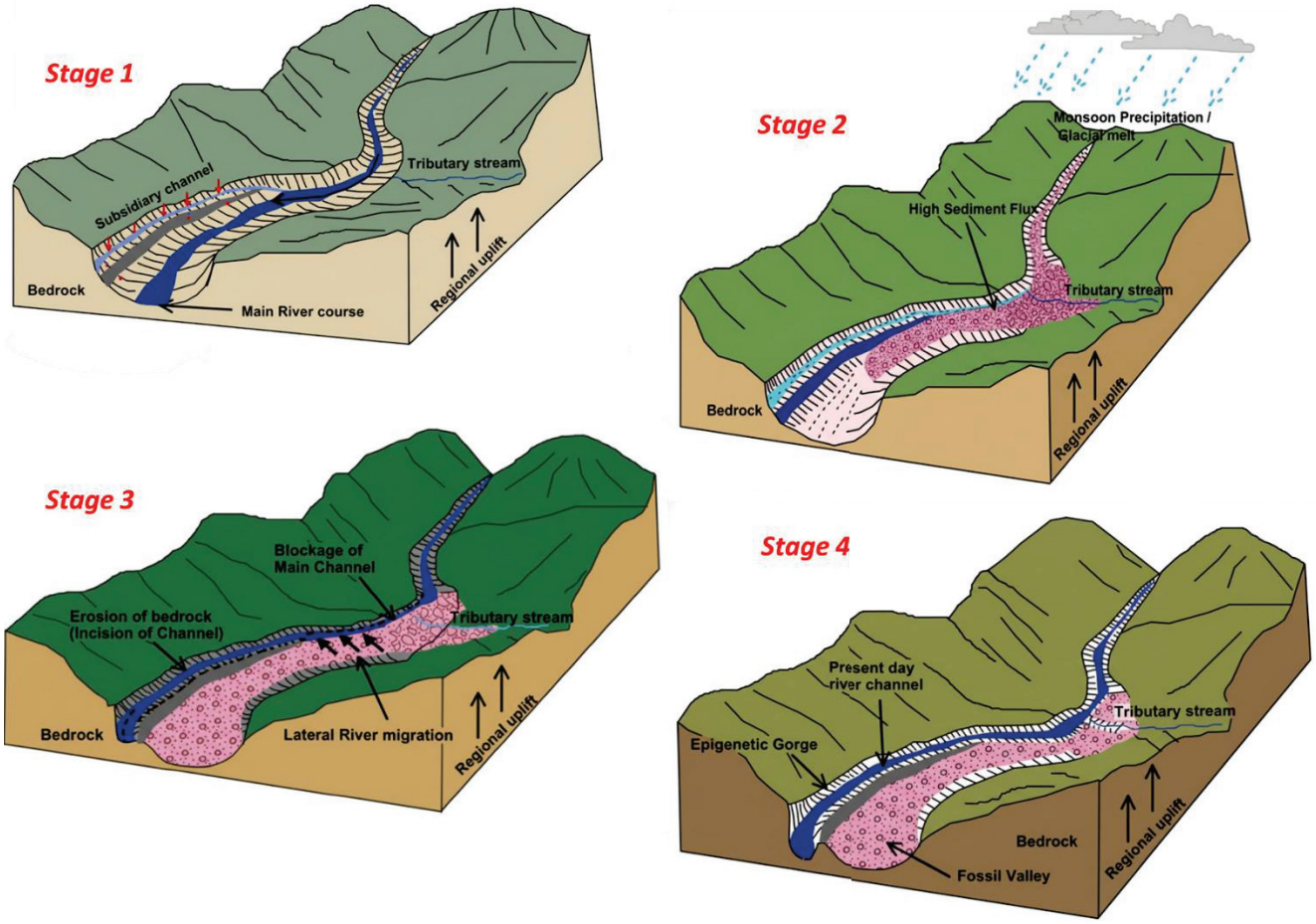

Figure 1, Block diagrams showing evolutionary stages of fossil valleys and associated gorges (modified after Kothyari and Juyal, 2013). Stage 1: Position of the river channel. Stage 2: Major valley fills aggradations occurred (during the early Holocene) climatic optimum. Stage 3: Enhanced sedimentation that led to the lateral river migration, thus occupying the subsidiary channel, and Stage 4: Present River course flowing through the gorge section.

The prime components of paleo-channel sediments are gravel and sand deposits, and their porosity, distribution of water and salt, and modifying transport, as well as high permeability, which act as subsurface conduits (Triantafilis and Buchanan, 2009). The permeable properties of the paleo-channels have created major concern due to the loss of irrigation water through deep drainage (Wray, 2009). The challenges posed by saturation of buried channels (or fossil valleys) have been recognized (Chakraborty et al., 2017) as an abnormal increase in the groundwater table, washing out of fines from the outlet, land subsidence due to saturation, decrease in reservoir storage capacity and weakening of abutment, etc.

In terms of the processes point of view, (i) before valley fill aggradation (in the present-day fossil valleys), the rivers were sediment-limited, and thus the ambient stream power was used to incise the channel (Fig.1). This probably happened because. (ii) The rivers did not migrate laterally to their present course (epigenetic gorge), as observed in cases of landslide-dam river courses (Ray and Srivastava, 2010). Landslide dams are also one of the major causes to change the river courses and to facilitate the formation of epigenetic valleys.

Geological challenges of epigenetic gorges in dams

The challenges associated with epigenetic gorges in the context of storage dams relate to their geological and hydraulic implications, potentially affecting dam safety and reservoir management. These channels can pose significant implications for dam construction and stability, including structural Integrity, water leakage and sediment management, etc., which may impact the lifespan of the dam and its reservoir. It is, therefore, imperative to conduct thorough geological assessments to identify such channels and evaluate their impact on the safety of dams.

Most epigenetic gorges documented in the literature occur about landslide dams, including examples from the northwest Himalaya along the Indus River (Hewitt, 1998), Central Nepal along trans-Himalayan rivers (Korup et al., 2006; Pratt-Sitaula et al., 2007).

The prime components of paleo-channel sediments are gravel and sand deposits, and their porosity, distribution of water and salt, and modifying transport, as well as high permeability, which act as subsurface conduits (Triantafilis and Buchanan, 2009). The permeable properties of the paleo-channels have created major concern due to the loss of irrigation water through deep drainage (Wray, 2009). The challenges posed by saturation of buried channels (or fossil valleys) have been recognized (Chakraborty et al., 2017) as an abnormal increase in the groundwater table, washing out of fines from the outlet, land subsidence due to saturation, decrease in reservoir storage capacity and weakening of abutment, etc.

Depending on the post-depositional environment, paleo-channels may be exposed to the surface or buried. Such a channel is no longer part of an active river system and generally remains scaled to the channel's flow. Paleo-channels are ancient riverbeds or stream valleys buried or abandoned over time, often concealed in shield (a case of Kundghat dam) and desertic areas. Identifying probable paleo-channels in peninsular terrain is challenging, where slope variation is minimal and geomorphologic signatures are often obscured. The potential challenges include

i. The bedrock erosion rates in epigenetic gorges can be very high and variable. This could lead to unexpected changes in the riverbed and surrounding geology near the dam and reservoir

ii. The formation and evolution of epigenetic gorges can influence sediment transport and deposition patterns in the river and reservoir, potentially impacting reservoir capacity and dam operation.

iii. The steep, often narrow nature of epigenetic gorges can affect the stability of the valley slopes surrounding the reservoir, potentially increasing the risk of landslides into the reservoir.

iv. If a dam is built within or near an epigenetic gorge, the geological structure and ongoing erosion could challenge the long-term stability and integrity of the dam's foundations.

v. The altered river course and incision rates associated with epigenetic gorges can change the hydrological regime of the river, potentially affecting water flow patterns into and out of the reservoir, and

vi. Designing and constructing dams in areas with complex geological features like epigenetic gorges can present unique engineering challenges, requiring thorough site investigation and specialized construction techniques.

In the Himalayan and Trans-Himalayan region, deep-buried channels/fossil valleys at many projects like Parbati HE Project Stage-II, Nimmo Bazgo hydroelectric Project, etc., have been identified during investigation stages (Chakraborty et al., 2017). These deeply buried channels pose significant challenges to the safety of the project. Paleo-channels in peninsular areas were formed due to river migration driven by neo-tectonic activity and monsoonal shifts during the Holocene period. The presence of faults and lineaments in the basin has influenced both the river's path and the location of these paleo-channels.

A variety of techniques have been used to map paleo-channels; mostly ground-based geophysical techniques including gravity, seismic and electrical methods, followed by drilling explorations. However, a preliminary assessment can be made by careful reconnaissance of topographic, geologic and geomorphic features and detailed engineering geological mapping of the dam site area.

To avoid problems due to paleo-channels concerning dam foundations, it is important to identify the buried channel at the investigation stage itself so that suitable geotechnical measures may be suggested for the overall safety of the project.

Buried channels can lead to severe damage in the storage dam projects if not identified and treated at an early stage of investigations. These buried/ paleo channels are mostly filled with riverine material and subsequently converted to old terrace deposits, which act as concealed pathways for the water conductor system.

Kundghat dam excavations

Kundghat dam (39.583 m high), an Earth and Rockfill structure across the River Bahaur, aims to impound a gross storage of 8.76 MCM at FRL (126.6 m) to harness the available water resources of the Bahaur River. The geological mapping of the dam site indicates that quartzite with subordinate schist is exposed on the right, while the left flank is occupied by the river-borne material, fluvial terrace, and slope wash without any rock outcrops.

Along the dam axis, a 351 m cut-off trench (COT) with the provision of a grout curtain has been designed as a principal measure for seepage control (Figure 2). Single line grout curtains were provided to initially try a widely spaced system of primary boles at a spacing of 6 m to 8 m, followed by secondary and tertiary holes at a progressively smaller spacing till the desired results of permeability value less than1 to 5 Lugeon (A Lugeon is defined as the water loss of 1litre/min/m of the drill hole under a pressure of 10 atmospheres maintained for 10 min in a drill hole of 46 mm to 76 mm diameter) are obtained.

The geological log of the COT reveals the presence of bedrock between 7 m and 14 m; however, the presence of a ‘paleo-channel between 110 m and 165 m was a geological surprise. The paleo river course was not picked up during geological mapping of the dam site area due to the cover of younger sediments (Fig.2).

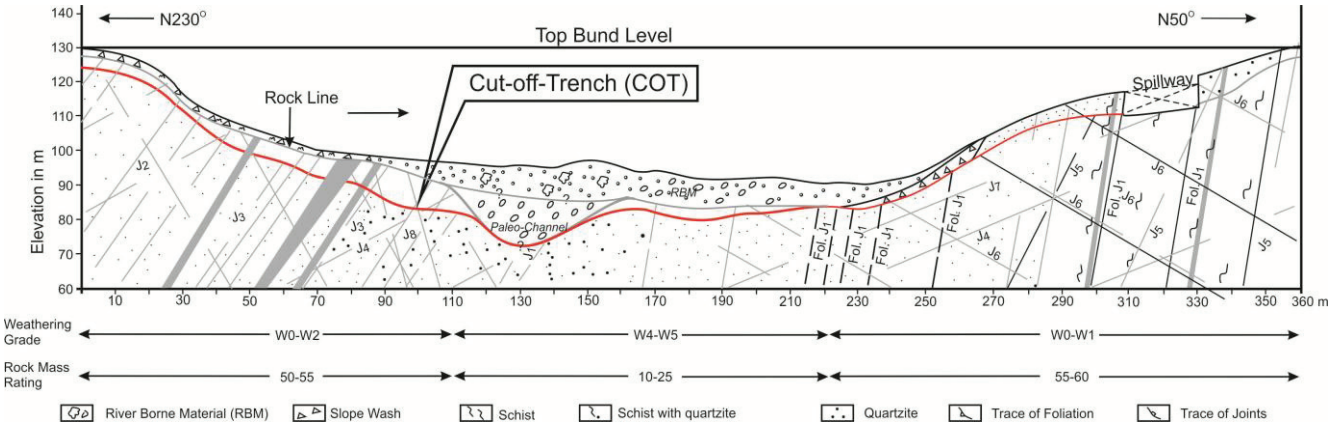

Figure 2, Geological section along the dam axis. The COT base (red line) shows the depth of the paleo-channel below the present bed level of the river.

Boulders, pebbles, and granules of varying sizes embedded in a sandy matrix comprised the paleo-channel material in about 55m section of COT posed a threat to the safety of the dam.

Table 1, Discontinuities observed in COT

Joint Set	Dip/ direction	Spacing (cm)	Continuity (m): Condition
Foliation / J1	40^0/SV/20 0°/20°	3 - 15	>5; S, SU,
J2	73°/110°	3 - 10	1-3 m; R, P, with 2 mm to 1 cm opening
J3	61°/ W	3 - 5	1 - 3 m, S, P
J4	65°-70° /310°	5 - 20	1 - 5 m, S, SR, P
J5	75°/280°	6 - 20	0.5 - 2 m; S, R, P
J6	28° /15°	40	2m, S, P
J7	25°-46° /295°	10	1.6 m; S, P
J8	75° /SV/ 30°	6-10	1.5 m; R, P

SV-Sub-Vertical, S-Smooth, P-Planar, SU-Slightly Undulating, R-Rough, SR-Slightly Rough, SR-Smooth Rough

Paleo-channel materials were filled with unconsolidated to semi-consolidated sediments that reflect the environment of the ancient river system. The material types found include gravel and coarse to medium sand, the coarser materials with slower-moving water.

Geo-log of the Cut-off-Trench (COT)

Geological logging of the COT section reveals the presence of bedrock between 7 m and 14 m, and a paleo-channel in the valley portion. The COT section may be categorized into four segments, viz., Chainages (CH) 0-112 m; 112-210 m;210-240 m;240-248 m, depending on the conditions encountered. The details of geological conditions along the COT are as below: -

(1) From CH. 00 to CH. 112.5 m (Left flank): Moderately weathered micaceous quartzite with mica schist bands classified as class-III rock. The foliation of the rock trend N750W-S750E with dips 400-670 in a southwesterly direction along with five sets of joints

(2) From CH. 112.5 m to CH. 210 m (Paleo-channel/fossil valley in River section): The section exposes moderate to high weathered (W4-W5 weathering Grade) quartzite and mica schist below the paleo-channel (9 m to 13 m deep) or the fossil valley of the river. A zone of crushed quartzite has been mapped between CH. 110 m and CH. 140 m, possibly because of the fault along which the paleo-channel is passing.

(3) From CH. 210 m- to CH. 240m (River portion): Fresh and hard quartzite are intercepted in this section. The rocks are traversed by two sets of joints aligned askew to the dam axis.

(4) From CH. 240 m- to CH. 348 m (Right flank): Hard quartzite with weathered mica schist bands has been encountered.

Structural discontinuities in COT

Discontinuities, such as faults or joints in the dam foundations, can influence the dam's stability and performance. They allow water seepage or affect the transmission of loads. Detailed mapping of the dam trench area highlights seven sets of discontinuity surfaces and a well-developed foliation plane; the details of their orientation, dip amount, spacing, and continuities are shown in Table 1. The provision of curtain grouting to check the seepage below the foundation of COT is mandated owing to closely spaced foliation (Karmakar et al., 2016) having a cross-cutting relation with the axis of the dam, along with other sets of joints.

Permeability values in COT (pre-grout)

Permeability tests are an integral part of any grouting operation, and to decide the spacing between the Primary, Secondary or even Tertiary holes. The drill holes at center line of COT, done with 6m spacing as primary holes, and an empirical criterion

$$D = \frac{2}{3}H + 8$$

where *D* is depth of the hole kept for grout curtain permeability, and *H* is the height of the reservoir water decides the depth of the hole. The average permeability values in sections 0-112 m, 112-210 m, 210-240 m, and 240-348 m were computed in 3m stages with cyclic pressure indicate order of permeability values <5 lugeons, 22 lugeons (and in some sections up to 44 lugeons), <1 to 5 lugeon and <1-2 lugeon respectively. In the secondary drill holes with 3m spacing, these values are reduced to <1-3 lugeon; however, in section (110-165 m), the permeability values were found to be anomalous, and it was difficult to determine the permeability values.

Grouting technique as mitigation measures

Grouting, a vital geotechnical technique has been used to enhance dam safety by improving the foundation and preventing water seepage involving following stages.

Curtain grouting in COT

A provision of curtain grouting down to the depth up to 3/4H (H is the height of water retention at that point) has been provided as a measure of seepage control, in addition to an upstream impervious layer up to 10H (clay blanketing) has been provided and tagged to COT to increase the path of percolation as well as to reduce the anticipated seepage below the foundation (Sharma, 2018).

Along the dam axis, a 351 m cut-off trench (COT) with the provision of a grout curtain has been designed as a prime measure for seepage control. After filling the COT with the clay of variable depth, number of drill holes in a pattern of three rows (upstream row, downstream row, and center line) have been drilled and Primary (6 m spacing) and Secondary grouting (3 m spacing) grouting operations have been done in the COT area ensuring permeability (1-5 lugeon).

TAM Grouting in the paleo channel section

Drilled using the ODEX (Overburden Drilling Excentric) system, a specialized drilling method designed to simultaneously drill a borehole and install a temporary or permanent casing through unstable ground, such as loose soil, sand, gravel, and formations with cobbles and boulders. The system uses a down-the-hole (DTH) hammer along with casing up to the channel material, which is a collapsible stratum, then further drilling within the rock section has been performed.

After completion of drilling TAM (Tube a' Manchette) perforated PVC pipe with sleeves on perforations then inserted into the hole. Water cement and bentonite (2-5 % by weight of Cement) solution (Sheath Grout) were then filled around the TAM Pipe in the drill hole, and the casing was withdrawn. A hydraulically operated double packer with inter-packer distance of 0.60 m is then inserted and packers are hydraulically expanded to seal the section.

The paleo channel section in a depth range of 9-14 m (Figure 3), between CH 110m and 165 m (55 m), following an 'Off-pattern' grouting holes were drilled to consolidate the entire paleo-channel material, ensuring permeability values (1-5 lugeons). The method is repeated in drill holes done in the entire channel material in an off-pattern manner. The progression of techniques such as cut-off-trench, curtain grouting, blanketing, specific section TAM grouting and off-pattern grouting found to be most effective mitigation for potential leakage especially along paleo-channel encountered in the COT excavation.

Discussion and lessons learned

Epigenetic gorges (paleo-channels or fossil valleys) consist of channel-lag deposits, which are unconsolidated sediments having high permeability. Paleo-channels are parts of rivers representing channels abandoned by migrating rivers as they shifted their courses to carve new water courses. Despite remaining cut off from the active river flow, these features remain part of the flow regime of the active river system. These channels were formed due to river migration driven by neo-tectonic activity and climatic shifts or variability during the Holocene period. In the peninsular shield area, such features are generally concealed and difficult to locate, while in younger mountains such as the Himalayas, the epigenetic gorges are obvious to locate during the geological mapping of the dam sites and their environs. The presence of faults and lineaments in the basin influences both the river's path and the location of these paleo-channels. Paleo-channels are ancient, buried riverbeds formed due to past tectonic shifts or climate changes.

Dams, although mainly built on active rivers, interact with paleo-channels in many ways. The paleo-channels may pose significant challenges if encountered in the foundation of dams, reservoirs and have a connection with downstream, may endanger the stability of the superstructure. Understanding these channels is crucial for assessing the geological stability and potential risks of dam sites. The relevance lies in how paleo-channels may influence water flow patterns, sediment transport, and the overall stability of the dam foundation. Studies of these features ensure proper civil design and construction, minimizing the risk of foundation failures and enhancing the long-term safety of the dam. In the context of dam construction and reservoir management, epigenetic gorges are crucial

because dams built near or across such gorges must account for the potential for differential erosion or seepage in reservoirs, and epigenetic gorges help model how water might bypass or undermine dam structures during extreme events.

Figure 3, Course of the paleo-channel intercepted in excavations of the Cut-off-Trench (Source: GoogleEarth).

Delineation of paleo-channel course in the Kundghat dam foundation was a unique case of such ancient channel within plateau of Chhotanagpur Gneissic Complex (CGC), mostly forested, where routine geological mapping could not locate the channel possibly due to slope wash cover (Figure 3). It is therefore imperative that treatment of paleo-channels in dam foundations should involve a comprehensive geological and engineering approach that includes

(i) site investigations (geological, geophysical, and drilling explorations)

(ii) foundation design to adjust the parameters of variations in soil and rock properties

(iii) grouting to fill voids to improve stability and permeability of channel material

(iv) cut-off walls to intercept potential seepage path and (v)engineering barriers such as clay or concrete cut-offs,

The successions of grouting techniques were found useful in addressing foundation leakage while managing the risks to the dam. Grouting, a geotechnical process, also helps to improve soil or rock properties by injecting a fluid material (grout) into a formation, which then hardens. The effectiveness of grouting depends heavily on understanding the ground geological conditions and selecting the right techniques for structural integrity and safety of the dams.

Acknowledgements

The author likes to thank the authorities of the Kundghat dam projects, the Water Resources Department, Government of Bihar for sharing the permeability and grouting data about the project and anonymous reviewers for purposeful suggestions in improving the manuscript.

Author contributions

Vinod wrote the manuscript, prepared the figures, and revised the article. He is the sole author of this article.

Data availability

No datasets were generated or analyzed during this study.

Declarations

The author declare that he has no known competing financial interests or personal relationships that could have appeared to influence the work reported in this article.

References

Chakraborty, A., Sharma, V., and Rath, S. (2017). Prognosis and treatment of buried channels in river valley projects: A geotechnical perspective. Journal of Engineering Geology, 42(1–2), 317–329.

Engeln von, O. D. (1942). Geomorphology: Systematic and regional (pp. 224–225). Macmillan.

Hewitt, K. (1998). Catastrophic landslides and their effects on the Upper Indus streams, Karakorum Himalaya, northern Pakistan. Geomorphology, 26(1–3), 47–80. https://doi.org/10.1016/S0169-555X(98)00051-5

Karmakar, R., Singh, S. K., and Ghoshal, T. B. (2016). [Unpublished report]. Geological Survey of India, field season 2015–2016.

Korup, O., Strom, A., and Weidinger, J. (2006). Fluvial response to large rock-slope failures: Examples from the Himalayas, the Tien Shan, and the Southern Alps in New Zealand. Geomorphology, 78(1–2), 3–21. https://doi.org/10.1016/j.geomorph.2006.01.019

Kothyari, G. C., and Juyal, N. (2013). Implications of fossil valleys and associated epigenetic gorges in parts of Central Himalaya. Current Science, 105(3), 383–387.

Ouimet, W. B., Whipple, K. X., Crosby, B. T., Johnson, J. P., and Schildgen, T. F. (2008). Epigenetic gorges in fluvial landscapes. Earth Surface Processes and Landforms, 33(13), 1993–2009. https://doi.org/10.1002/esp.1650

Pant, G. (1975). Observations on the fossil valleys and epigenetic gorges of the Bhagirathi and Alaknanda rivers. Himalayan Geology, 5, 193–206.

Pratt-Sitaula, B., Garde, M., Burbank, D., Oskin, M., Heimsath, A., and Gabet, E. (2007). Bedload-to-suspended load ratio and rapid bedrock incision from Himalayan landslide-dam lake record. Quaternary Research, 68(1), 111–120. https://doi.org/10.1016/j.yqres.2007.03.005

Ray, Y., and Srivastava, P. (2010). Widespread aggradation in the mountainous catchment of the Alaknanda–Ganga River System: Timescales and implications to hinterland–foreland relationships. Quaternary Science Reviews, 29(17–18), 2238–2260. https://doi.org/10.1016/j.quascirev.2010.05.014

Sharma, V. K. (2018). A geotechnical note on construction stage investigations at Kundaghat Dam Project, Sikandra Block, Jamui District, Bihar [Unpublished report]. Water Resources Department, Government of Bihar.

Triantafilis, J., and Buchanan, S. (2009). Identifying common near-surface and subsurface stratigraphic units using 'Em34 water science 107' signal data and fuzzy k-means analysis in the Darling River valley. Australian Journal of Earth Sciences, 56(4), 535–558. https://doi.org/10.1080/08120090902806330

Wray, R. A. (2009). Paleochannels of the Namoi River floodplain, New South Wales, Australia: The use of multispectral Landsat imagery to highlight a Late Quaternary change in fluvial regime. Australian Geographer, 40(1), 29–49. https://doi.org/10.1080/00049180802657007

Research Article DOI: https://doi.org/10.64862/ajeg.2025.201.02 Open Access

Numerical Modeling of Debris Flow Originating from Topographic Hollows at Koyalghari and Simaltal Area along Narayangadh-Mugling Highway

Aakriti Koirala[1, 2*] and Ranjan Kumar Dahal[1]

[1]Central Department of Geology, Tribhuvan University, Kirtipur, Kathmandu, Nepal
[2]Geotech Solutions International, Dhobighat, Lalitpur, Nepal

(*Corresponding E-mail: aakritikoirala111@gmail.com)

Received: November 26, 2024, Accepted: June 11, 2025

Abstract: Assessment of debris flow runout extent is essential for evaluating landslide hazards and formulating effective land-use plans. This study employed the openly available LISEM (LImburg Soil Erosion Model) to simulate debris flow runout using diverse geospatial and geotechnical input data. By incorporating the spatial distribution of soil geotechnical parameters, the model effectively estimated debris flow runout based on debris height. The research integrates rainfall-induced slope failure and runout dynamics through a physically based modeling approach to predict potential landslide impact zones under extreme rainfall conditions corresponding to 5-, 10-, and 25-year return periods. The study area is the Koyalghari region along the Narayangadh-Mugling Highway in central Nepal. Model validation was conducted in the Simaltal area using the Cohen's Kappa statistic, yielding a value of approximately 0.7, which indicates substantial agreement with observed debris flow patterns. For the analyzed rainfall scenarios, the estimated average debris flow height ranged from 0.92 m to 1.1 m on the highway, highlighting the potential for severe damage to road infrastructure and traffic during extreme events. Overall, the study demonstrates that a physically based model incorporating geotechnical soil parameters can reliably estimate debris flow runout and deposit height, offering valuable insights for hazard assessment, risk mitigation, and land-use planning in landslide-prone regions such as the Narayangadh-Mugling Highway.

Keywords: ***Cohens Kappa, Debris flow, LISEM model, Physical based modelling, Runout distance, Mugling.***

Introduction

The mountainous areas of Nepal are naturally unstable and particularly vulnerable to landslides for several reasons like their rugged topography, which is the result of their narrow north-south distance. Additionally, the presence of soft soil cover, high intensity monsoon rainfall and frequent earthquake amplify the risk (Upreti and Dhital, 1996). Rainfall plays a crucial role in triggering debris flow from topographic hollow, which are natural depressions in the landscape where colluvial material (loose, unconsolidated soil and rock) accumulates over time. In densely populated mountainous areas of Nepal, human life and property remain vulnerable to the wide-spreading effects of rainfall-induced debris flow. This debris flow originating from topographic hollows due to rainfall can travel considerable distances across sloped natural terrain covering a larger area than the topographic hollow. Hazard analysis in these mountainous regions requires an analysis of both the debris flow initiation and runout areas. Despite the risks posed by debris flows, people continue to inhabit the middle mountain and low valleys of Nepal. Understanding the origin of debris flow from topographic hollow is essential for disaster resilience especially in the context of a mountainous country like Nepal.

Debris flow modeling can be carried out by three general approaches: physical modeling, empirical modeling, and dynamic modeling (Chen and Lee, 2000). The distinction between these approaches is that empirical modeling is based on well-documented observations and typically allows for the practical estimation of travel distance without taking debris flow rheology into account, while physical modeling is based on field observation and supported by controlled laboratory experiment (Quan et al., 2014). Furthermore, dynamic modeling is carried out through the application of momentum and energy conservation laws through numerical methods (Hussin, 2011).

The dynamic method is numerically solved using physically based models derived from fluid mechanics. They can offer more precise predictions; however, they require more detailed input data and are computationally intensive than other methods. LISEM (LImberg Soil Erosion Model) developed by Faculty of Geo-Information Science and Earth Observation (ITC) of Twente University is a physically based dynamic model that offers a more comprehensive analysis by considering the physical processes involved in debris flow runout. It uses a physically based approach to model the movement of water and solid material down a slope considering the physical processes involved in debris flow and the interaction with the topography, offering a more realistic representation than simpler models (Bout et al., 2018). LISEM includes

mathematical equations related to debris flow. Users can also construct a physically based model through a script that integrates the selected tools and arranges them in the desired order, providing flexibility in the model setup. A more comprehensive scripting environment is offered by the script editor, which uses a modified version of the AngelScript language. The runout was simulated in OpenLISEM using a simple runout modeling or "FlowDebris" function that can simulate two-phase runout flow or flows with different solid contents and flow properties through the integration of solids and water dynamics based on the Two-Phase flow equations proposed by Pudasaini (2012).

Study area

The study area of the research is located at Simaltal and Koyalghari in Ichhakamana Gaupalika, Chitwan district (Figure 1). The area is about 72 km southwest of the capital city, i.e. Kathmandu.

The Koyalghari area lies in the latitude of 27° 48' 45" and longitude of 84° 30' 31'' and Simaltal area lies in the latitude of 27° 49' 11'' and longitude of 84° 28' 39''.

The hollow in Koyalghari area and Simaltal area covers about 2663.25 sq. m. area and 2732.23 sq. m. area respectively. The major highways that connect the study area to most parts of Nepal includes Mahendra Highway, Prithvi Highway and Madan Bhandari Highway. Geologically, the study area lies in the Nourpul Formation of the Lower Nawakot Group of the Nawakot Complex (Stöcklin and Bhattarai, 1977). The formation is part of the Lesser Himalaya Sequence (LHS), which is separated from the Siwalik by the Main Boundary Thrust (MBT) near Jogimara village in Narayangadh-Mugling section. The lithology around the study area comprises grey-green slate, grey phyllite, pink dolomite, grey metasandstone, pink, grey, dirty white quartzite etc. This rock succession was overlain by the silty to clayey colluvial soil of low to high plasticity in the topographic hollow.

The nearest rainfall station from the research area is Devghat station. The rainfall data of Devghat station obtained from Department of Hydrology and Metrology (DHM) shows that the monsoon season (June to September) brings heavy rainfall that accounts for around 80% of the total annual precipitation of the area (Figure 2). These rainfalls are responsible for numbers of shallow landslides along the highway during monsoon.

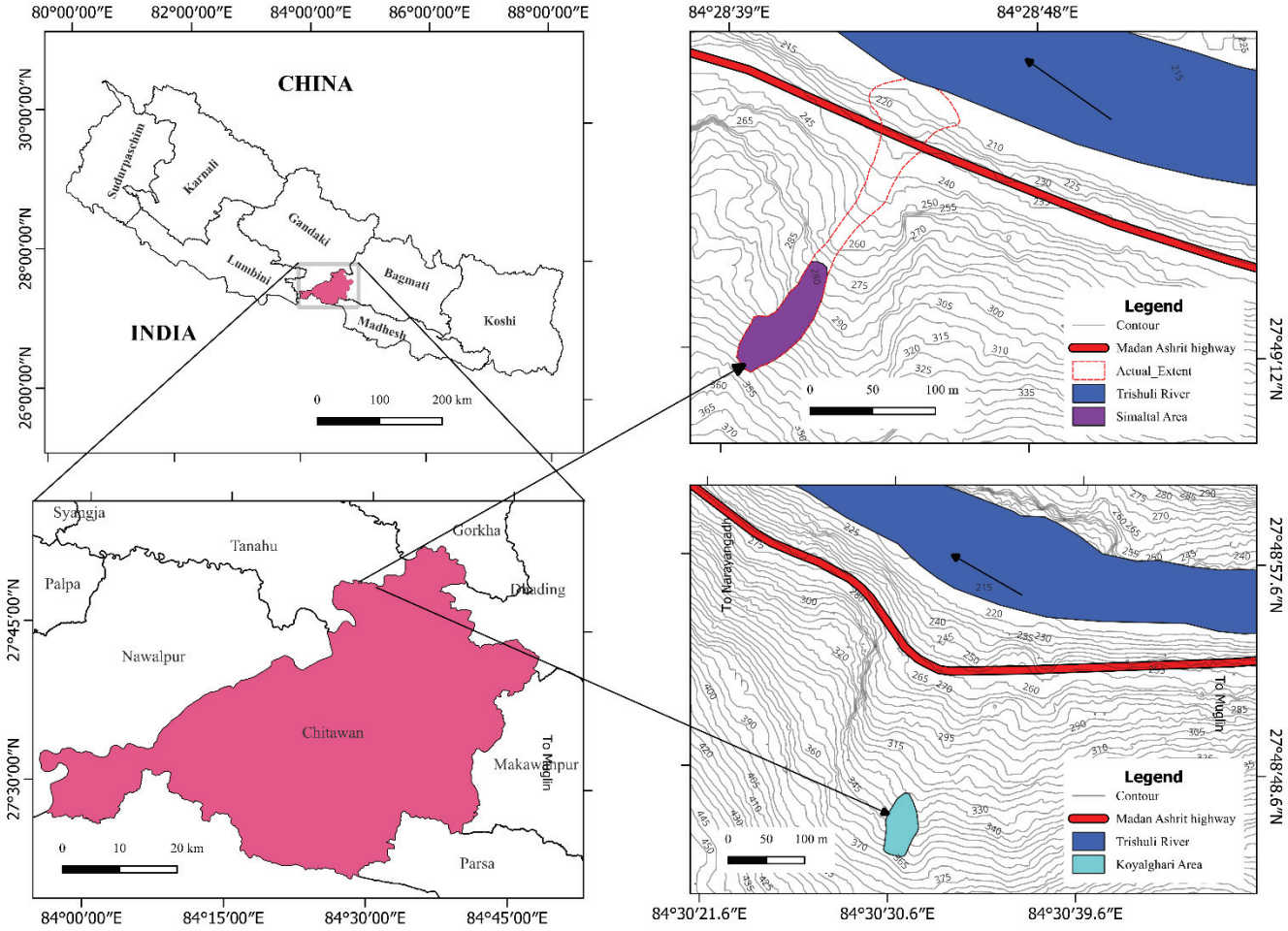

Figure 1, Location map of study area.

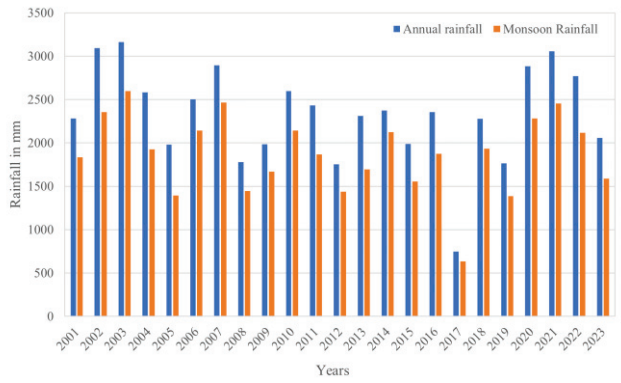

Figure 2, Total monsoon and annual rainfall of each year from 2001 to 2023 in Devghat Station (Source: DHM).

Physical based modelling in LISEM

The objective of the present study was achieved by following methods as presented in the flowchart below (Figure 3).

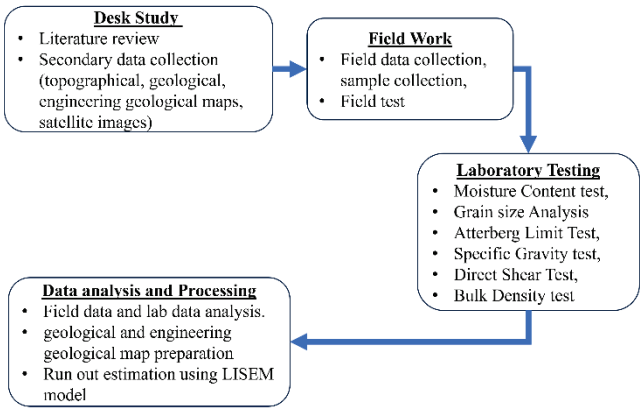

Figure 3, Overview of methods used during study.

For geotechnical investigation, laboratory tests conducted on the collected samples included moisture content, grain size analysis, Atterberg limits, specific gravity, unit weight, porosity and direct shear tests whereas in situ tests conducted includes infiltration test and DCPT. For simulations, geotechnical properties determined from different samples were utilized.

The flow chart of the methods used for modeling debris flow in the LISEM model is shown in Figure 4.

Primary inputs

The primary inputs for the model are grouped into 3 categories: geospatial data, ground truth, and rainfall data. Geospatial data includes Digital Elevation Model, soil depth, and soil hydraulic properties and runout parameters like manning's 'n'. The data related to soil parameters obtained from the average value of the field test and lab test were rasterized to obtain the required input map. The ground truth data is the actual impact area of past debris flow which is used for model validation. It is the observed runout of the debris flow at Simaltal in 2010 obtained from the google earth image.

Two types of rainfall data were used as observed and forecasted. Observed precipitation data for past events was obtained from the DHM to validate the model while forecasted precipitation data was obtained based on extreme rainfall with return periods of 5, 10 and 25 years after processing 23-year daily rainfall data. The various sources of data used in LISEM model are given in Table 1.

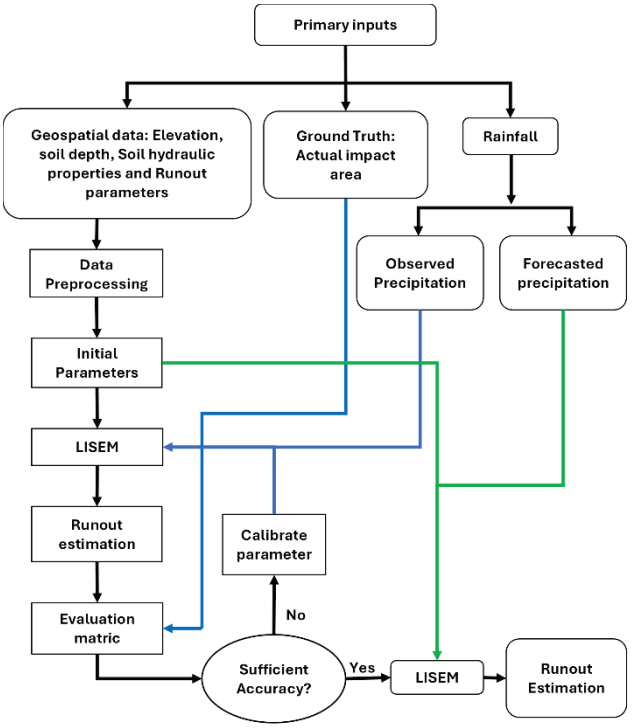

Figure 4, Flowchart of LISEM model employed for debris runout estimation.

Table 1, Data sources required for LISEM model

Data	Input data	Source
Geospatial data	Elevation (5-m DEM resampled into 1 m)	Durham University
	Soil depth	DCPT
	Saturated Hydraulic Conductivity	Infiltration test
	Porosity	Laboratory test
	Particle density	
	Dominant grain size	Sieve Analysis
	Cohesion	Direct Shear test
	Internal Friction Angle (IFA)	
	Manning's n	Manning's n table from Chow, 1959
Ground Truth	Actual debris runout extent	Google Earth pro
Rainfall	Precipitation	23-year rainfall record from DHM

Data preprocessing

This section outlines the data sources and preprocessing methods used to prepare maps for the physically based model. All input data underwent preprocessing steps to ensure compatibility with LISEM. This step includes formatting the data into a specific file, ensuring spatial and temporal consistency between different data layers and filling any data gaps or outliers. The rainfall data were also processed to determine extreme rainfall for 5, 10 and 25 yr return period based on Gumbel method.

Initial parameters

LISEM requires various initial parameters to control the debris flow simulation. These parameters include initial solid internal friction angle, cohesion, rock size, solid density, solid height and water height. The values of these parameters are determined by laboratory test results of the collected sample. The raster map of each initial parameter was prepared using a raster calculator in QGIS. The initial solid internal friction angle, cohesion and solid density was taken from the average of the value obtained from the laboratory test. Similarly, initial rock size was obtained from the average Characteristic Grain Size (D_{10}).

LISEM modelling

The core part of the methods involves running the LISEM model. At first the start time, end time of simulation and time step were selected as per requirement. Then directory of all input maps, rainfall data and output directory were chosen. Similarly, the two options in the SPH model as 'include initial solid' and 'include initial fluid' were selected for simulation. Finally, after running the model the debris flow runout process was simulated considering factors like topography, past rainfall intensity, and debris material properties. In the Simaltal area the past rainfall data was used whereas in the Koyalghari area the extreme rainfall data (forecasted precipitation) was used.

Runout estimation and validation

LISEM generated the debris flow runout zone in the study area in terms of solid height and fluid height. The model was validated in the Simaltal debris flow of 2010. Common metrics for evaluating debris flow models include the root mean squared error (RMSE) and Cohen's kappa. In the present study the accuracy of the model was calculated based on Cohen's kappa (Cohen 1960) by using "MapContinuousCohensKappa" function in a scripting environment of the LISEM model. These metrics enable the comparison of accuracy based on several parameters and are widely used for quantitative evaluations. The Cohen's Kappa matric is preferred over others because it helps to estimate interrater reliability i.e. rater agreement by considering chance agreement. This makes it an effective tool for validating the reliability of models or maps in a variety of fields, including environmental science and risk assessment. The formula to calculate Cohen's kappa (κ) modified from Cohen 1960 for machine learning application based on 2x2 confusion matrix described by Chicco et al. (2021) is given in Equation 1:

$$\kappa = \frac{2*(TP*TN-FP*FN)}{(TP+FP)*(FP+TN)+(TP+FN)*(FN+TN)} \quad (1)$$

For the calculation of Cohen's Kappa, first confusion matrix was constructed as in Table 2. The matrix compares the location of the actual impact area referred to as observed, and the simulated runout area labeled as predicted. In this case, the debris height was chosen to compare the observed and predicted values in the confusion matrix. During accuracy assessment minimum debris flow height should be specified below which the runout is not considered because this small value might not be visible in satellite image of actual runout. Hence, it classifies according to the threshold height and delineate predicted debris height of each pixel into two regions as the runout area and outside (where no runout is expected during the simulation period). Finally, Cohen's Kappa was calculated with the confusion matrix obtained by counting the number of pixels classified as False Positive (FP), False Negative (FN), True Positive (TP) and True Negative (TN). Cohen's kappa value can be classified into various classes based on Table 3.

Table 2, Confusion matrix based simulated debris height (modified from Rossi et al., 2010)

		Predicted	
		Positive	Negative
Observed	Positive	True Positive (TP): Debris height > 0.45 m in 1	True Negative (TN): Debris height < 0.45 m in 2
	Negative	False Positive (FP): Debris height > 0.45 m in 2	False Negative (FN): Debris height < 0.45 m in 1

The number 1 refers to the runout area of 2010 debris flow event, and the number 2 is the outside the area, in which it is assumed that no debris runout occurred.

Table 3, Interpretation Cohen's Kappa value (Landis and Koch, 1977)

Cohen's Kappa Value	Interpretation of Cohen's Kappa Value
< 0.0	Poor agreement
0.0 - 0.20	Slight agreement
0.21 - 0.40	Fair agreement
0.41 - 0.60	Moderate agreement
0.61 - 0.80	Substantial agreement
0.81 – 1.00	Almost perfect agreement

Slope stability and failure volume estimation

To simulate the debris flow in LISEM model from a topographic hollow, a crucial assumption was made regarding the failure mechanism. Instead of employing a separate slope stability model to calculate a Factor of Safety and a specific failed volume, the approach assumes a worst-case, physically possible scenario: that the entire colluvial deposit within the topographic hollow fails and mobilizes simultaneously after extreme rainfall event.

This assumption is based on the known characteristics of debris flows originating from these specific geomorphic features. Topographic hollows are inherently unstable and highly susceptible to complete failure when saturated by intense rainfall. The high permeability and low cohesion of this material, combined with the convergent subsurface flow of water during a storm, lead to a rapid increase in pore water pressure and a sudden loss of shear strength, which can trigger a catastrophic failure of the entire colluvial mass.

By assuming the mobilization of the entire volume of colluvial mass, a conservative, upper-bound estimate of the initial solid and fluid volume was made. This volume directly provides input parameters of "initial solid height" and "initial fluid height" using equation 2 and equation 3 respectively. This method helps in simulating debris flow run out and focus on how the material moves and settles afterward.

Result

Geologically, the study area lies in the Nourpul Formation of the Lesser Himalaya Zone. The slope under study is largely composed of phyllite and quartzite fragments and is characterized by a predominance of colluvial deposits. The area is mostly covered up to 3 m thick colluvial soil, primarily low plasticity silt (ML) and low plasticity clay (CL). The terrain, with slopes facing the Northeast, has gentle angles averaging 30 degrees (Figure 5).

Runout parameter maps

The runout was estimated using opensource software called LISEM which requires various input maps. The input map of the soil parameter was determined from the average value of geotechnical parameter given in Table 4 obtained from field and lab test.

Digital elevation model (DEM)

The DEM of the study area was prepared and it indicates the highest elevation of about 600 m, and the lowest elevation of 210 m is located near the Narayangadh-Mugling Highway in Koyalghari area. Whereas the elevation in the Simaltal area varies from 210 m to 480 m. The landslide scarp of the Simaltal area was at 340 m elevation whereas the deposition was at 215 m elevation on the Trishuli River as shown in Figure 6.

Table 4, Summary of values of various parameters obtained from field and laboratory test for hollow at Simaltal and Koyalghari

Parameters	Values in Simaltal area	Values in Koyalghari area
Cohesion (kN/sq. m.)	13.83	16.51
Internal Friction Angle (radians)	0.46	0.46
Soil density (kg/m^3)	1757.76	1640.12
Porosity	0.323	0.385
Specific gravity	2.58	2.51
Characteristic Grain Size, D_{10} (m)	2.62E-04	1.19E-04
Moisture content (%)	5.04	17.21

Manning's "n"

Manning's 'n' map was prepared from land use map based on Chow (1959). The land use map, as shown in Figure 7, **Error! Reference source not found.**was obtained from ESRI, which was based on Sentinel image. The land use map shows medium to dense brush is dominant in Koyalghari area followed by scatter brush. Similarly, in the Simaltal area, dense brush is dominant. The value of 'n' ranges from 0.04 to 0.1 in the Koyalghari area and the Simaltal area.

Soil depth map

Soil depth map was prepared from point map of soil depth obtained by Dynamic cone penetration test (DCPT) using ordinary kriging interpolation in GIS. The soil depth ranges from 0.6 m to 2.5 m in Koyalghari area whereas it ranges from 2.3 m to 4.5 m in Simaltal area as shown in Figure 8.

Initial solid height

Initial Solid height map was obtained from porosity and soil depth. The highest value of initial solid height is 3.045 m at Simaltal area and lowest value is 1.533 at Koyalghari area (Figure 9). Initial solid height map was prepared in QGIS using Equation 2 modified from Das (2008):

$$Solid\ height = (1 - Porosity) \times Soil\ depth \quad (2)$$

Initial Water Height

Initial water height map was based on water content at maximum saturation and soil depth. The highest value of initial water height is 1.453 m at Simaltal area and lowest value is 0.385 at Koyalghari area (Figure 10). It was prepared in QGIS using Equation 3 modified from Das (2008):

$$Water\ height = Porosity \times Soil\ depth \quad (3)$$

Initial solid cohesion

The initial cohesion map was prepared using direct shear test data obtained from the laboratory. The average value of cohesion in Koyalghari area is 16.51 kPa whereas that of Simaltal area is 13.83 kPa.

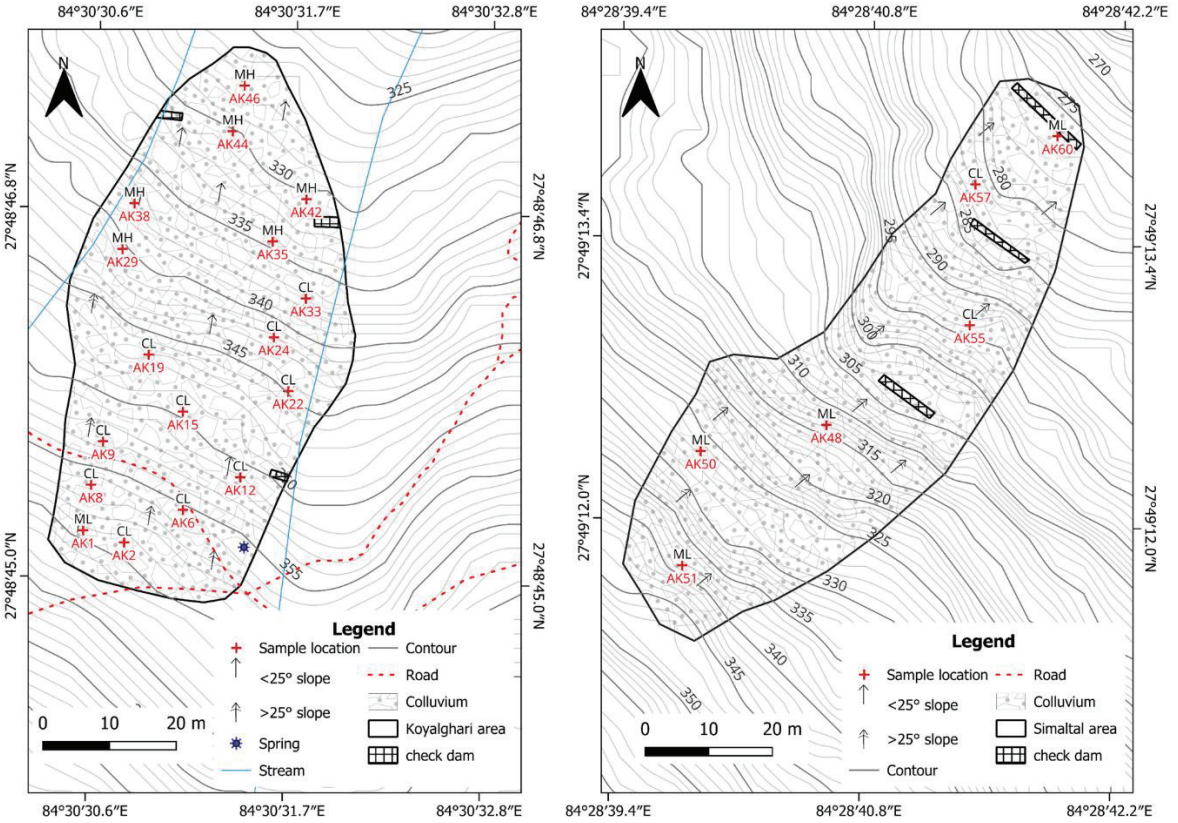

Figure 5, Engineering geological map of Koyalghari area (left) and Simaltal area (right).

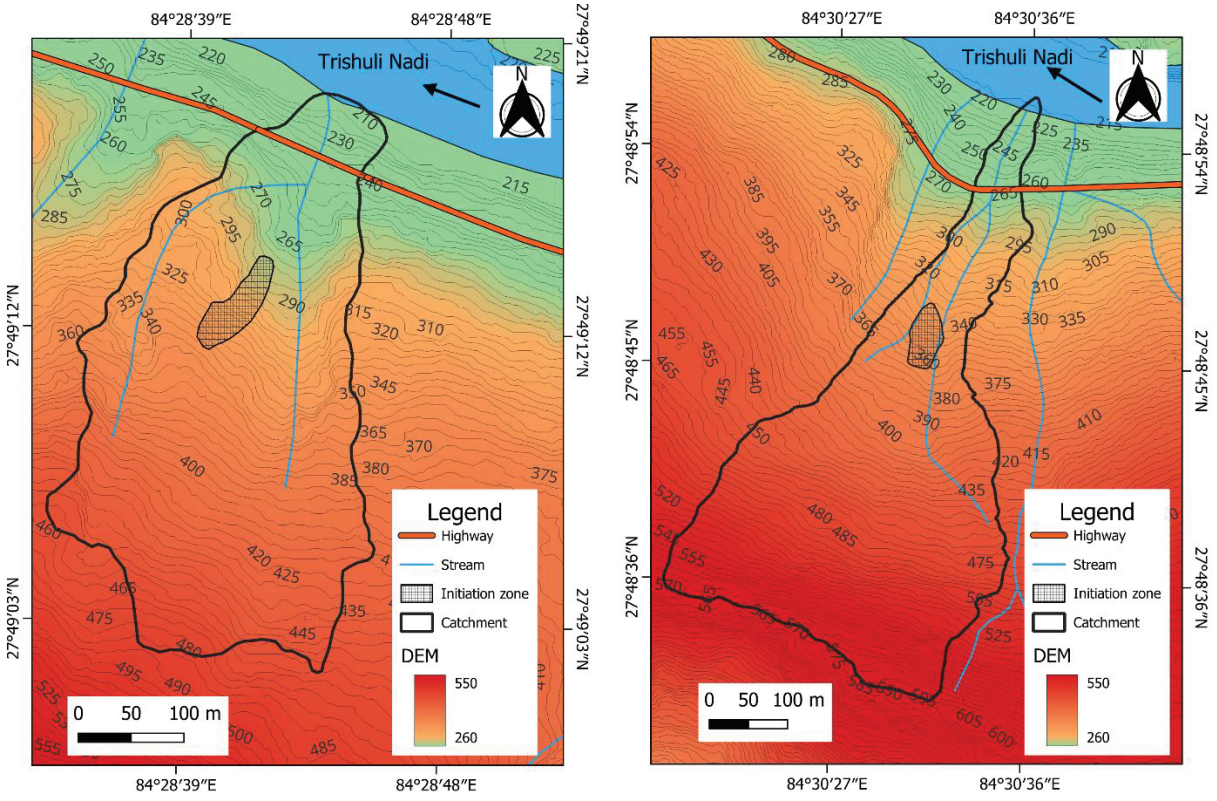

Figure 6, DEM of Simaltal area (left) and Koyalghari area (right).

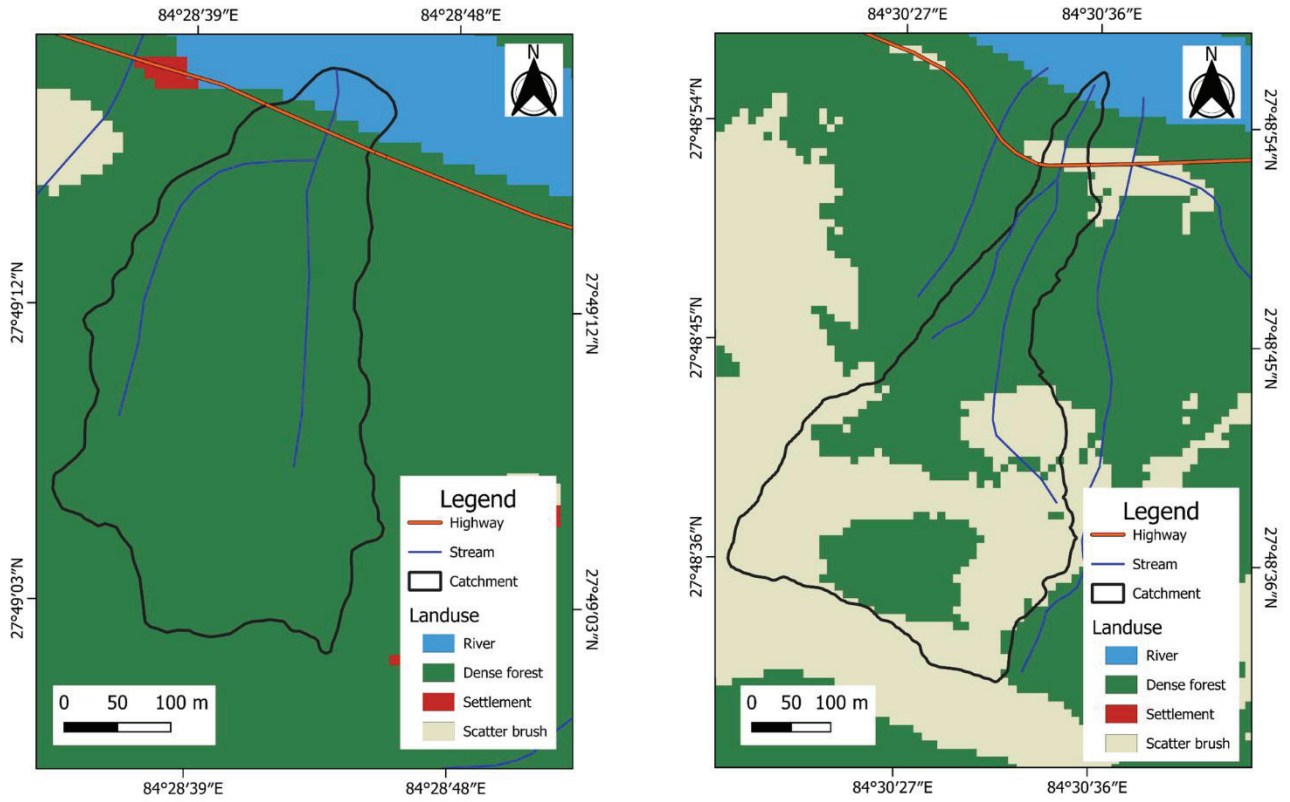

Figure 7, Landuse map of the Simaltal area (left) and Koyalghari area (right).

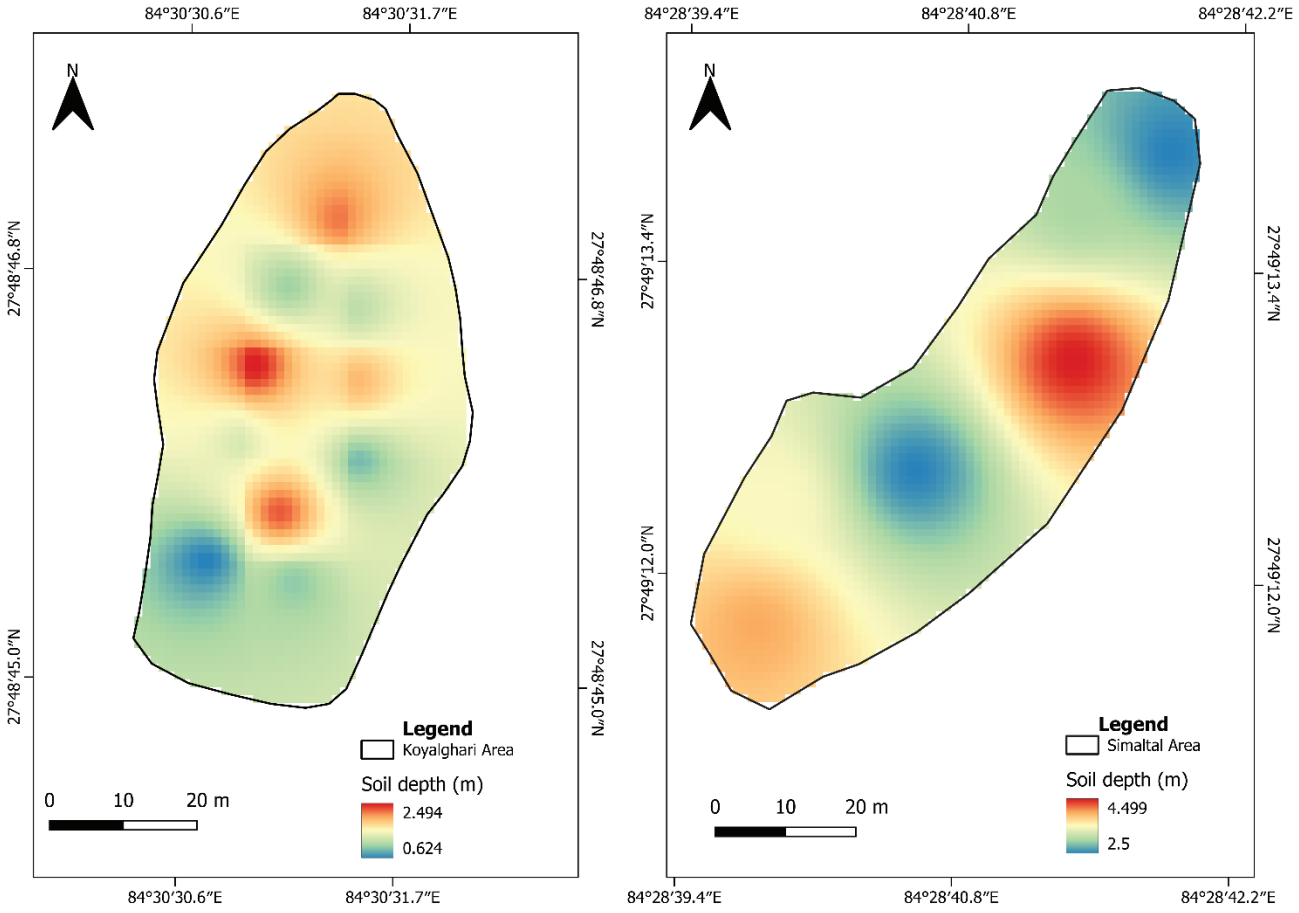

Figure 8, Soil depth map of Simaltal area (right) and Koyalghari area (left).

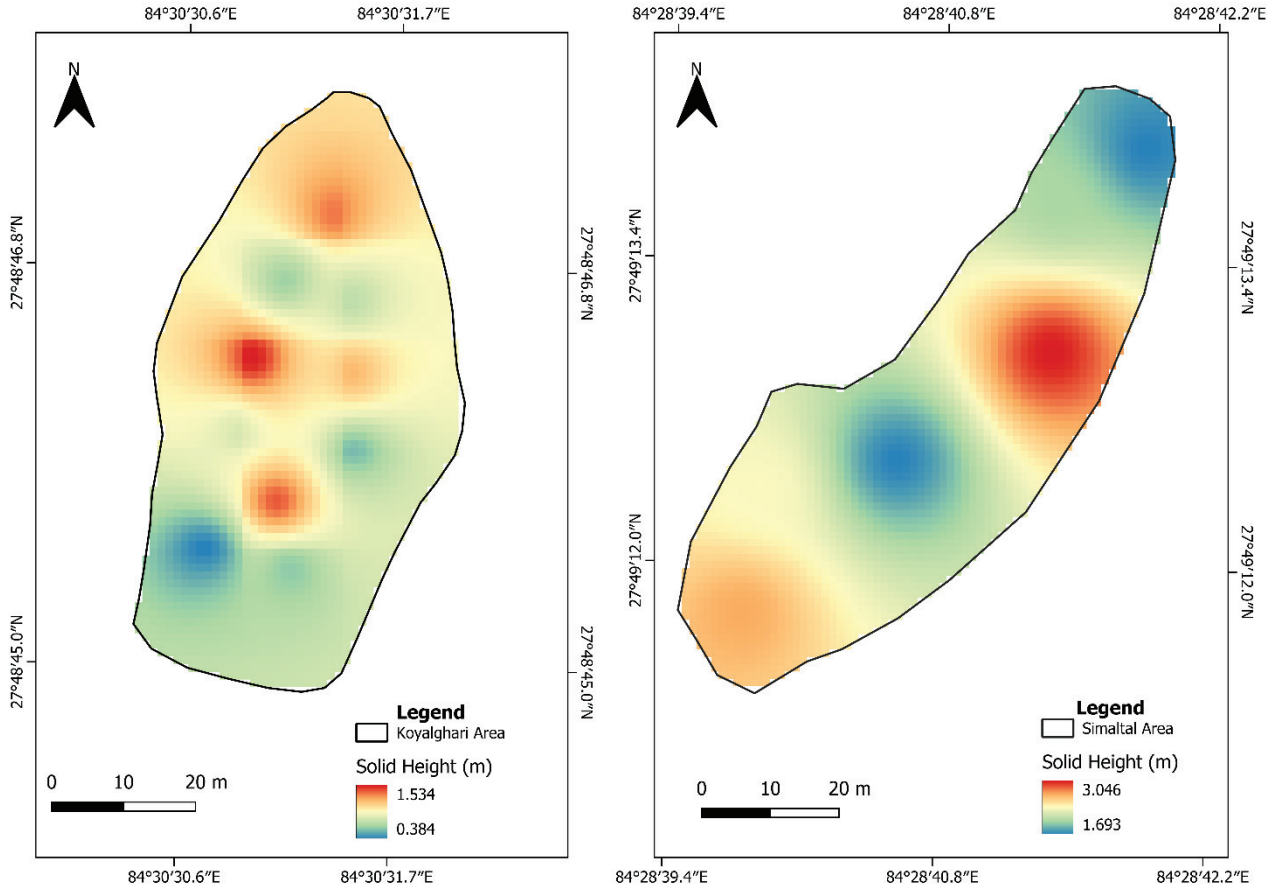

Figure 9, Map of solid height at Simaltal area (right) and Koyalghari area (left).

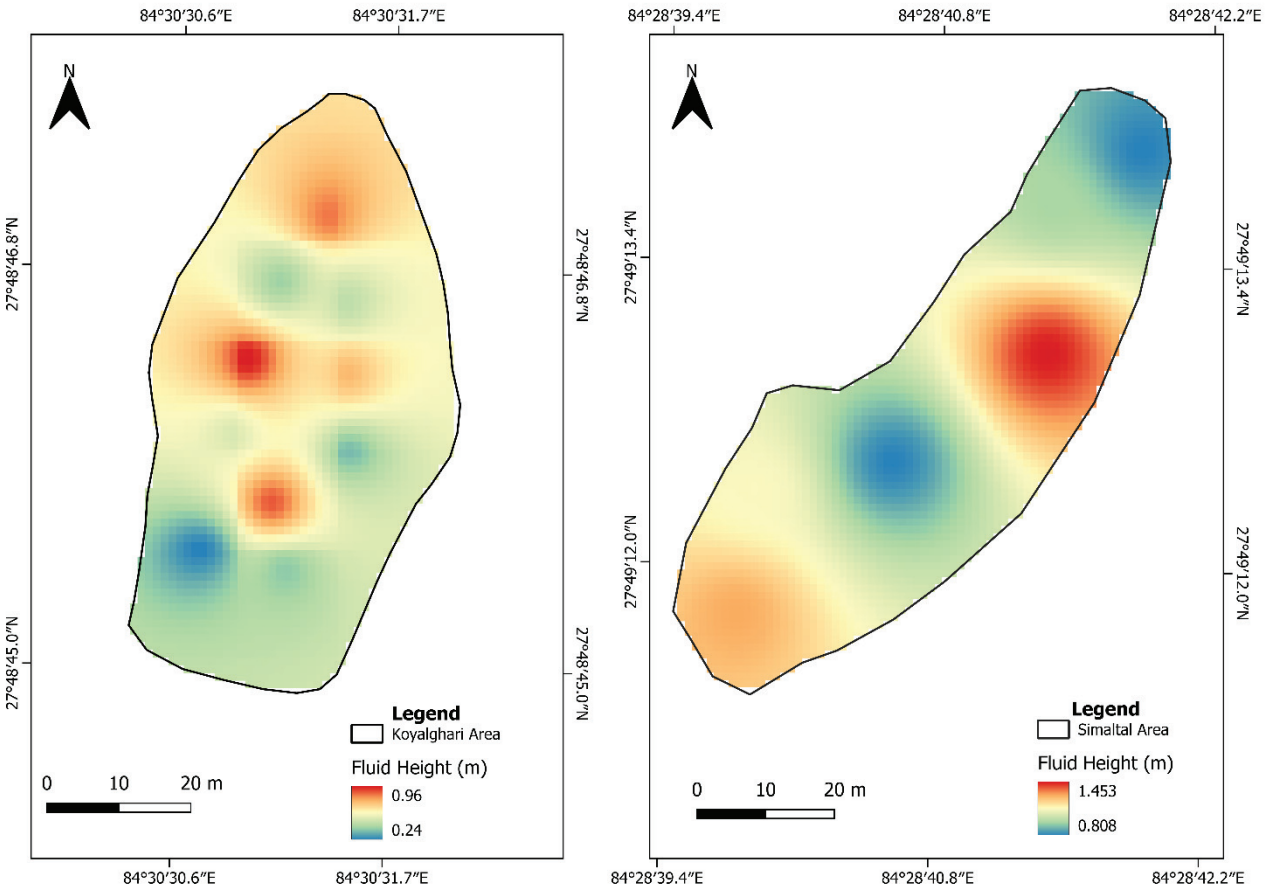

Figure 10, Map of initial fluid height at Simaltal area (right) and Koyalghari area (left).

Initial solid internal friction angle

The Initial Solid Internal Friction Angle map was also prepared using direct shear test data obtained from the laboratory. The average value of internal friction angles in both Koyalghari area and Simaltal area is 0.46 radian.

Initial solid density

The initial solid density map was prepared using soil density data obtained from the laboratory. The average value of solid density in Koyalghari area is 1,640.12 kg/m^3 whereas that of the Simaltal area is 1,757.76 kg/m^3.

Initial solid rock size

The initial Solid Rock size map was prepared from grain size analysis based on D_{10} value. The average value of initial rock size in Koyalghari area is $1.19x10^{-04}$ m whereas that of Simaltal area is $2.62x10^{-04}$ m.

Simulation result

Runout modeling was performed in LISEM model for two areas i.e. first in the Simaltal area to represent debris flow occurred in 2010 using actual precipitation that triggered debris flow and then in the study hollow using extreme rainfall intensity. The satellite image of the Simaltal area of 2010 debris flow is shown in Figure 11. This event was triggered by rainfall of 6th September 2010. The simulation result gives a map of maximum and final debris height and maximum and final debris velocity. The maximum debris height of 9.243 m was obtained at central part (Figure 12) of debris runout whereas the maximum velocity of 29.99 m/s was obtained at initiation part (Figure 13). The debris flow runout covers total area of 15,492.24 sq. m.. On the highway the average maximum debris flow height was 1.107 m and ran out to extend beyond the highway depositing debris finally at the bank of the Trishuli River. The debris flow affected about 60 m of highway from chainage 23+630 m to 23+690 m which aligns with satellite image.

The accuracy of the runout modeled in Simaltal area was calculated using Cohen's Kappa. The sensitivity analysis was carried out changing debris flow height during accuracy estimation to understand how different thresholds height impacts the performance of a model. This process helps to identify the optimal threshold value that balances sensitivity (true positive rate) and specificity (true negative rate), ultimately improving the model's accuracy. Map obtained using observed precipitation in the Simaltal area that resulted in maximum Cohen's kappa value is shown in Figure 14. The value of Cohens kappa at various threshold heights is shown in Figure 15. The maximum value of Cohen's Kappa was 0.7453 using the threshold height of 0.45 m. The total runout area obtained using threshold height of 0.45 m is 10,844.91 sq. m.

The actual runout extent was mapped from satellite imagery obtained 3 months after the event. By this time, lower-height debris areas were likely restored by vegetation growth and were therefore not visible in the satellite images, leading to an apparent mismatch if a lower threshold were used. Furthermore, the runout extent above 0.45 m debris height visually matches with the actual debris flow extent of the satellite image. This justifies the selection of threshold height 0.45 m for estimation of Cohens Kappa value.

Figure 11, Satellite image of debris flow at Simaltal triggered by 2010 rainfall from GoogleEarth (2010/11/02).

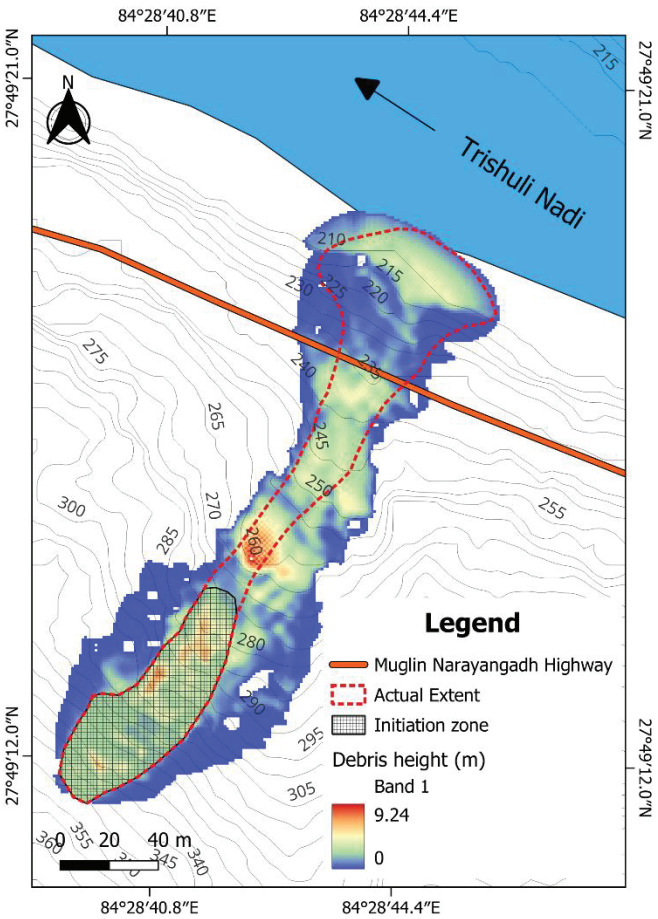

Figure 12, Debris flow runout in Simaltal area obtained from LISEM model considering all range of debris height.

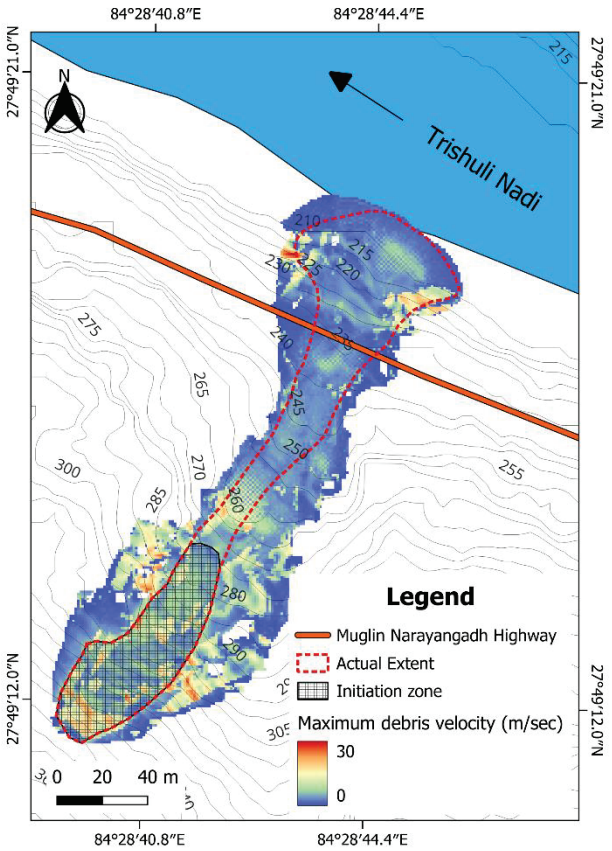

Figure 13, Maximum debris velocity in Simaltal area.

Simulation was also performed in Koyalghari area along Narayangadh-Mugling Highway section. The hollow in the area was modelled for various extreme events based on 23-year rainfall data. The rainfall data of 1-day and 3-day maximum were used to model the runout. Based on the result, the total area of runout for various rainfall events is shown in Table 5. The average debris flow height at the highway due to material from the hollow at various rainfall events are given in Table 6. Among the simulated rainfall, the maximum debris height at highway was 2.3 m for 3-day maximum rainfall of 2006 (Figure 16, Figure 17 and Figure 18).

Table 5, Runout area at highway for various rainfall events

Maximum rainfall	Total runout area (sq. m.) of debris flow for various return period rainfall			
	Actual	5-yrs	10-yrs	25-yrs
1 day	16767.64	16400.77	16419.17	16702.09
3 days	16484.72	15859.10	16081.06	16165.02

Table 6, Average debris height at Highway in Koyalghari area for various rainfall periods

Maximum rainfall	Average debris height (m) at highway for various return period rainfall			
	Actual	5-yrs	10-yrs	25-yrs
1 day	0.9626	0.9266	0.9482	0.9689
3 days	1.1153	0.9563	0.9341	0.9333

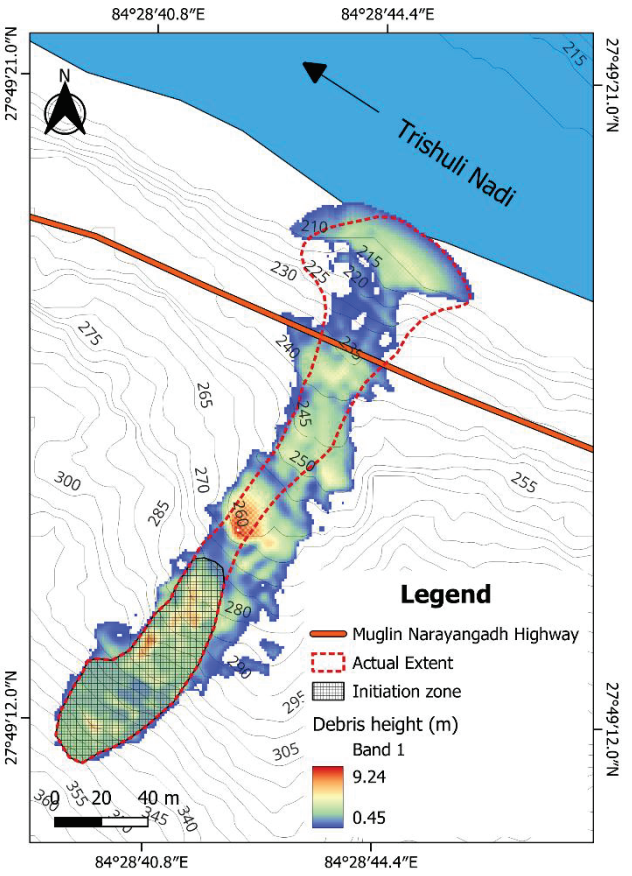

Figure 14, Debris flow runout in Simaltal area for threshold height that results maximum value of Cohens Kappa.

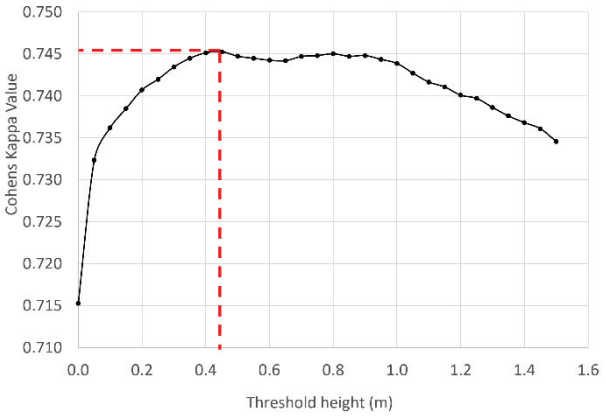

Figure 15, Cohens Kappa value for various threshold heights.

Discussion

Unlike earlier empirical and statistical approaches to debris flow modeling (e.g., Chen and Lee, 2000), which often relied on general observations and simplified assumptions about flow behavior, this study utilized a physically based dynamic model. The integration of geotechnical parameters specific to the local colluvial deposits, such as cohesion, internal friction angle and porosity, allowed for more accurate simulations of debris flow behavior under different rainfall scenarios.

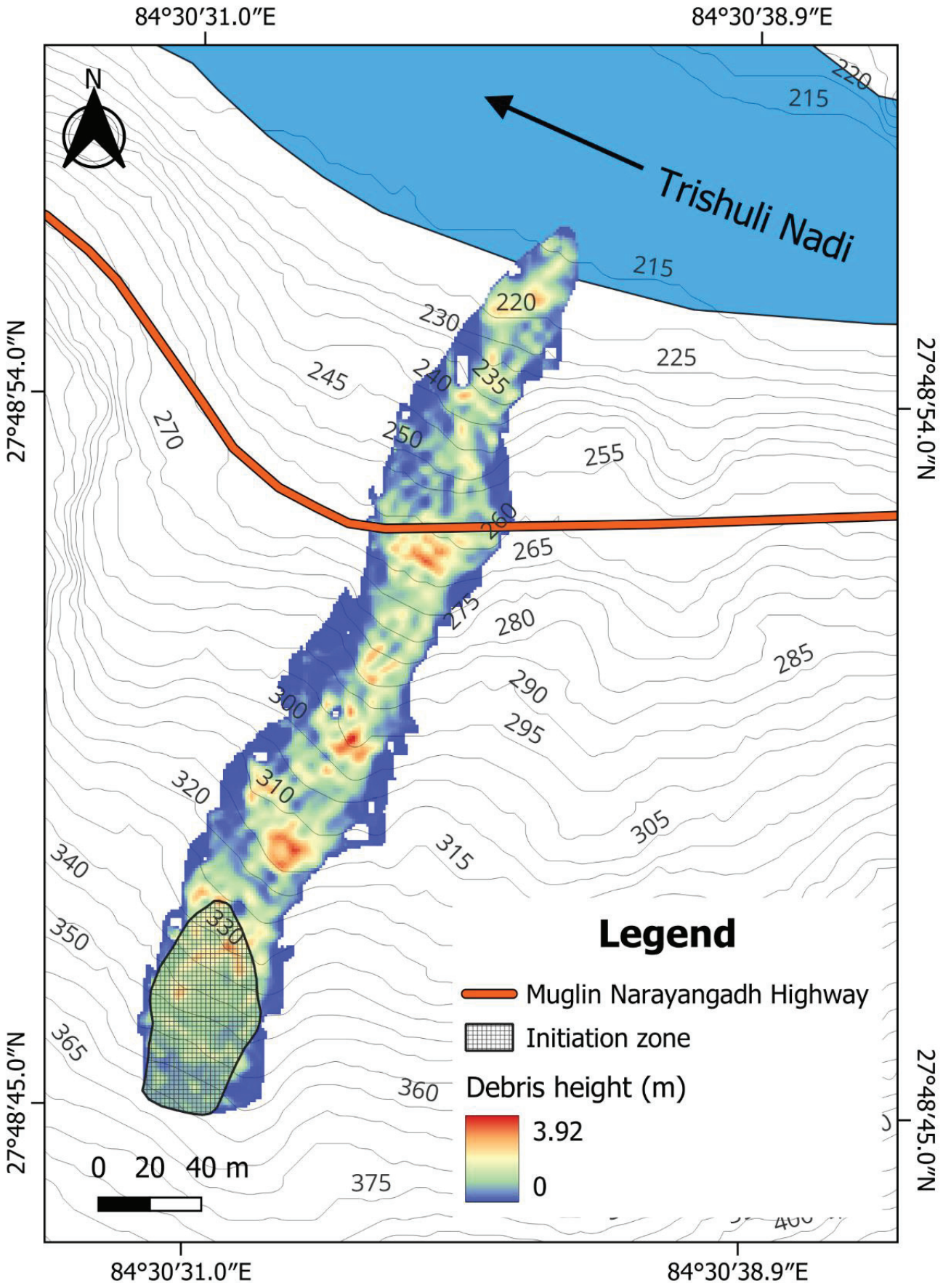

Figure 16, Debris height initiated from Koyalghari area for 3-day maximum rainfall of 2006.

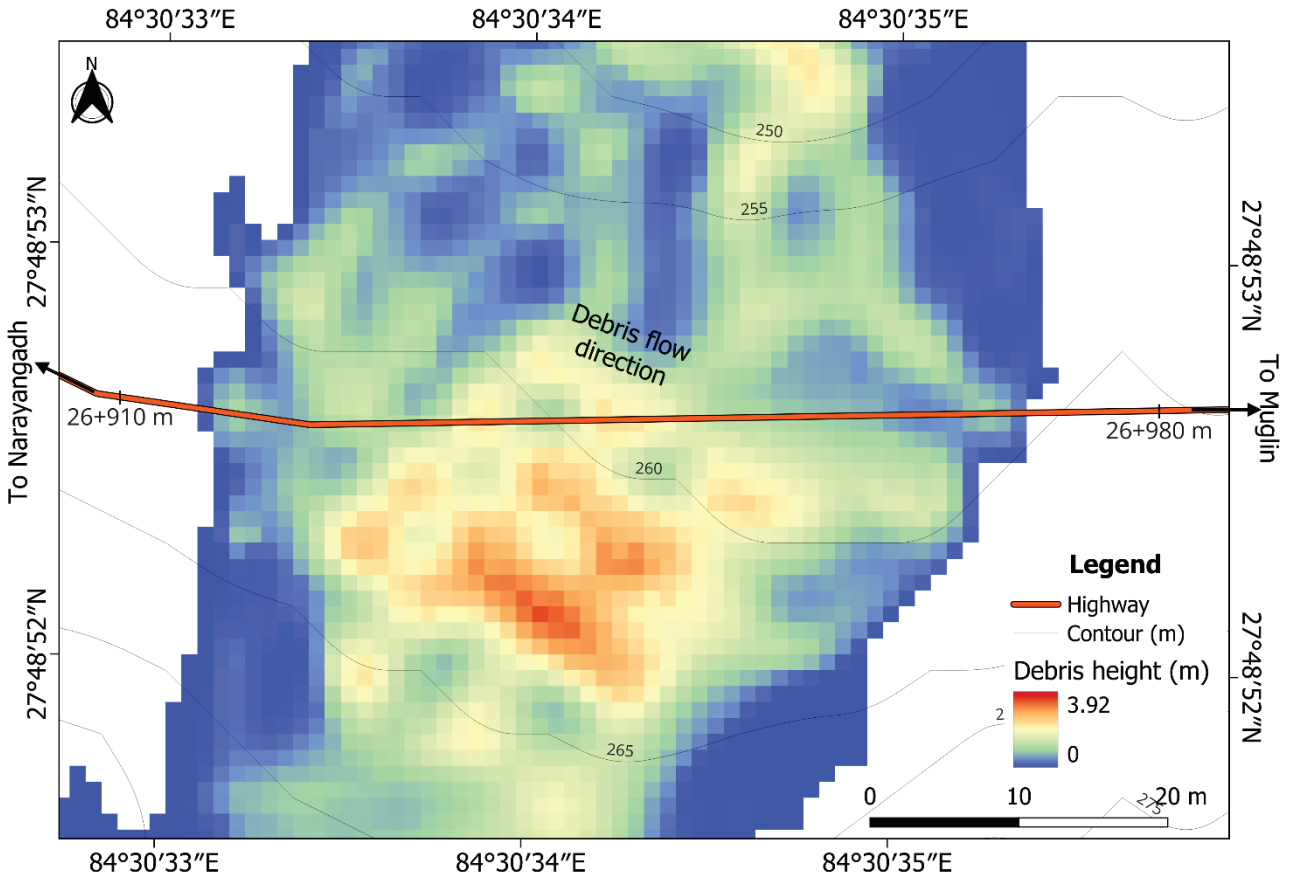

Figure 17, Debris height at Koayalghari area of the Narayangadh-Mugling Highway for 3-day max. rainfall of 2006.

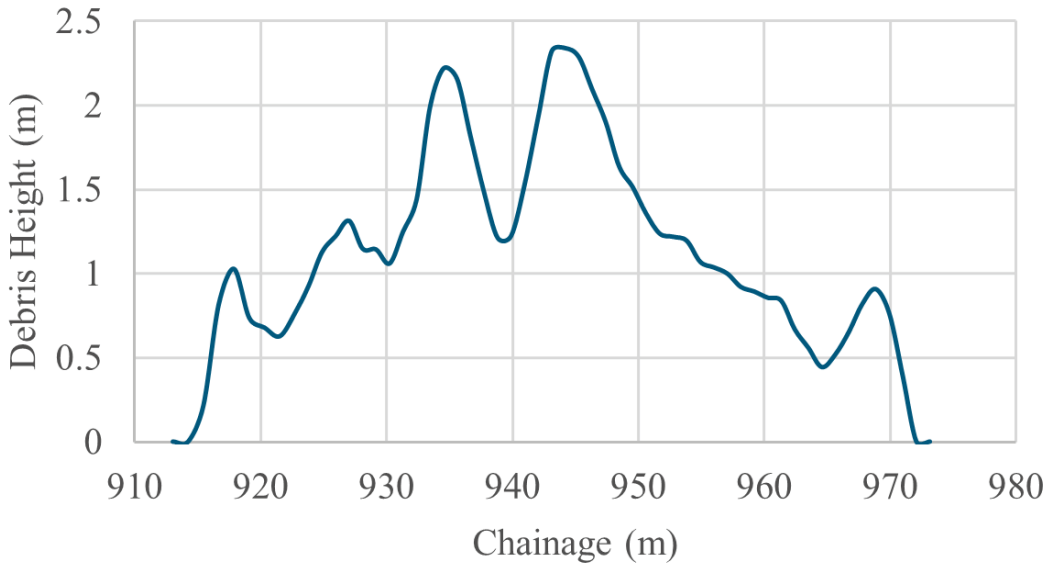

Figure 18, Debris height profile along highway for 3-day max rainfall of 2006 from chainage 26 km+910 m.

This approach is in line with the dynamic modeling method outlined by Pudasaini (2012), but this study takes it further by validating the model with actual historical events in the Simaltal area.

One of the key advancements in this study is the use of Cohen's Kappa for validating model accuracy, which is not commonly applied in debris flow studies. Like the approach used by Rossi et al. (2010) in their assessment of landslide susceptibility models, this validation method demonstrates substantial agreement between simulated and observed runout areas, lending credibility to the model's reliability. Such rigorous validation techniques were not emphasized in earlier debris flow modeling efforts, particularly in the context of the Nepal Himalayas.

While some studies, such as Paudel et al. (2021), have used GIS-based empirical models to assess debris flow runout in Kulekhani watersheds, this research distinguishes itself by using a physically based dynamic model. This approach moves beyond empirical

correlations and offers a more robust tool for hazard management in a geologically complex and dynamic environment like the Lesser Himalaya Sequence. By demonstrating a substantial agreement with historical runout patterns using Cohen's kappa, the findings support the application of advanced physically based models for hazard assessment in landslide-prone regions in Nepal. This is a crucial step toward developing more accurate and proactive early warning systems for critical transportation corridors.

The findings of the study are consistent with and build upon previous research on landslide hazards in the Nepal Himalaya. The significance of high-intensity monsoon rainfall in triggering shallow landslides and debris flows, as observed in the study area, has been well-documented by others, such as Dahal and Hasegawa (2008), who established representative rainfall thresholds for landslides in the region. The potential for debris flows originating from topographic hollows to travel considerable distances and affect vital infrastructure, like the Narayangadh-Mugling Highway, is a key concern in Nepal. The potential threat to infrastructure demonstrates the need for early warning systems and robust hazard management strategies.

Additionally, the results align with global observations that debris flows triggered by extreme rainfall can cause extensive damage, as described by Jakob and Hungr (2005) and Hungr et al. (2005) in their comprehensive analysis of debris flow hazards. The prediction of debris flows in study area with heights exceeding 1 m during extreme rainfall events shows similar findings of Berti and Simoni (2007) who have documented comparable debris flow heights and runout distances.

This study enhances understanding of debris flow runout modeling by integrating geotechnical parameters into the LISEM model and validating it with historical data. It provides a significant advancement over empirical and statistical methods, which often rely on simplified assumptions and may lack precision when conditions vary from historical observations. However, the model relies on geotechnical parameters like cohesion and the internal friction angle, which introduces a level of uncertainty. These parameters are derived from samples collected in a limited number of locations and may not fully represent the spatial variability of the soil, which can lead to disagreements in the output of the model. Slight variations in the cohesion, internal friction angle, porosity or soil depth alters the rheology of the mixture and volume of debris which thereby affecting the predicted runout extent and height. Similarly, Pudasaini (2012) two-phase flow equations also make certain assumptions about fluid mechanics and solid-water interactions that may not perfectly capture the complex rheology of real-world debris flows, which often include a mixture of fine sediment, large boulders, and entrained woody debris. Further, the capability of models to simulate entrainment and deposition processes, while an improvement over simpler models is still a simplification of highly dynamic natural phenomena.

Compared to earlier works, which either lacked dynamic modeling approaches or omitted crucial validation steps, this research demonstrates importance of incorporating both rainfall and geotechnical factors for accurate hazard prediction. The predicted average debris flow of 0.92 m to 1.1 m at the highway is substantial enough to not only bury highway and block drainage culverts but also to potentially sweep away passing vehicles. The result of the study clearly demonstrated the capacity of these flows to extend beyond the highway and deposit debris at the bank of the Trishuli River. These findings align with global observations that rainfall-triggered debris flows can cause extensive damage and are comparable to documented events in other mountainous regions, which have recorded similar debris flow heights and runout distances. It supports the applicability of physically based models, such as LISEM, in debris flow-prone regions like Nepal, contributing to debris flow hazard assessment and risk mitigation. The use of this physically based model provides a valuable tool for authorities to develop more robust land-use plans and early warning systems to protect vulnerable infrastructure and human life.

Conclusion

The study successfully applied the LISEM model to simulate and estimate debris flow runout in topographic hollow based on debris height at Koyalghari area. The model validation in the Simaltal area demonstrated substantial accuracy and supported the conclusion that physically based models can reliably predict debris flow runout in similar geotechnical and topographical settings. The findings indicate that the debris flow runout encompasses 13.74% of the catchment area that is triggered by 2010 rainfall. The kappa value for validation area ranges from 0.716 (2 m height) to 0.745 (0.45 m height) which shows substantial agreement (Landis and Koch, 1977) with the actual landslide runout. The average debris flow ranges from 0.92 m to 1.12 m for various extreme rainfall events, which shows the risk to infrastructure along the Narayangadh-Mugling Highway. The accuracy shows that this model can serve as a valuable tool for estimating debris flow risks and providing hazard mitigation strategies in mountainous regions of Nepal.

For future studies more refined input data can be integrated, which includes updated geotechnical parameters and high-resolution topographical maps, which help to improve the precision of the model. Additionally, the incorporation of real-time rainfall monitoring data would enhance the predictive capability of early warning systems to protect human lives and infrastructure. Finally, the application of the LISEM model demonstrates its potential for widespread use in debris flow-prone regions to estimate road section affected by the potential debris flow.

Author contributions

Aarikti and Ranjan wrote the manuscript, prepared figures and tables. Both authors reviewed the article.

Data availability

No datasets were generated or analyzed during the current study.

Declarations

The authors declare that they have no known competing financial interests or personal relationships that could have appeared to influence the work reported in this article.

References

Berti, M., and Simoni, A. (2007). Prediction of debris flow inundation areas using empirical mobility relationships. Geomorphology, 90(1–2), 144–161. https://doi.org/10.1016/j.geomorph.2007.01.014

Bout, B., Lombardo, L., van Westen, C. J., and Jetten, V. G. (2018). Integration of two-phase solid fluid equations in a catchment model for flash floods, debris flows and shallow slope failures. Environmental Modelling and Software, 105, 1–16. https://doi.org/10.1016/j.envsoft.2018.03.019

Chen, H., and Lee, C. (2000). Numerical simulation of debris flows. Canadian Geotechnical Journal, 37(1), 146–160. https://doi.org/10.1139/t99-091

Chicco, D., Warrens, M. J., and Jurman, G. (2021). The Matthews correlation coefficient (MCC) is more informative than Cohen's kappa and Brier score in binary classification assessment. IEEE Access, 9, 78368–78381. https://doi.org/10.1109/ACCESS.2021.3084050

Chow, V. T. (1959). Open-channel hydraulics. McGraw-Hill.

Cohen, J. (1960). A coefficient of agreement for nominal scales. Educational and Psychological Measurement, 20(1), 37–46. https://doi.org/10.1177/001316446002000104

Dahal, R. K., and Hasegawa, S. (2008). Representative rainfall thresholds for landslides in the Nepal Himalaya. Geomorphology, 100(3–4), 429–443. https://doi.org/10.1016/j.geomorph.2008.01.014

Das, B. M. (2008). Advanced soil mechanics. Taylor and Francis.

Hungr, O., McDougall, S., and Bovis, M. (2005). Entrainment of material by debris flows. In M. Jakob and O. Hungr (Eds.), Debris-flow hazards and related phenomena (pp. 135–158). Springer.

Hussin, H. Y. (2011). Probabilistic run-out modeling of a debris flow in Barcelonnette, France (Master's thesis). University of Twente, Faculty of Geo-Information and Earth Observation (ITC).

Jakob, M., and Hungr, O. (Eds.). (2005). Debris-flow hazards and related phenomena. Springer. https://doi.org/10.1007/b138657

Landis, J. R., and Koch, G. G. (1977). The measurement of observer agreement for categorical data. Biometrics, 33(1), 159–174. https://doi.org/10.2307/2529310

Paudel, B., Fall, M., and Daneshfar, B. (2021). GIS-based assessment of debris flow runout in Kulekhani Watershed, Nepal. Geotechnical and Geological Engineering, 39, 2755–2775. https://doi.org/10.1007/s10706-021-01678-9

Pudasaini, S. P. (2012). A general two-phase debris flow model. Journal of Geophysical Research: Earth Surface, 117(F3), 1–28. https://doi.org/10.1029/2011JF002186

Quan Luna, B., Blahut, J., Camera, C., van Westen, C., Apuani, T., Jetten, V., and Sterlacchini, S. (2014). Physically based dynamic run-out modelling for quantitative debris flow risk assessment: A case study in Tresenda, northern Italy. Environmental Earth Sciences, 72, 645–661. https://doi.org/10.1007/s12665-013-2989-0

Rossi, M., Guzzetti, F., Reichenbach, P., Mondini, A. C., and Peruccacci, S. (2010). Optimal landslide susceptibility modeling based on multiple forecasts. Geomorphology, 278, 160–175. https://doi.org/10.1016/j.geomorph.2016.11.021

Stöcklin, J., and Bhattarai, K. (1977). Geology of Kathmandu area and Central Mahabharat range: Nepal Himalaya [Unpublished report]. Department of Mines and Geology/UNDP.

Upreti, B. N., and Dhital, M. (1996). Landslide studies and management in Nepal. International Centre for Integrated Mountain Development (ICIMOD).

Research Article DOI: https://doi.org/10.64862/ajeg.2025.201.03 Open Access

Engineering Geological Study and Slope Stability Analysis along the Kanti-Rajpath from Chun Danda to the Simat Khola, Central Nepal

Anjila Babu Malla[1, 2*]

[1]Department of Earth Science, Shimane University, Japan
[2]Geotech Solutions International, Dhobighat, Lalitpur, Nepal

(*Corresponding E-mail: mallaanjila22@gmail.com)

Received: January 09, 2025, Accepted: June 15, 2025

Abstract: **Stability analysis of the cut slope of a road section is necessary to prevent damage to the road and the surrounding environment. The study encompasses engineering geological assessment, the cut and fill slope failure analysis of the road section of the Kanti-Rajpath from Chun Danda to the Simat Khola, Makwanpur. Four different cut and downslope critical slopes were selected to represent the overall road section for stability modeling. Four slopes were chosen based on high cut-angle, lithology and visible slope instability to represent the range of conditions along the alignment. The maximum 1-day monsoon rainfall data was used for seepage modeling using the FEM-based software SEEP/W and stability analysis to calculate the Factor of Safety (FOS) using SLOPE/W software of GeoStudio package. The results indicate that the slope appears to be marginally stable to unstable under the given rainfall condition. Our results indicate FOS values of 0.78–1.9, underscoring the need for drainage and slope-angle control. Approximately 7 km of the 20 km road section, especially at the gully portions which are highly vulnerable, needs to be managed. Since the highway serves a direct connection between the capital and the Terai, slope management of this road section is critical for the nation's economic growth.**

Keywords: ***FEM-based cut slope stability, Kanti Rajpath, Engineering geological map.***

Introduction

Slope failures are widely occurring throughout the world, particularly along the road cut slopes constructed in hilly/mountainous regions often leading to loss of life and property (Sharma et al., 2017; Shrestha, 2021; Singh et al., 2008). Whenever slopes are modified from their natural state for road construction and widening activities, slope instability may occur due to improper modifications (Sarkar et al., 2016). Slope failure can result in the loss of life and property; hence it's important to double-check the requisite slope's stability. Slope geometry, slope material type, strength, hydrological condition, structural discontinuities, lithological and weathering conditions etc. are the different factors which initiate the slope failure. Slope stability analysis simply means to calculate the factor of safety of any slip surface associated with a failing slope and find out the critical failure surface. If the factor of safety (FOS) is greater than 1, it means slope is stable and less than 1 means already failed.

After 1970, stability analysis started to be performed using various software such as GeoStudio, PLAXIS, Slide etc. The most widely used analytical method is the Limit Equilibrium Method-LEM (Anbazhagan, 2017; Jinyu et al., 2010; Kharel and Acharya, 2017) but nowadays the numerical methods (Finite Element Methods-FEM, Finite Difference Method-FDM) have become popular in case of slope stability problems for the prediction of unknown states by solving appropriate governing equations which can predict and control the real slope system. Numerical modeling will simplify the complexity of nature with the sparse data and proper understanding of the analysis.

Recent studies in Nepal have increasingly incorporated more detailed field data, geophysical investigations, and numerical modelling. For example, Shrestha et al. (2023) used 2D-ERT and lab tests to model cut-slopes in the Lesser Himalaya and showed that slope angle reductions or soil-nailing can improve factor of safety substantially. Bhandari et al. (2023) evaluated a 60 m high rock cut slope, showing how discontinuities, groundwater, and seismic loads affect stability. Most commonly the performance of traditional LEM and recent numerical method FEM has been compared and combined to examine the stability of road cut slopes, natural slopes of soft material, post-quake slopes, embankments etc. (Ansari et al., 2020; Burman et al., 2015; Bushira et al., 2018; Dahal et al., 2009; Hammouri et al., 2008; Huo and Zhai, 2012; Kumala, 2015; Lim et al., 2017; Wang et al., 2013). In Nepal, rainfall is the major triggering factor for the roadside slope failures (Dahal et al., 2006). The application of roadside cut slope stability assessment can help minimize failures caused by slope modifications (Lee et al., 2009). However, there remains a gap in applying these more advanced methods to many of Nepal's alternative or less-studied routes (such as Kanti-Rajpath), especially for engineering geological

mapping combined with FEM-based modelling across full road sections.

Kanti Rajpath is an alternative route that connects Capital city Kathmandu to Terai region of Nepal. In 1959, the late King Mahendra came to Kathmandu from Hetauda on his own taxi, but now it is challenging task for taxis also to go smoothly through this road section due to the problem of landslides, slope instability, road cracks and water runoff (Figure 1). Makwanpur Gadhi is a potential place for tourism in Makwanpur district, and it is very difficult nowadays to reach that place from the capital.

The research site is a road section of the Kanti-Rajpath from Chun Danda Road junction to the Simat Khola bridge, Thingan, Makwanpur District of Central Nepal (Figure 2). The research aims to prepare a detailed engineering geological map along the road section and highlight the current slope stability situation of the Kanti-Rajpath and identify required mitigating measures for stable slopes. This paper includes the FEM based stability analysis and engineering geological mapping of the road section of Kanti Rajpath to present the stability condition of that section.

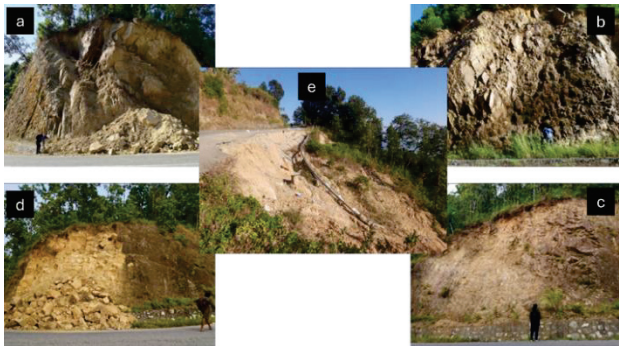

Figure 1, Representative slope conditions along the selected road section; a) Rockfall at Jitpur Bhanjyan, b) Joint sets at Taplakhar, c) Slope condition at Shikhar Kateri, d) Rock fall at Shikhar Kateri and e) Down slope failure at Bar Bhanjyan.

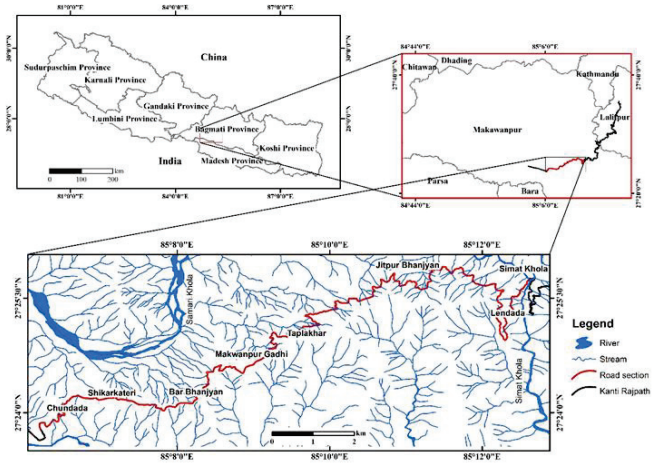

Figure 2, Location map of the study area.

Geological setting

Geologically, the stretch of road section of the Kanti-Rajpath belongs to the Siwalik, comprising sedimentary rocks such as mudstone, sandstone to pebbly sandstone and conglomerate. The Siwalik is the youngest southernmost Himalaya zone which is bounded by the Main Boundary Thrust in the north and the Main Frontal Thrust in the south. It is overlain on the plain of Indo Gangetic Basin in the south. Siwalik is divided into Lower Siwalik, Middle Siwalik, and Upper Siwalik subgroup (Auden, 1935). The stratigraphy of the Siwalik Group at different area of Nepal has also been established (Auden, 1935; Corvinus and Nanda, 1994; Glennie and Ziegler, 1964; Rai and Yoshida, 2020; Tokuoka et al., 1990; Ulak and Nakayama, 1998; Ulak, 2009; Yoshida and Arita, 1982). Ulak and Nakayama (1998) studied the Siwalik Group of Central Nepal and divided into subgroup: the Rapti Formation, the Amlekhgunj Formation, the Churia Khola Formation, and the Churia Mai Formation.

Geomorphology

The road section of the Kanti-Rajpath from Chun Danda to the Simat Khola lies within rugged Siwalik terrain, characterized by moderate to high relief and steeply dissected slopes. Similar to other Siwalik areas of central Nepal, slope angles typically exceed 30˚ to more than 45˚ in cut slopes (Subedi and Tamrakar, 2020). Numerous active gullies incise the road corridor and deliver large sediments during monsoon storms, well documented in nearby Siwalik catchments (Ghimire et al., 2006). Small streams and tributaries drain the slopes causing stream-bank erosion and debris flow during intense rainfall (Ghimire et al., 2013). The alternating beds of sandstone, mudstone and conglomerate typical of the Siwalik further influence erosion and slope instability. This combination of steep slopes, gullies and weak lithology makes the road corridor highly susceptible to failures.

Methods

Field mapping

Engineering geological mapping of the study area was carried out along the cut slopes and downslope sections of the Kanti-Rajpath Highway. All the information about the geological, geomorphological, hydrological, and hydrogeological aspects were incorporated into a 1:10,000 scale engineering geological map. The mapping included lithology, soil type, soil depth, Unified Soil Classification system (USCS soil classification), streams, weathering grade, seepages and landslides. Geological Strength Index (GSI) were determined for the assessment of rock mass quality. GSI value was evaluated using surface condition and structure ratings based on visual field estimation and applied here using the chart established by

(Sonmez and Ulusay, 1999) for a more quantitative numerical basis of strength of Siwalik rocks.

Kinematic analysis

Kinematic analysis of potential rock slope failures was performed on joint data collected from different slopes (T8, T11, T39, T40, T56, T58, T62, T73, T77, T89) along the Kanti-Rajpath Highway (Figure 3). At each site the attitudes (dip amount and dip direction) of all major discontinuity sets were measured using a Brunton compass.

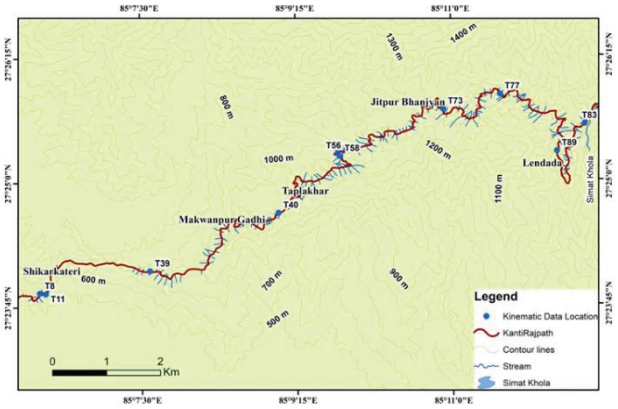

Figure 3, Kinematic data collected location along the study road section.

The discontinuity data were plotted on lower-hemisphere stereographic projections using Dips v6.0 software. In these projections, great circles represent discontinuity planes, and their intersections indicate potential wedge lines. Potential planar, wedge and toppling failures were then evaluated using the failure criteria given by Hoek and Bray (1981).

Slope selection and FEM-based stability modelling

To represent the range of conditions along the road (Figure 4), four representative cut and downslope soil slopes (SS1–SS4: Figure 5, Figure 6, Figure 7, Figure 8) were selected based on slope angle, lithology and visible slope instability and spatial coverage.

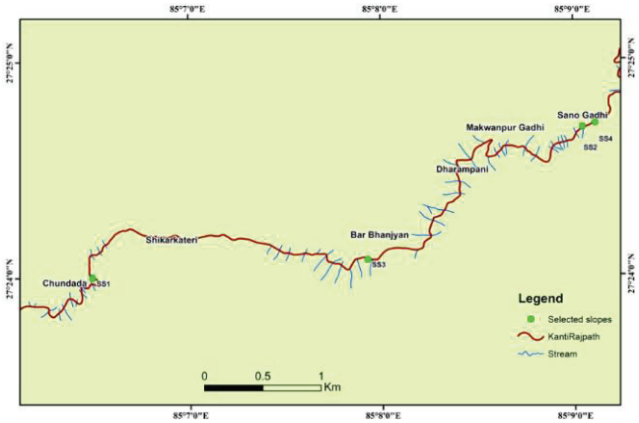

Figure 4, Map showing the locations of selected slopes for stability analysis.

Subsoil samples were collected from landslide (colluvial) material using hand auger, sampler and geological hammer. All soil samples were sealed in airtight plastic bags and labeled with sample number and GPS coordinates. Remolded samples were prepared from disturbed material; no intact cores were recovered. The samples were tested in the laboratory following ASTM standards: grain size analysis by sieve and hydrometer (ASTM D422), Atterberg limits (ASTM D4318), and direct shear tests (ASTM D3080). Direct shear tests were conducted on remolded soil specimens at normal loads of 19, 38 and 76 kPa with a displacement rate of 0.5-1.0 mm/min.

Figure 5, Slope SS1.

Figure 6, Slope SS2.

Figure 7, Slope SS3.

Figure 8, Slope SS4.

Slope stability analysis was performed using FEM based stability analysis in GeoStudio 2021. GeoStudio is a coupled hydrological slope stability model in which both SEEP/W and SLOPE/W are collectively used for simulation. SEEP/W is a FEM based program in GeoStudio which simulates the distribution of pore water pressure (PWP) in the slopes. To predict the porewater pressure developed due to the rainfall infiltration, hydrological models have been used widely. SEEP/W uses a numerical discretization technique to solve Darcy's equations for unsaturated and saturated flow conditions and runs the following water-flow governing equation in each time step to compute two-dimensional seepage (Eq. 1).

$$\frac{dy}{dx}\left(K_x \frac{dH}{dx}\right) + \frac{d}{dy}\left(K_y \frac{dH}{dy}\right) + q = m_w^2 \rho_w \frac{dH}{dt} \quad (1)$$

Where,

K_x, K_y is the coefficient of permeability in x-direction and y-direction,

H is the hydraulic head or total head,

q is the applied flux at the boundary,

m_w is the slope of the soil-water characteristic curve, and

ρ_w is the unit weight of water.

For the seepage analysis, it is needed to provide permeability function, the characteristic curve of soil-water, boundary flux and water table to define the slope problem.

The geometry of slope was obtained by ranging rod for profile and compass bearing survey for boundary. These obtained geometries were sketched on the geo-slope blank document to proceed with the modeling. The interface of soil and rock surface was drawn as per the slip surface observed in the field. The thickness of the colluvium soil layers was selected as per the field observation. The measured hill slope and cut slope angle were used for modeling. Contact between soil and rock was geometrically planar, having soil layers parallel to the ground surface. The hydraulic conductivity functions and volumetric water content functions were defined as per the lab and field test data of grain size distributions of colluvial soil. The boundary conditions used are the null flux to the upslope and interface of soil and rock, null flux with potential seepage face on the downslope, and rainfall with potential seepage face along the slope face. Water tables are considered at the boundary of soil and rock. After defining all these, the modeling was run.

The Morgenstern-Price (1965) method was used to calculate the FOS. It satisfies both the force and moment equilibrium, so can be applied to any kind of slip. The result of transient seepage analysis can be used as the parent analysis for the stability analysis through SLOPE/W with the definition of material (Mohr-Coulomb model) and entry and exit of the slip surface because SLOPE/W lacks the dynamic modeling of pore water pressure.

Results

The study road section from Chun Danda to Simat Khola lies in the Siwalik Zone of Central Nepal and comprised the Lower Siwalik Formation, Middle Siwalik Formation (Lower Middle Siwalik and Upper Middle Siwalik member) of Siwalik in Central Nepal. The Lower Siwalik comprises variegated mudstone, shales interbedded with thinly bedded fine grained sandstone. The lower Middle Siwalik (MS1) consists of moderately thick beds of medium-grained sandstone interbedded with "pepper and salt" textured medium-grained sandstone. The upper Middle Siwalik (MS2) consists of interbeds of medium-grained sandstone, calcareous mudstone with a moderately thick bed of pebbly sandstone with moderate weathering (Table 1). Weathering and lithological variations strongly influence the engineering behavior of the slopes along the road.

Table 1, Siwalik lithostratigraphy of the study region.

Formation/Member	Lithology	Grain size
Upper Middle Siwalik (MS2)	Medium-grained sandstone, calcareous mudstone with pebbly sandstone	Sand-gravel
Lower Middle Siwalik (MS1)	Moderately thick medium-grained sandstone interbedded with "pepper and salt" sandstone	Sand
Lower Siwalik	Variegated mudstone & shale with thin fine-grained sandstone	Clay-silt

Engineering geology of the road section

The engineering geological mapping of the 20 km road section includes lithology, soil type, soil classification, weathering pattern, the presence of gullies and seepages, and slope failures, along with mass strength indices. The 1:10,000 scale engineering geological map (Figure 9) shows lithology, soil classification, weathering pattern, gullies, seepages, slope failures with corresponding GSI values.

The mapped terrain is rugged, with moderate to high relief, steep slopes (20°–70°), and deeply incised gullies. Residual soil depth ranges from <1 m in fresh Lower Siwalik to 1–1.5 m in highly weathered MS1 sandstone. Small landslides (<30 m) occur in the lower section, while larger failures are observed near Bar Bhanjyan, Gadhi, Jitpur Bhanjyan, and Gairigau. Wide road cuts, steep slopes, and weak lithology are the main engineering challenges for this road section.

Kinematic analysis

Lower-hemisphere stereographic projections show three main joint sets within the Siwalik rocks along the study section (Table 2). The plotted data of slopes revealed wedge failure is the most common potential mode at most sites (up to 56.7 % at T77), followed by plane failure (up to 30 %) and toppling (generally <25 %).

Table 2, Joint sets and potential failure modes.

Site	J1 (°/°)	J2 (°/°)	J3 (°/°)	Plane (%)	Wedge (%)	Toppling (%)
T8	345/55	105/68	125/60	28.0	51.2	24.6
T11	350/60	116/30	240/73	3.3	26.3	5.8
T39	050/20	195/65	290/88	18.5	31.7	20.3
T40	070/35	190/65	275/75	0.0	9.3	4.6
T56	350/35	190/75	268/75	30.0	37.9	3.5
T58	340/25	216/83	155/78	16.7	37.1	2.3
T62	345/25	265/80	170/80	5.4	14.3	5.1
T73	010/55	100/72	195/85	14	21.3	4.5
T77	010/50	105/70	270/66	24.0	56.7	3.7
T89	004/36	090/78	130/71	0.0	1.9	8.6

Slope condition and stability modelling

Slope material of SS1 (cut slope) and SS3 (down slope) consist of clay to very fine sand, representing moderately weathered Lower and Lower Middle Siwalik slopes. SS2 (cut slope) and SS4 (down slope) comprise sandy sediments, representing highly weathered Lower Middle Siwalik slopes with "pepper and salt" texture (Table 3).

The maximum 1-day annual rainfall from Makwanpur Gadhi station (2010–2020) was used for modeling. The rainfall was applied in 240-time steps of 6-minute intensity to simulate transient seepage using SEEP/W (GeoStudio). The results were used as input for slope stability analysis in SLOPE/W, where the Mohr-Coulomb failure model was applied, and entry and exit points of the slip surface were defined manually due to SLOPE/W's limitations in modeling dynamic pore pressures. The slope profiles and stability results are shown in Figure 10, Figure 11, Figure 12 and Figure 13.

The parameters required for stability analysis, including unit weight, cohesion, internal friction angle, and saturated water content of each soil layer, are presented in Table 4.

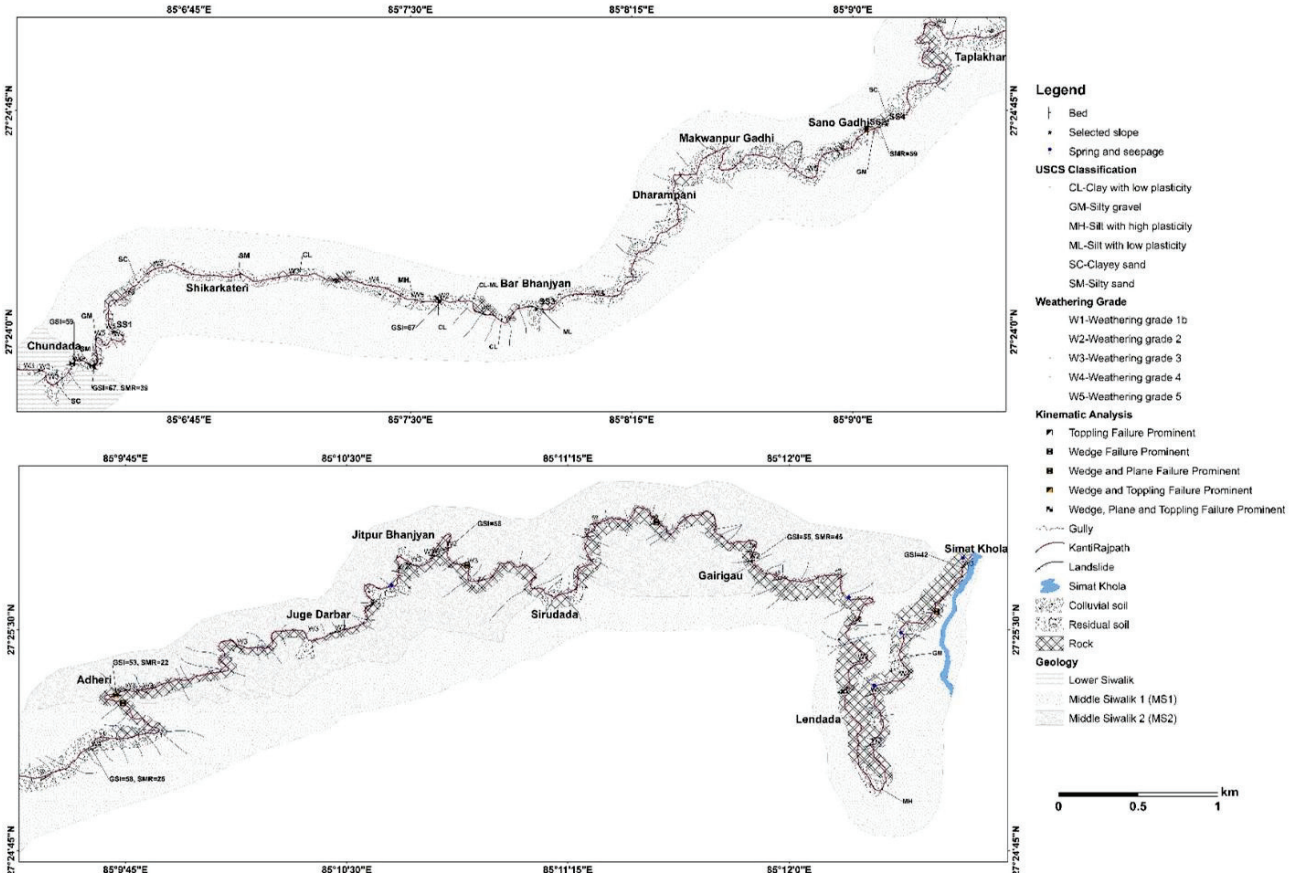

Figure 9, Engineering geological map of the study area.

Table 3, Summary of key parameters of selected slopes.

Slope ID	Location	Slope Type	Height (m)	Soil Type
SS1	Chundanda	Cut slope	10–15	Clay to very fine sand
SS2	Gadhi Bazaar	Cut slope	25	Sandy sediments
SS3	Bar Bhanjyan	Downslope	32	Clay to very fine sand
SS4	Gadhi Bazaar	Downslope	70	Sandy sediments

Table 4, Data used for slope stability analysis.

Layers	Cohesion (kN/m^2)	Frictional angle (°)	Unit weight (kN/m^3)	Liquid limit	Saturated Water Content
SS-1a	32.55	17	19.306	32.47	0.38
SS-1b	4.58	38	15.386	44.41	0.43
SS-1c	5.96	36	17.542	34.28	0.43
SS-1d	2.12	33	16.464	17.42	0.46
SS-2	5.33	29	16.85	17.24	0.43
SS-3	3.69	39	15.19	33.41	0.46
SS-4	11.7	25	16.95	18.13	0.43

The maximum 1-day annual monsoon rainfall of Makwanpur Gadhi station (2010-2020) was modeled in the simulation. The monsoon rainfall event of 1 day maximum was divided into 240 steps of 6-minute intensity and seepage into the soil was simulated using SEEP/W, GeoStudio. FEM-based transient seepage and stability modeling of four representative slopes under 1-day maximum rainfall showed FOS ranging from 0.78 to 1.946. Small cut slopes like SS1 (Chun Danda) were stable (FOS = 1.8), while steep cut slopes and tall downslope failures like SS2 (Gadhi Bazaar, FOS = 0.814) and SS4 (Gadhi Bazaar, FOS = 0.78) were unstable. Maximum pore pressures ranged from 2.03 to 5.39 kPa. The slope profiles with their stability analysis results are shown in Figure 10, Figure 11, Figure 12 and Figure 13.

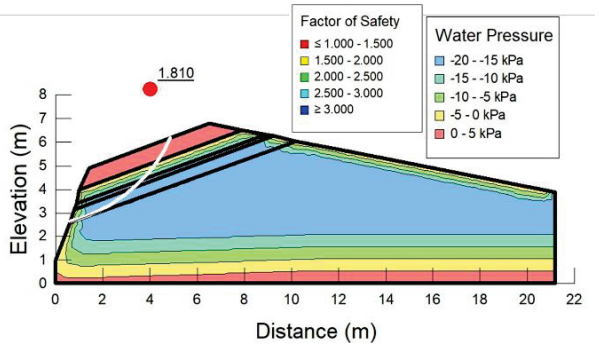

Figure 10, Stability analysis of SS1.

Discussion

Slope failures in the Siwalik region are widely reported due to the combination of weak lithology, steep slopes, and intense monsoonal rainfall. Road-cut slopes are particularly vulnerable as excavation alters the natural slope geometry, reduces stability and increases susceptibility to rainfall-induced landslides.

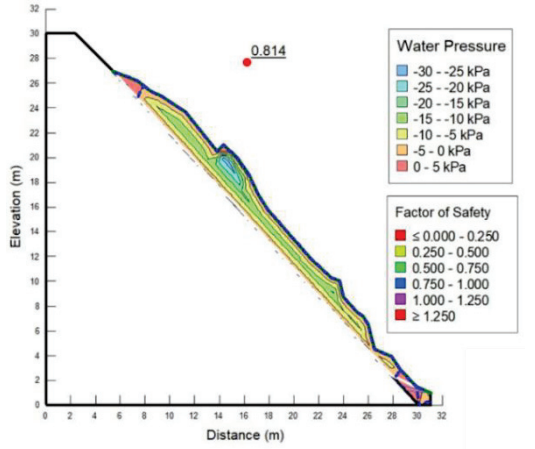

Figure 11, Stability analysis of SS2.

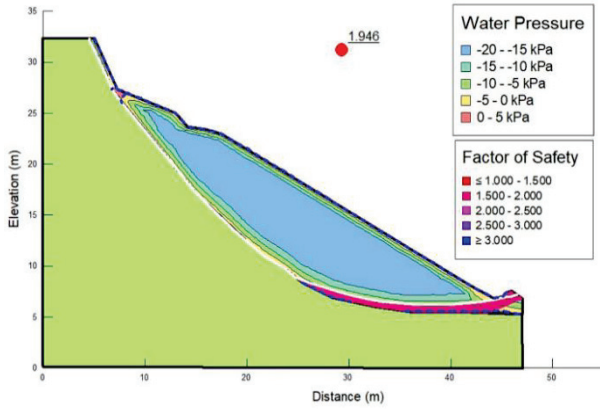

Figure 12, Stability analysis of SS3.

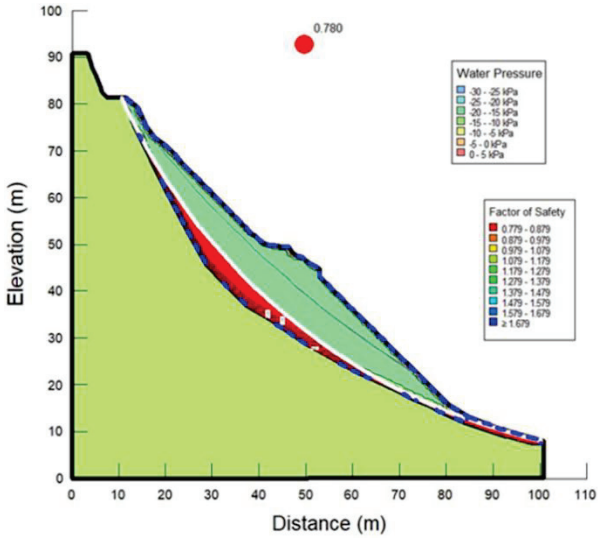

Figure 13, Stability analysis of SS4.

The computed FOS values (0.78-1.95) along the Kanti-Rajpath align closely with findings from other Himalayan studies. Ansari et al. (2020) reported FOS 0.7-1.8 for Lesser Himalaya road cuts, Sharma et al. (2017) observed similar instabilities in unconsolidated hill slopes in India, and Dahal et al. (2006) identified rainfall infiltration as the dominant trigger for slope failures. This comparison underscores that Siwalik road-cut slopes are highly sensitive to rainfall, lithology and slope geometry.

This study is novel in combining detailed engineering geological mapping with FEM-based transient seepage modeling. This integrated approach allows identification of high-risk slopes, quantification of rainfall-induced pore pressures, and understanding of failure mechanisms, particularly wedge-dominated failures. The results provide practical guidance for slope stabilization, including slope-angle optimization, drainage improvement, and reinforcement of weak lithologies. This approach is directly applicable for landslide mitigation and road maintenance in Siwalik terrains.

Conclusion

The following conclusions are drawn exclusively from this study.

- The lower and Middle Siwalik slopes, particularly the lower Middle Siwalik contain thick weathered sandy soils, contributing to slope instability.
- FEM-based slope stability analysis under 1-day maximum rainfall shows FPS value ranging from 0.78 to 1.946, indicating slopes are unstable to marginally stable.
- Approximately 7 km of the 20 km road section exhibit stability issues, including rockfall, circular failures, and planar sliding, especially near Chun Danda, Bar Bhanjyan, Gadhi, Jitpur Bhanjyan and Gairigau.
- Avoid vertical or very steep cut slopes to reduce risk of failure
- Implement drainage, optimize slope angles and use retaining structures where needed.
- Monitor the vulnerable slopes, especially in gully areas.
- Integrate engineering geological mapping and slope stability assessment into future road planning in the Siwalik terrains.

Author contributions

Anjla wrote the manuscript, prepared the figures, and revised the article. She is the sole author.

Data availability

No datasets were generated or analyzed during the current study.

Declarations

The author declare that she has no known competing financial interests or personal relationships that could have appeared to influence the work reported in this article.

References

Anbazhagan, S., Ramesh, V., and Saranaathan, S. E. (2017). Cut slope stability assessment along Ghat road section of Kolli Hills, India. Natural Hazards, 86(3), 1081–1104. https://doi.org/10.1007/s11069-016-2731-0

Ansari, T. A., Singh, K. H., Singh, T. N., and Tripathi, J. N. (2020). Stability analysis of road cut slope near Devprayag in Lesser Himalaya, India. Journal of Earth System Science, 129(1), 132. https://doi.org/10.1007/s12040-020-01394-0

Auden, J. B. (1935). Traverses in the Himalayan. In Records of the Geological Survey of India (Vol. 69, pp. 123–167).

Bhandari, K., Panthi, K. K., and Basnet, C. B. (2023). Stability assessment of desander cut slope of Seti Khola hydropower project. Journal of Nepal Geological Society, 65, 57–62. https://doi.org/10.3126/jngs.v65i01.57747

Burman, A., Acharya, S., Sahay, R., and Maity, D. (2015). A comparative study of slope stability analysis using traditional limit equilibrium method and finite element method. Asian Journal of Civil Engineering, 16, 467–492.

Bushira, K. M., Gebregiorgis, Y. B., Verma, R. K., and Sheng, Z. (2018). Cut soil slope stability analysis along national highway at Wozeka–Gidole road, Ethiopia. Modeling Earth Systems and Environment, 4(2), 591–600. https://doi.org/10.1007/s40808-018-0465-6

Corvinus, G., and Nanda, A. C. (1994). Stratigraphy and palaeontology of the Siwalik Group of Surai Khola and Rato Khola in Nepal. Neues Jahrbuch für Geologie und Paläontologie - Abhandlungen, 191(1), 25–68. https://doi.org/10.1127/njgpa/191/1994/25

Dahal, R., Hasegawa, S., Masuda, T., and Yamanaka, M. (2006). Roadside slope failures in Nepal during torrential rainfall and their mitigation. In Disaster Mitigation of Debris Flow, Slope Failures and Landslides (Interpraevent 2007) (Vol. 2).

Dahal, R. K., Hasegawa, S., Yamanaka, M., Dhakal, S., Bhandary, N. P., and Yatabe, R. (2009). Comparative analysis of contributing parameters for rainfall-triggered landslides in the Lesser Himalaya of Nepal. Environmental Geology, 58(3), 567–586. https://doi.org/10.1007/s00254-008-1531-6

Ghimire, S., Higaki, D., and Bhattarai, T. (2013). Estimation of soil erosion rates and eroded sediment in a degraded catchment of the Siwalik Hills, Nepal. Land, 2(3), 370–391. https://doi.org/10.3390/land2030370

Ghimire, S. K., Higaki, D., and Bhattarai, T. P. (2006). Gully erosion in the Siwalik Hills, Nepal: Estimation of sediment production from active ephemeral gullies. Earth Surface Processes and Landforms, 31(2), 155–165. https://doi.org/10.1002/esp.1320

Glennie, K. W., and Ziegler, M. A. (1964). The Siwaliks formation of Nepal. In 22nd Session Reports (Vol. 25, pp. 82–95). Delhi.

Hammouri, N. A., Malkawi, A. I. H., and Yamin, M. M. A. (2008). Stability analysis of slopes using the finite element method and limiting equilibrium approach. Bulletin of Engineering Geology and the Environment, 67(4), 471–478. https://doi.org/10.1007/s10064-008-0156-z

Hoek, E., and Bray, J. D. (1981). Rock slope engineering (3rd ed.). CRC Press.

Huo, Y. X., and Zhai, H. F. (2012). The study on slope stability analysis based on finite element method. Advanced Materials Research, 575, 70–74. https://doi.org/10.4028/www.scientific.net/AMR.575.70

Kharel, G., and Acharya, I. P. (2017). Stability analysis of cut-slope: A case study of Kathmandu–Nijghad fast track. In Proceedings of IOE Graduate Conference (Vol. 5, pp. 171–174).

Kumala Sari, P., and Lastiasih, Y. (2015). Slope stability evaluation using limit equilibrium method (LEM) and finite element method (FEM) for Indonesia soft soil.

Lee, L. M., Gofar, N., and Rahardjo, H. (2009). A simple model for preliminary evaluation of rainfall-induced slope instability. Engineering Geology, 108(3–4), 272–285. https://doi.org/10.1016/j.enggeo.2009.06.011

Li, J., Qing, Y., and Maotian, L. (2010). Limit equilibrium analysis of the influence of matric suction on unsaturated soil slope stability. Journal of Convergence Information Technology, 5(10), 167–175. https://doi.org/10.4156/jcit.vol5.issue10.21

Lim, K., Li, A. J., Schmid, A., and Lyamin, A. V. (2017). Slope-stability assessments using finite-element limit-analysis methods. International Journal of Geomechanics, 17(2), 06016017. https://doi.org/10.1061/(ASCE)GM.1943-5622.0000715

Rai, L. K., and Yoshida, K. (2020). Lithostratigraphy of the Siwalik Group along the Muksar Khola section, Siraha–Udayapur District, Eastern Nepal Himalaya. Journal of Nepal Geological Society, 60, 207–224. https://doi.org/10.3126/jngs.v60i0.31275

Sarkar, K., Singh, A. K., Niyogi, A., Behera, P. K., Verma, A. K., and Singh, T. N. (2016). The assessment of slope stability along NH-22 in Rampur–Jhakri area, Himachal Pradesh. Journal of the Geological Society of India, 88(3), 387–393. https://doi.org/10.1007/s12594-016-0500-z

Sharma, L. K., Umrao, R. K., Singh, R., Ahmad, M., and Singh, T. N. (2017). Geotechnical characterization of road cut hill slope forming unconsolidated geo-

materials: A case study. Geotechnical and Geological Engineering, 35(1), 503–515. https://doi.org/10.1007/s10706-016-0093-8

Shrestha, J. K. (2021). Impact of road cuts in slope stability in hilly regions of Nepal. Journal of Advanced College of Engineering and Management, 6, 43–55. https://doi.org/10.3126/jacem.v6i0.38289

Shrestha, K. K., Paudyal, K. R., and Thapa, P. B. (2023). Numerical modelling of cut-slope stability in the Lesser Himalayan terrain of west-central Nepal. Journal of Nepal Geological Society, 66, 75–90. https://doi.org/10.3126/jngs.v66i01.57933

Singh, T. N., Gulati, A., Dontha, L., and Bhardwaj, V. (2008). Evaluating cut slope failure by numerical analysis: A case study. Natural Hazards, 47(2), 263–279. https://doi.org/10.1007/s11069-008-9219-5

Sonmez, H., and Ulusay, R. (1999). Modifications to the Geological Strength Index (GSI) and their applicability to stability of slopes. International Journal of Rock Mechanics and Mining Sciences, 36(6), 743–760. https://doi.org/10.1016/S0148-9062(99)00043-1

Subedi, M., and Tamrakar, N. K. (2020). Fluvial geomorphology and basin development of Karra Khola basin, Hetauda, Central Nepal. Journal of Geological Research, 2(4). https://doi.org/10.30564/jgr.v2i4.2250

Tokuoka, T., Takayasu, K., Yamasaki, H., Tanaka, S., Konomatsu, M., Sah, R. B., and Ray, S. M. (1990). Stratigraphy and geologic structures of the Churia (Siwalik) Group in the Tinau Khola–Binai Khola area, west-central Nepal. Memoirs of the Faculty of Science, Shimane University, 24, 71–88.

Ulak, P. D. (2009). Lithostratigraphy and late Cenozoic fluvial styles of Siwalik Group along Kankai River section, East Nepal Himalaya. Bulletin of the Department of Geology, 12, 63–74. https://doi.org/10.3126/bdg.v12i0.2251

Ulak, P. D., and Nakayama, K. (1998). Lithostratigraphy and evolution of the fluvial style in the Siwalik Group in the Hetauda–Bakiya Khola area, Central Nepal. Bulletin of the Department of Geology, Tribhuvan University, 6, 1–14.

Wang, Q., Yao, L. H., and Zhang, N. (2013). Application study on the stability of Xiufengsi landslide by using limit equilibrium method and finite element method. Advanced Materials Research, 671–674, 180–185. https://doi.org/10.4028/www.scientific.net/AMR.671-674.180

Yoshida, M., and Arita, K. (1982). On the Siwaliks observed along some routes in central Nepal. Journal of Nepal Geological Society, 2, 59–66. https://doi.org/10.3126/jngs.v2i0.36174

Research Article DOI: https://doi.org/10.64862/ajeg.2025.201.04 Open Access

Comprehensive Evaluation and Practical Stabilization of Roadside Rock-Cut Slopes along the Narayangadh–Mugling Highway Section

Shankar Pantha[1*], Manita Timilsina[2] and Kabita Maharjan[2]

[1]KL Dugar Group, Dillibazar, Kathmandu, Nepal
[2]Geotech Solutions International, Dhobighat, Lalitpur, Nepal

(*Corresponding E-mail: panthashankar100@gmail.com)

Received: September 12, 2024, Accepted: June 15, 2025

Abstract: **The Narayangadh–Mugling Highway corridor in Nepal is highly vulnerable to recurrent rock-cut slope failures—including rockslides, rockfalls, toppling, and debris flows—that pose significant risks to life, infrastructure, and transportation. Two representative high-risk slopes were investigated through geological mapping, discontinuity surveys, and slope geometry measurements. Laboratory testing determined rock strength parameters and discontinuity shear strength. Rock mass quality was evaluated using RMR_{basic} and Slope Mass Rating (SMR) systems. Kinematic analysis identified potential planar, wedge, and toppling failures, while numerical modeling with SLIDE 5.0 computed factors of safety (FoS) under existing and remedial conditions. Both slopes were found to be critically unstable under current conditions. Installation of rock anchors at −150° significantly improved stability, while slope re-profiling to 60° (1H:1.73V) further enhanced performance. The combined approach of re-profiling with anchoring was identified as the most economical solution. The study provides practical insights for designing targeted slope stabilization measures, offering guidance for reducing geohazard risks along this critical transportation corridor.**

Keywords: ***Slope stability analysis, Rock anchors, Optimum rock-cut slope angle, Kinematic analysis, RMR_{basic}, SMR.***

Introduction

Slope failures are common along rock-cut slopes in mountainous road corridors, often causing fatalities, injuries, and economic losses (Ahmad and Joshi, 2010; Aleotti and Chowdhury, 1999). These failures may occur as rockslides, rockfalls, topples, debris flows, or combinations thereof (Brunsden et al., 1981; Gerrard, 1994; Owen, 1991; Regmi et al., 2013a, 2013b; Shroder and Bishop, 1998), and their prevention is critical for maintaining transportation infrastructure (Sharma et al., 2013).

Inappropriate excavation techniques, steep cut angles, and blasting-induced vibrations can reduce slope stability by enlarging pre-existing cracks and activating minor faults (Singh et al., 2013; Umrao et al., 2011). In the Himalayas, slope failures are often linked to lithological variability, unfavorable discontinuity orientations, weak overburden, and hydrological influences (Kainthola et al., 2015).

The 36 km Narayangadh–Mugling Highway corridor, a crucial link between the capital and the Terai plains carrying over 90% of consumer goods, industrial raw materials, and fuel (World Bank, 2025), traverses high mountains, rolling hills, and flat terrain. This corridor is highly susceptible to landslides, with frequent rockslides, topples, and debris flows (Khanal and Dahal, 2024), including notable events such as the burial of a police vehicle in 2017 (Onlinekhabar, 2017). Despite these recurrent hazards, existing studies provide limited guidance on site-specific mitigation strategies that integrate geological, geotechnical, and numerical stability analyses.

Rock mass classification systems such as RMR_{basic} (Bieniawski, 1973; Bieniawski, 1976; Bieniawski, 1989) and SMR (Romana, 1985; Romana, 1995) provide quantitative measures of rock quality, while kinematic analysis evaluates planar, wedge, and toppling failure potential based on slope–discontinuity relationships (Goodman, 1995; Goodman, 2000; Haswanto and Abd-Ghani, 2008). Numerical limit equilibrium modeling using SLIDE 5.0 (Rocscience, 2006) enables factors of safety (FoS) computations for complex surfaces, and mitigation measures such as rock anchors and slope re-profiling are commonly applied (Kliche, 1999).

In this study, these tools were applied to two representative high-risk slopes (RS-1 and RS-2) selected through systematic field assessment. Selection criteria included frequent past failures, representative geological and geotechnical conditions (weathered rock, critical discontinuities, weak overburden), proximity to essential road infrastructure, and accessibility for detailed monitoring. These slopes exemplify the failure mechanisms observed throughout the corridor. The study provides a comprehensive evaluation of slope stability, integrating field investigations, laboratory testing, rock mass classification, kinematic analysis, and numerical modeling to develop practical stabilization measures tailored to the corridor's challenging terrain.

Study area

The 36 km Narayangadh–Mugling Highway corridor lies in Chitwan District, central Nepal, spanning 84°25'00"–84°35'E and 27°45'00"–27°52'30"N (Figure 1).

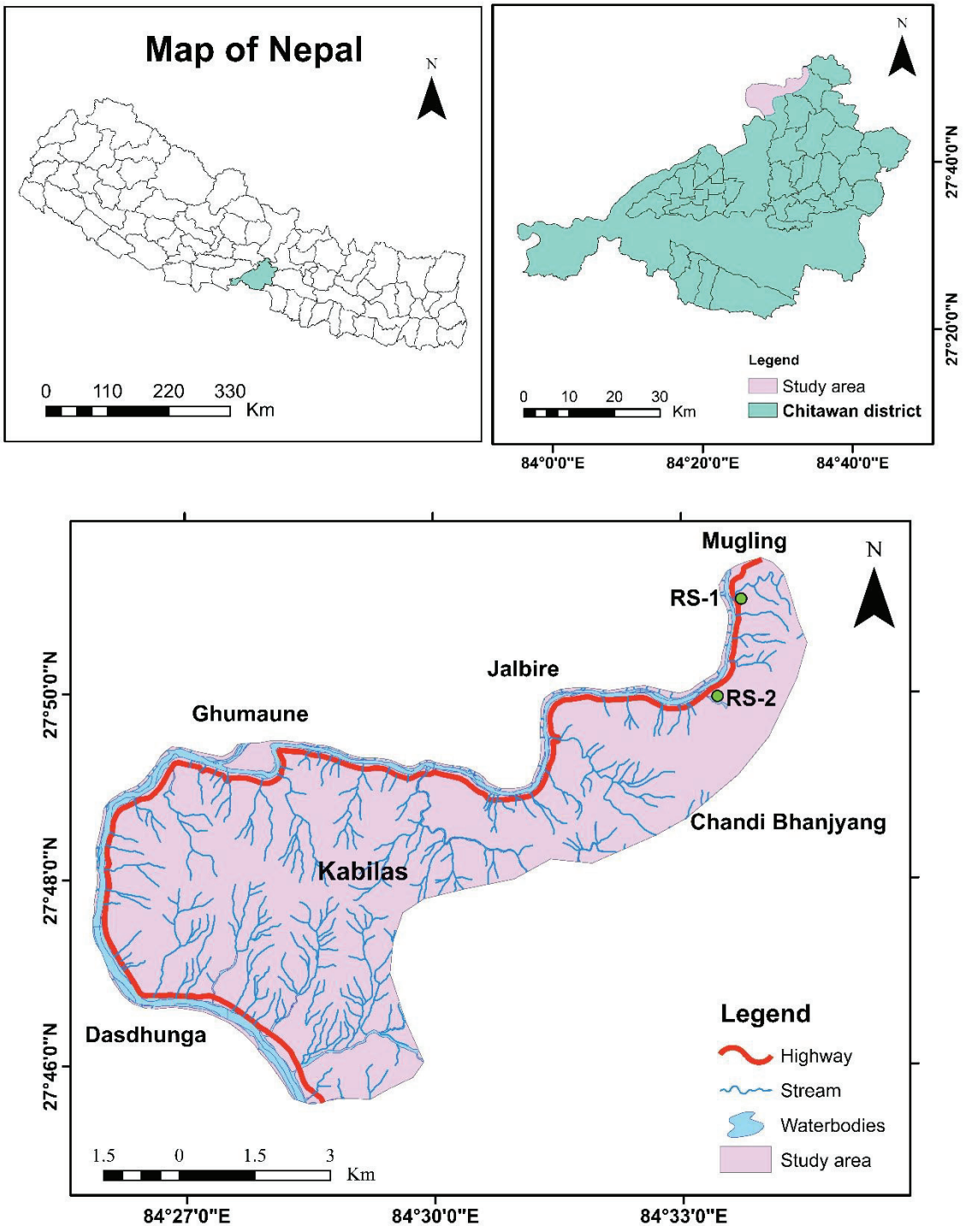

Figure 1, Location map showing the study area within Chitwan District, Central Nepal.

Geological condition

The corridor lies within the Mahabharat Synclinorium, characterized by tightly folded structures, sheared zones, and thrust faults. Lithostratigraphy resembles the Nawakot Complex (Paudyal, 2014) and includes Kuncha, Lower Siwalik, Fagfog Quartzite, Dandagaon Phyllite, Purebensi Quartzite, Amdanda Phyllite, Dhading Dolomite, and Benighat Slate (Figure 2). Dominant rocks are metasandstone, phyllite, dolomite, quartzite, slate, mudstone, sandstone, colluvium soil, and minor greenschist and hematite beds.

Elevations range from ~200 m in river valleys to 500 m along hills. The terrain is rugged, with steep slopes, deeply incised gorges, and variable lithology, creating conditions prone to slope instability.

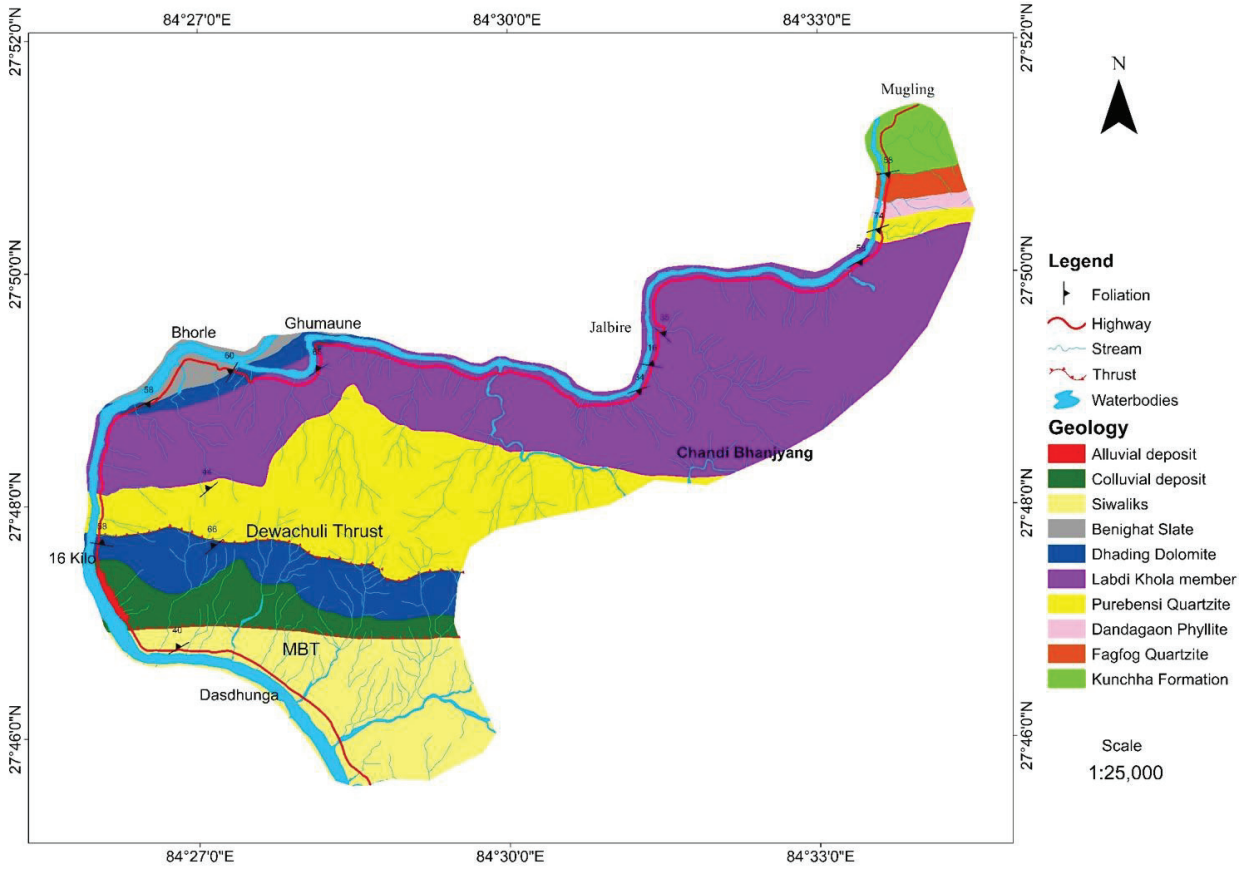

Figure 2, Geological map of the study area along the Narayangadh–Mugling Highway section (modified after Paudyal, 2014).

Methodology

Field investigation

The two slopes, RS-1 and RS-2, were selected as representative high-risk sites based on a combination of field observations and historical data (Figure 3). Field investigations recorded slope geometry, discontinuity characteristics (orientation, spacing, persistence, aperture, infill, weathering), groundwater, and hydrological influences, providing essential input for RMR_{basic}, SMR, and kinematic analyses.

Figure 3, Field photographs of rock-cut slopes

Laboratory testing

Rock samples underwent Point Load Index testing (50 samples) to determine intact rock strength. Results were used to derive cohesion, friction angle, and unit weight.

Data analysis

RMR_{basic}: Based on intact rock strength, RQD, discontinuity spacing/condition, and groundwater (Bieniawski, 1973). Orientation parameters excluded.

$$RQD = 115 - 3.3J_v \qquad (1)$$

$(Jv\ between\ 4-44;\ empirical\ approximation)$

$$SMR = RMR_{basic} + (F1 \times F2 \times F3) + F4 \quad (2)$$

Factors F1-F3 account for slope-discontinuity orientation; F4 accounts for excavation method.

Stability analysis

Stability analyses were conducted using SLIDE 5.0 with the Morgenstern–Price method to evaluate vertical slice equilibrium for both circular and non-circular failure surfaces. Input parameters included unit weight (γ), cohesion (c), friction angle (ϕ), groundwater conditions, and detailed slope geometry. Critical slip surfaces were identified through an automated search algorithm, and rock anchors were modeled considering their length, spacing, orientation, and capacity.

Results and discussion

For detailed analysis, two of the most vulnerable rock-cut slopes along the Narayangadh–Mugling Highway section in the Lesser Himalaya region of central Nepal were selected. The rock masses in this area are heavily jointed, typically exhibiting two to three dominant joint sets. Field investigations thoroughly examined discontinuity characteristics affecting slope stability, including orientation, spacing, persistence, aperture, roughness, infilling, and weathering. These data informed kinematic and limit equilibrium analyses alongside rock mass classification using the Rock Mass Rating (RMR) and Slope Mass Rating (SMR) systems.

Discontinuity spacing, defined as the perpendicular distance between adjacent joints, controls block size and influences permeability and seepage within the rock mass. Measurements of spacing and other discontinuity conditions were carefully recorded and averaged for RMR calculation. Although the study was conducted in the dry season with negligible groundwater presence, seasonal variations may affect hydrological conditions.

Rock mass classification

RMR_{basic} values were computed by summing parameter ratings, classifying both slopes (RS-1 and RS-2) within the fair rock category (Class III) with scores of 58 and 48, respectively. Table 1 summarizes the parameter ratings and classifications for the slopes investigated.

Kinematic analysis

Kinematic analysis of RS-1 and RS-2 demonstrates that slope stability is strongly influenced by the orientation of discontinuities relative to the slope face.

Discontinuity orientation is a critical factor influencing structurally controlled failure modes in jointed rock masses. During field investigations, the relative orientations of slopes and discontinuities were measured and stereographically projected to qualitatively assess whether the orientation adjustment factors are favorable or unfavorable for stability.

Table 1, Rock Mass Rating (RMR_{basic}) values for RS-1 and RS-2

Slopes	RS-1	RS-2
Strength of intact rock (R1)	7	7
RQD	13	8
Spacing of discontinuity (R3)	10	8
Condition of discontinuity (R4)	13	10
Groundwater condition (R5)	15	15
RMR_{basic}	58	48
Class	III	III
Grading	Fair	Fair

The most critical discontinuity set, together with slope face orientation, was used to calculate factorial adjustment factors (F1, F2, and F3). Bieniawski's Rock Mass Rating (RMR), based on RMR_{basic}, was modified to the Slope Mass Rating (SMR) by incorporating these factors. Additionally, excavation-related adjustment factor F4 was determined through detailed visual inspection at each site.

The SMR values accounting for toppling and planar failure modes, slope-discontinuity relationships, and excavation method yielded a classification of fairly stable Class III with an SMR of 50 for RS-1, and unstable Class IV with an SMR of 40 for RS-2 (Table 2).

Table 2, Slope Mass Rating (SMR) values for RS-1 and RS-2 (Failure mode T = Toppling; P = Planar)

Slopes	RS-1		RS-2
Failure	T	W	T
F1*F2*F3	0	0	0
F4	-8	-8	-8
RMR	58	58	48
SMR	50	50	40
Class	III	III	IV
Stability	PS	PS	UN
Probability of failure	0.4	0.4	0.6

RS-1 shows potential for both toppling and wedge failures, while RS-2 is more critically affected, with a higher likelihood of toppling failure. These findings underscore the role of joint set orientation and slope geometry in controlling failure mechanisms and provide a basis for selecting suitable stabilization measures (Figure 4).

Geotechnical properties

The investigated rock slopes show moderate weathering and are primarily composed of slate, phyllite, gritty phyllite, and metasandstone. The rock masses are extensively fractured and jointed, influencing their mechanical behavior. Laboratory point load tests were

conducted to assess the intact rock strength indices for slopes RS-1 and RS-2. Complementary geomechanical parameters, including cohesion and internal friction angles, were derived using the RocLab software (Figure 5). The comprehensive geotechnical properties of both slopes are detailed in Table 3.

Stability analysis and result

A detailed stability assessment of the selected rock slopes was carried out using SLIDE 5.0, applying the Morgenstern and Price method to compute the factor of safety (FoS). This quantitative analysis was complemented by qualitative evaluations using the RMR and SMR classifications, providing a comprehensive understanding of slope stability. Under dry conditions, the FoS values for RS-1 and RS-2 were calculated as 0.96 and 0.81, respectively, both well below the acceptable threshold of 1.0. These results indicate that the slopes are critically unstable, with a high likelihood of failure under existing conditions. Consequently, immediate reinforcement measures and continuous monitoring are essential to mitigate risks and ensure long-term slope safety.

The assessment further reveals that several rock-cut slopes along the Narayangadh–Muglingg road are unstable during the dry season, with failure potentially occurring at any time (Figure 6). The observed and anticipated failure mechanisms include planar sliding along persistent discontinuities, wedge failures at the intersection of joint sets, toppling of isolated blocks, and circular failures associated with weathered rock masses. These instabilities are exacerbated by the presence of highly weathered rock, weak overburden materials, and unfavorable discontinuity orientations, all of which collectively increase the susceptibility of the slopes to failure. Such conditions pose a significant hazard to road safety and highlight the urgent need for systematic stabilization and monitoring measures.

Both qualitative and quantitative approaches consistently indicate marginal stability of the investigated slopes. According to the SMR classification, RS-1 is rated as “Partially Stable,” whereas RS-2 is classified as “Unstable,” in agreement with the low FoS values obtained from the SLIDE analysis. This consistency between empirical classification and numerical modeling confirms that both slopes are highly susceptible to failure under the current conditions.

These results highlight the need for targeted slope stabilization measures. Potential interventions include controlled slope re-profiling to reduce steepness, installation of rock anchors or bolts to enhance cohesion, construction of retaining structures, drainage improvements to limit water-induced weakening, and routine monitoring to detect early signs of instability.

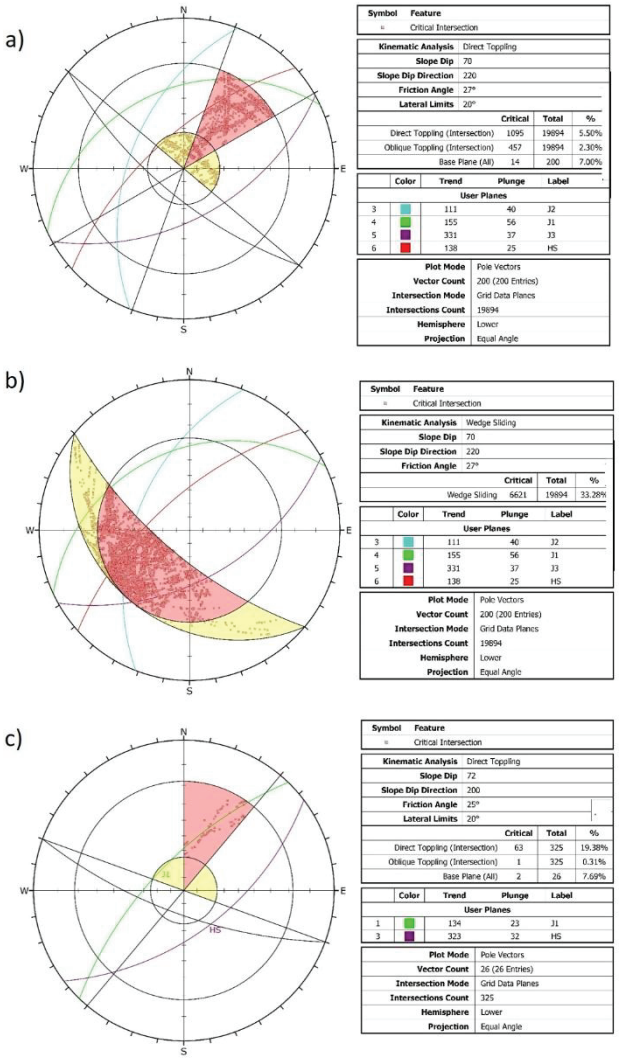

Figure 4, (a) and (b) Kinematic analysis results for slope RS-1 showing toppling and wedge failure modes; (c) Kinematic analysis results for slope RS-2 indicating toppling failure susceptibility

Table 3, Geotechnical properties of slope materials 2

Slopes	RS-1	RS-2
Avg. slope angle (^{O})	70	71
Cohesion (MPa)	0.089	0.077
Friction angle (^{O})	27.09	25.31
Unit weight (KN/m^3)	20	19
Point load strength index (MPa)	3.74	3.38

In this study, the effectiveness of rock anchor installation and slope re-profiling was examined in detail, demonstrating their capability to improve slope stability. Incorporating these measures within a slope-specific risk assessment framework can markedly enhance road safety and reduce both economic and human losses from slope failures. For critical slopes and lifeline structures, such as major highways, dams, railways, and urban slopes, a higher margin of stability is required. Accordingly, the factor of safety (FoS) is typically designed to be greater than 1.5 to account for the potentially severe consequences of failure (Hoek and Bray, 1981; Duncan et al., 2005).

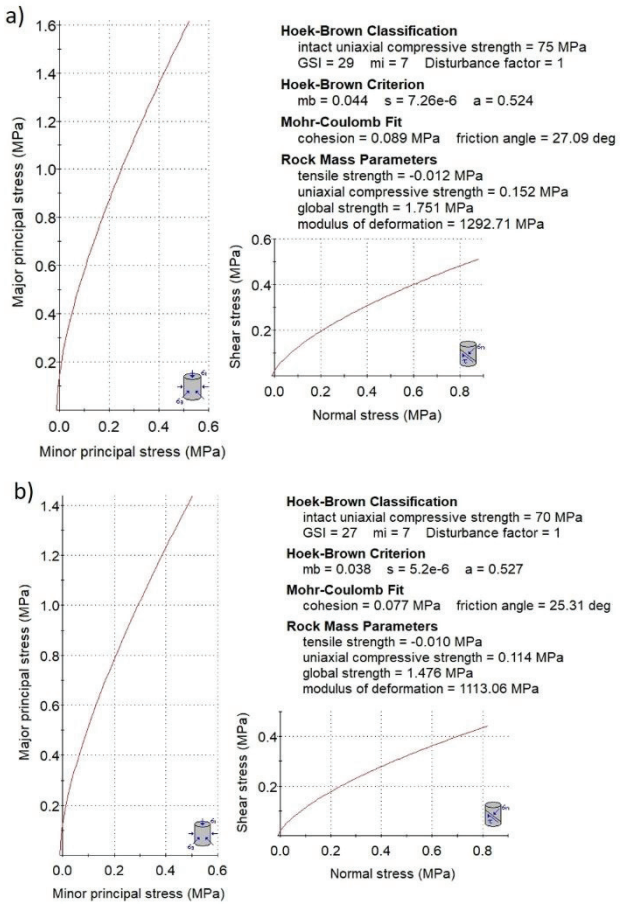

Figure 5, (a) Geomechanical parameters derived for slope RS-1 including cohesion, friction angle, unit weight, and point load strength index; (b) Geomechanical parameters determined for slope RS-2.

Effect of rock anchors on slope stability

The influence of rock anchors on slope stability was analyzed using SLIDE 5.0, with anchor parameters defined in terms of type, length, spacing, orientation, and capacity. The modeled end anchors had lengths of 12 m and 15 m, with capacities of 400 kN and 500 kN. Anchors were spaced at 1 m along the slope, with an out-of-plane spacing of 1 m. They can be installed at inclinations of −90°, −120°, −150°, and −180° relative to the horizontal slope face, where negative angles indicate inclinations measured downward from the horizontal, with larger negative values corresponding to steeper orientations pointing back into the slope. Stability analyses indicated that an installation angle of −150° provided the highest improvement in factor of safety (FoS = 1.55 for RS-1 and 1.53 for RS-2), outperforming other tested orientations (FoS range: 0.46–1.27 for RS-1; 0.39–1.15 for RS-2). Details are shown in Table 4 and Figure 7. This orientation was particularly effective for slopes dipping near 70°, optimizing load transfer and enhancing resistance against potential failure planes. The results align with Baharvand et al. (2015), who reported −150° as the optimal inclination for slopes around 60° and −165° for slopes near 75°.

The required anchor capacities were determined based on the stabilizing forces necessary to achieve the target factor of safety (FoS) calculated in SLIDE. For slope RS-1, anchors were designed with a capacity of 100 kN, reflecting their relatively lower stabilization requirement, while RS-2 required 350 kN anchors due to higher instability. These capacities were verified assuming an anchor FoS greater than 1.8, ensuring that each anchor could adequately resist anticipated loads from potential planar or toppling failure mechanisms. The design considered slope geometry, rock mass strength, and potential failure surfaces, providing sufficient reinforcement without unnecessary overdesign.

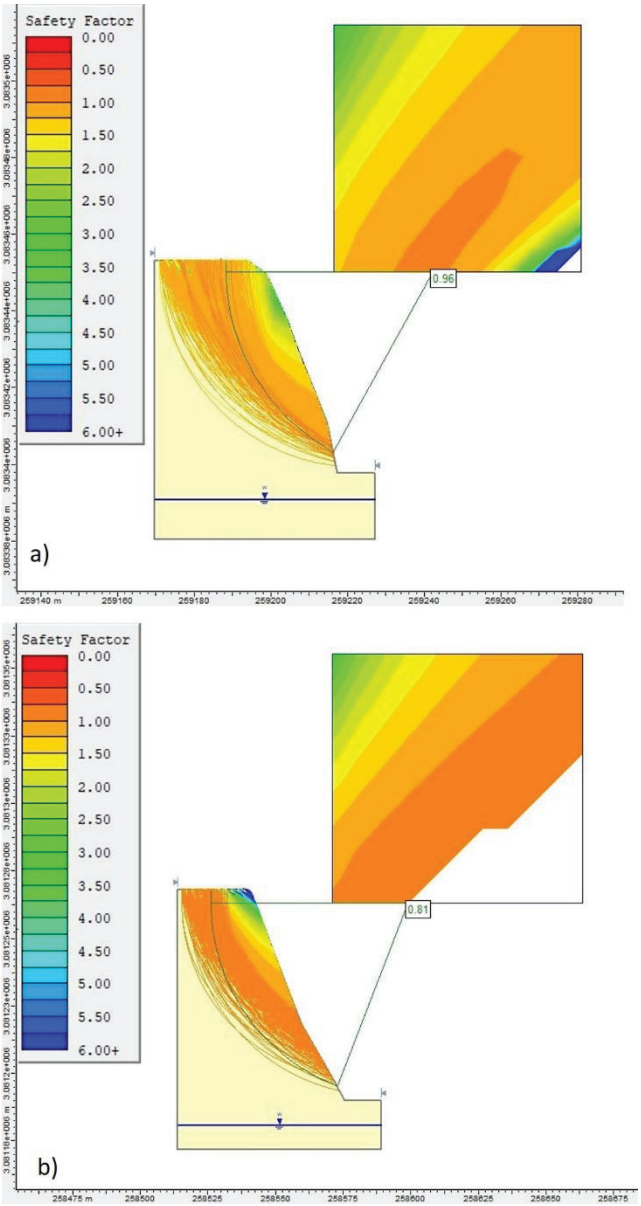

Figure 6, (a) Stability analysis results showing the factor of safety for rock-cut slope RS-1 using SLIDE software; (b) Stability analysis results for rock-cut slope RS-2.

Influence of cut slope angle on rock slope stability

The influence of cut slope angles on stability was analyzed using SLIDE 5.0 by modeling slopes with dip angles of 45°, 50°, 55°, and 60°. Factors of safety (FoS) were computed for each configuration (Table 5). Results

indicate that the 45° bench-cut slope exhibited higher stability compared to the others (Figure 8).

Table 4, Stability results after rock anchor installation

Slopes	RS-1				RS-2			
Anchor type	End anchored				End anchored			
Anchor length (m)	12				15			
Distance between anchors (m)	1				1			
Out-of-plane spacing (m)	1				1			
Anchor capacity (kN)	400				500			
Anchor direction from horizontal (°)	-90	-120	-150	-180	-90	-120	-150	-180
FoS before rock anchor	0.96	0.96	0.96	0.96	0.81	0.81	0.81	0.81
FoS after rock anchor	0.46	1.20	1.55	1.27	0.39	1.01	1.53	1.15

Implementing a 45° slope requires substantially more excavation, increasing construction costs, material handling, and environmental disturbance. Thus, only slope re-profiling is not enough to stable these cut slopes along the Narayangadh-Mugling Road section. But by integrating a 60° slope with strategically designed rock anchors, sufficient stability can be achieved without incurring the high costs and operational challenges associated with a gentler 45° slope.

A qualitative cost–benefit evaluation suggests that a 60° cut slope reinforced with rock anchors achieves an effective balance among safety, constructability, and long-term maintenance requirements (Figure 9; Table 6). For steeper slopes nearing 70°, this design approach optimizes both structural performance and economic efficiency, providing a practical solution for slope stabilization in challenging terrains.

Table 5, Stability results after cut slope reprofiling

Slope	Suitable cut angle (o)	FoS before slope refiling	FoS before slope refiling
RS-1	45 (1H:1V)	0.96	1.7
	50 (1H:1.16V)	0.96	1.57
	55 (1H:1.43V)	0.96	1.48
	60 (1H:1.73V)	0.96	1.39
RS-2	45 (1H:1V)	0.81	1.35
	50 (1H:1.16V)	0.81	1.25
	55 (1H:1.43V)	0.81	1.17
	60 (1H:1.73V)	0.81	1.1

Design life and maintenance considerations

The proposed stabilization measures, particularly rock anchors and slope reprofiling, are expected to achieve a design life of 20–30 years when implemented with adequate corrosion protection and strict quality control. Their long-term performance depends on a structured maintenance program, including periodic anchor head inspections, re-tensioning as required, and routine cleaning and repair of drainage systems. Post-event inspections after intense rainfall or seismic activity are also critical to ensure continued stability. Integrating these maintenance provisions enhances both the durability and cost-effectiveness of the proposed solutions' description.

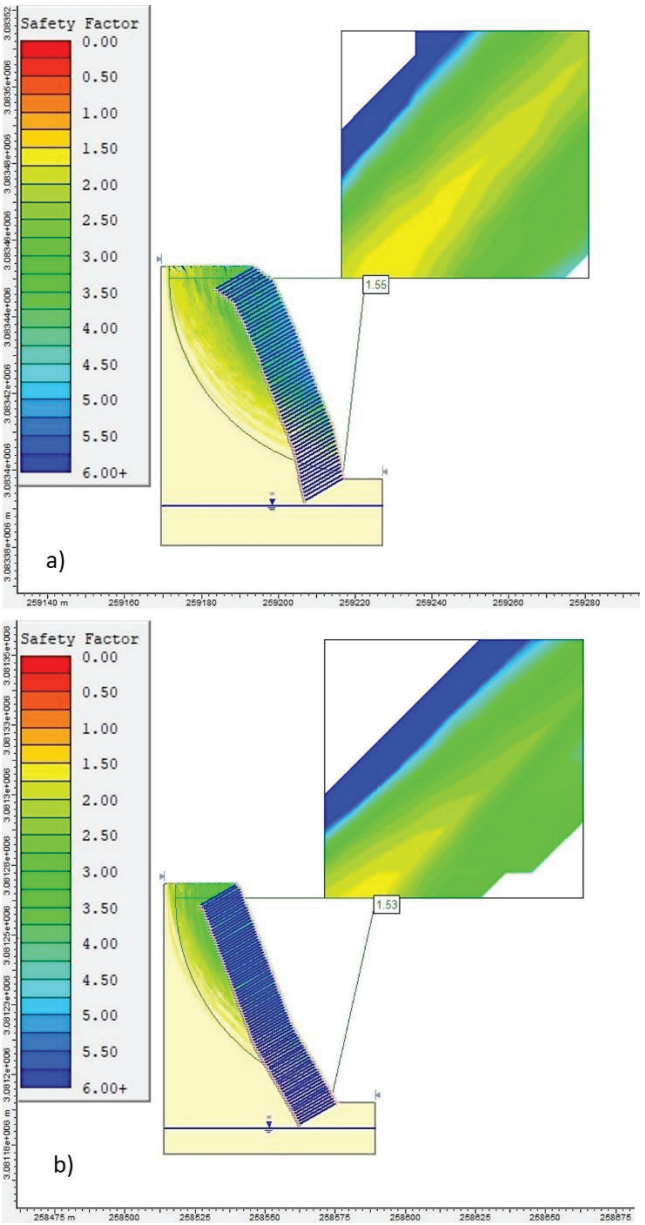

Figure 7, (a) Stability analysis of rock-cut slope RS-1 after installation of rock anchors showing improved factor of safety; (b) Stability analysis of rock-cut slope RS-2 after installation of rock anchors demonstrating enhanced slope stability.

Conclusions

Roadside rock-cut slopes along the Narayangadh–Mugling Highway, central Nepal, are highly susceptible to planar, wedge, toppling, and circular failures. Field investigations and modeling confirm that slopes RS-1 and RS-2 are critically unstable (FoS < 1.0), in agreement with RMR_{basic} and SMR assessments.

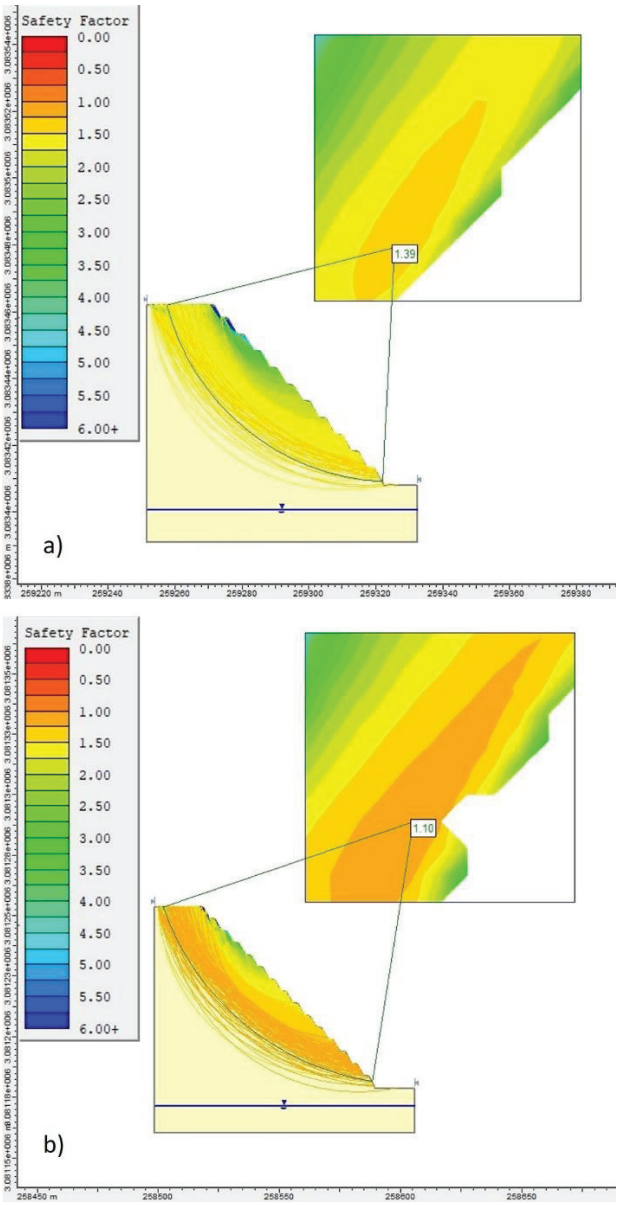

Figure 8, (a) Stability analysis results of rock-cut slope RS- 1 after slope inclination was modified to 60°; (b) Stability analysis results of rock-cut slope RS- 2 after slope inclination was modified to 60° (1H:1V)

Table 6, Stability analysis results after cut slope modification and anchor reinforcement

Slope	RS-1	RS-2
Anchor type	End anchored	End anchored
Anchor length (m)	5	10
Anchor length (m)	8	15
Distance between anchors (m)	1	1
Out-of-plane spacing (m)	1	1
Anchor capacity (KN)	200	300
Anchor direction from horizontal (0)	-150	-150
Slope Re-profiling	60	60
Pre-reprofiling and anchor FoS	0.96	0.81
Post-reprofiling and anchor FoS	1.56	1.51

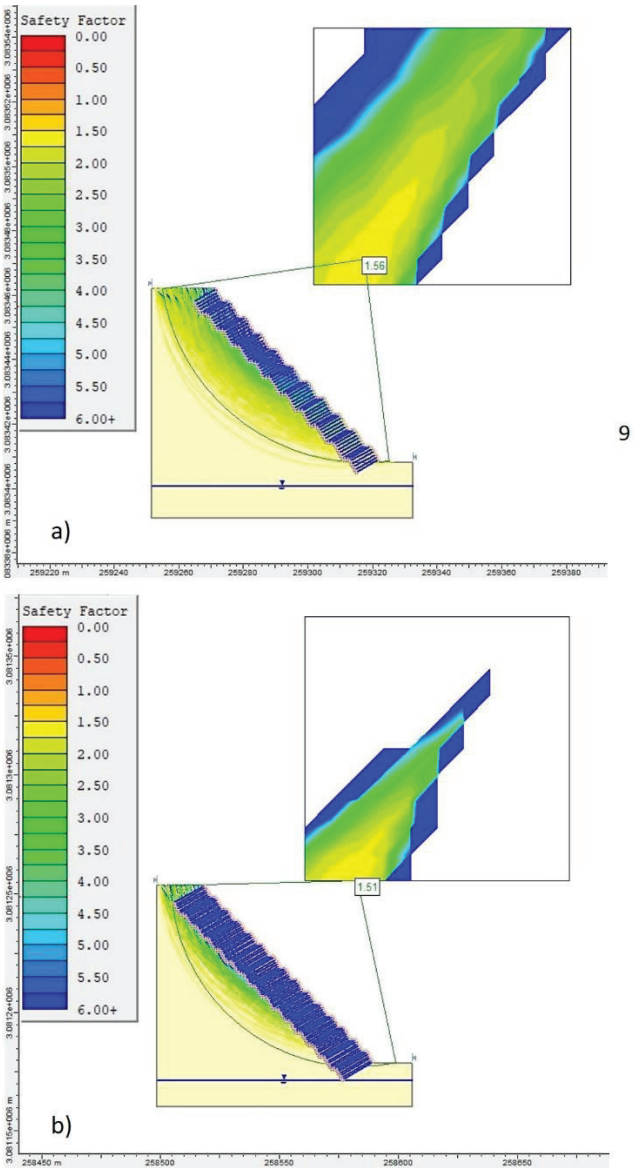

Figure 9, (a) Stability analysis of rock-cut slope RS-1 following slope reprofiling and rock anchor installation; (b) Stability analysis of rock-cut slope RS-2 following slope reprofiling and rock anchor installation.

Rock anchors (−150°, 8–15 m, 200–300 kN) effectively stabilize these slopes, offering a cost-efficient alternative to extensive re-profiling. A 60° slope with anchors achieves FoS up to 1.56 while minimizing excavation and environmental impact.

Key factors for sustainable stabilization include slope geometry, discontinuity orientation, and anchor design. Combined interventions, targeted re-profiling, rock anchors, benching, drainage, and monitoring—provide a practical framework for securing high-risk Himalayan Road slopes.

Limitations and future work

This study did not consider seismic loading, which is critical in the earthquake-prone Himalayan region. Future analyses incorporating dynamic forces could alter factors of safety assessments and rock anchor design, providing a more comprehensive evaluation of

slope stability under combined static and dynamic conditions.

Acknowledgements

Special thanks to Geotech Solutions International for valuable support. We are thankful to two anonymous reviewers for their comments and suggestions, which helped to rectify the manuscript.

Author contributions

Shankar wrote the main manuscript text, Manita and Kabita prepared figures and revise the article. All authors also reviewed it.

Data availability

No datasets were generated or analyzed during this study.

Declarations

The authors declare that they have no known competing financial interests or personal relationships that could have appeared to influence the work reported in this article.

References

Ahmad, R., and Joshi, M. N. (2010). Assessment of landslide susceptibility on land degradation processes in Chamoli and surrounding areas using RS and GIS technique. International Geoinformatics Research and Development Journal, 1(3).

Aleotti, P., and Chowdhury, R. (1999). Landslide hazard assessment: Summary review and new perspectives. Bulletin of Engineering Geology and the Environment, 58(1), 21–44. https://doi.org/10.1007/s100640050066

Baharvand, M., and Hosseinitoudeshki, V. (2015). The effect of installation angle of rock bolts on the stability of rock slopes. Journal of Novel Applied Sciences, 4(1), 67–71.

Bieniawski, Z. T. (1973). Engineering classification of jointed rock masses. Civil Engineering (South Africa), 15, 335–344.

Bieniawski, Z. T. (1976). Rock mass classifications in engineering. In Proceedings of the Symposium on Exploration Rock Engineering (pp. 97–106). Johannesburg.

Bieniawski, Z. T. (1989). Engineering rock mass classification. Wiley.

Brunsden, D., Jones, D. K. C., Martin, R. P., and Doornkamp, J. C. (1981). The geomorphological character of part of the Low Himalaya of eastern Nepal. Zeitschrift für Geomorphologie Supplementband, 40, 25–72.

Duncan, J. M., Wright, S. G., and Brandon, T. L. (2005). Soil strength and slope stability (2nd ed.). John Wiley and Sons.

Gerrard, J. (1994). The landslide hazard in the Himalayas: Geological control and human action. Geomorphology, 10(3), 221–230. https://doi.org/10.1016/0169-555X(94)90041-8

Goodman, R. E. (1995). Block theory and its application. Géotechnique, 45(3), 383–423. https://doi.org/10.1680/geot.1995.45.3.383

Goodman, R. E. (2000). Introduction to rock mechanics. John Wiley and Sons.

Haswanto, W. A., and Abd-Ghani, R. (2008). Kinematic and block theory applications to rock slope stability analysis at Fraser's Hill, Pahang, Malaysia. Electronic Journal of Geotechnical Engineering, 13(D).

Hoek, E., and Bray, J. W. (1981). Rock slope engineering (3rd ed.). Institute of Mining and Metallurgy.

Kainthola, A., Singh, P. K., and Singh, T. N. (2015). Stability investigation of road-cut slope in basaltic rock mass, Mahabaleshwar, India. Geoscience Frontiers, 6(6), 837–845. https://doi.org/10.1016/j.gsf.2014.06.006

Khanal, S., and Dahal, R.K. (2024). Influence of Precipitation Variability on Pore Water Pressure and Surface Layer Failures in Naturally Undulating Slopes at Nau Kilo, Narayanghat–Mugling Road, Central Nepal. Asian Journal of Engineering Geology, 1(1 and 2), 39-48. https://doi.org/10.64862/ajeg.112.05

Kliche, A. C. (1999). Rock slope stability. Society for Mining, Metallurgy, and Exploration.

OnlineKhabar (2017). Two killed, Two missing as landslide buries police van in Chitwan. Available at: https://english.onlinekhabar.com/2-killed-2-missing-as-landslide-buries-police-van-in-chitwan.html

Owen, L. A. (1991). Mass movement deposits in the Karakoram Mountains: Their sedimentary characteristics, recognition, and role in landform evolution. Geomorphology, 35(4), 401–424. https://doi.org/10.1016/0169-555X(91)90007-E

Paudyal, K. (2014). Geological and petrological evolution of Mugling–Damauli area of central Nepal, Lesser Himalaya (Doctoral dissertation). Tribhuvan University, Nepal.

Regmi, A. D., Yoshida, K., Dhital, M. R., and Devkota, K. (2013a). Effect of rock weathering, clay mineralogy, and geological structures on the formation of a large landslide: A case study from Dumre Besei, Lesser Himalaya, Nepal. Landslides, 10(4), 483–494. https://doi.org/10.1007/s10346-011-0311-7

Regmi, A. D., Devkota, K. C., Yoshida, K., Pradhan, B., Pourghasemi, H. R., Kumamoto, T., and Akgün, K. (2013b). Application and comparison of frequency ratio, statistical index, and weights-of-evidence

models in landslide susceptibility mapping in central Nepal Himalaya. Arabian Journal of Geosciences, 6(7), 2727–2743. https://doi.org/10.1007/s12517-012-0807-z

Rocscience. (2006). Slide 5.0: 2D limit equilibrium slope stability analysis [Computer software]. Rocscience Inc.

Romana, M. (1985). New adjustment ratings for application of Bieniawski classification to slopes. In International Symposium on the Role of Rock Mechanics (ISRM) (pp. 49–53). Zacatecas.

Romana, M. (1995). The geomechanics classification SMR for slope correction. In Proceedings of the 8th International ISRM Congress (pp. 1085–1092).

Sharma, R. K., Mehta, B. S., and Jamwal, C. S. (2013). Cut slope stability evaluation of NH-21 along the Natayan–Gambhrola section, Bilaspur District, Himachal Pradesh, India. Natural Hazards, 66(1), 249–270. https://doi.org/10.1007/s11069-012-0469-x

Shroder, J. F., and Bishop, M. P. (1998). Mass movement in the Himalaya: New insights and research directions. Geomorphology, 26(1–3), 13–35. https://doi.org/10.1016/S0169-555X(98)00052-7

Singh, P. K., Kainthola, A., and Singh, T. N. (2013). Rock mass assessment along the right bank of the River Sutlej, Luhri, Himachal Pradesh, India. Geomatics, Natural Hazards and Risk, 5(3), 205–222. https://doi.org/10.1080/19475705.2013.834486

Umrao, R. K., Singh, R., Ahmad, M., and Singh, T. N. (2011). Stability analysis of cut slopes using continuous slope mass rating and kinematic analysis in Rudraprayag District, Uttarakhand. Geomaterials, 1(2), 79–87. https://doi.org/10.4236/gm.2011.12012

World Bank (2025). Protecting slopes to build resilient roads in Nepal. Available at: https://www.worldbank.org/en/news/feature/2025/02/10/protecting-slopes-to-build-resilient-roads-in-nepal

Research Article DOI: https://doi.org/10.64862/ajeg.2025.201.05 Open Access

Subsurface Characterization in Rugged Himalayan Terrain Using 2D ERT: Implication for Hydropower Development in Karnali, Nepal

Kapil Karki[1*, 3], Gyanendra Raj Sapkota[2, 3], Dilandra Raj Pathak[3], Rishi Raj Baral[4], Praveen Upadhyay Kandel[5], Faraz Ul Haq[6], and Muhammad Fahim Aslam[6]

[1]Department of Earth Science, The University of Memphis, 3720 Alumni Ave, Memphis, TN 38152
[2]Department of Geosciences, Texas Tech University, 1200 Memorial Circle, Lubbock, TX 79409, USA
[3]Quartz Group Pvt. Ltd., Kirtipur, Nepal
[4]Explorer Geophysical Consultants Pvt. Ltd., Kathmandu 44600, Nepal
[5]Geotech Solutions International, Dhobighat, Lalitpur, Nepal
[6]Department of Civil Engineering, The University of Memphis, TN, 38152, USA

*(*Corresponding E-mail: kkarki@memphis.edu)*

Received: January 25, 2025, Accepted: June 25, 2025

Abstract: Hydropower development in the tectonically active and geologically complex Himalayan region requires advanced geophysical methods capable of resolving subsurface heterogeneity in rugged terrain. Two-dimensional Electrical Resistivity Tomography (2D ERT) is particularly effective in such environments due to its adaptability, resolution, and ability to delineate lithological and structural variations. In Nepal, ERT has become an essential tool for assessing overburden thickness, bedrock quality, aquifer characteristics, and potential instability zones critical for hydropower development. This study presents the application of 2D ERT at the proposed Peaking Run-of-River (PROR) hydropower project in the Mugu Karnali highlands of western Nepal. Sixteen high-resolution resistivity profiles were collected using the Wenner array with 5 m electrode spacing to image the subsurface. The results reveal distinct resistivity values from very low to very high (20 Ω·m - 4,500 Ω·m) corresponding to colluvium, weathered bedrock, and competent crystalline formations, including schist, quartzite, and granitic gneiss. Fractured and saturated bedrock zones were also identified, providing insights into site stability and foundation suitability. The resistivity models confirm that the project area possesses competent bedrock conditions appropriate for key hydropower structures. The successful application of ERT in this high relief, folded, and thrusted Himalayan setting underscores its reliability for geotechnical and hydropower feasibility studies. These findings demonstrate that integrating geophysical methods like ERT into project planning enhances the accuracy of subsurface evaluation and supports sustainable hydropower development in rural Nepal.

Keywords: 2D Electrical resistivity tomography (ERT), Wenner array, Peaking run-of-river, Hydropower.

Introduction

The Himalayan range, stretching over 2,400 km, has been pivotal in advancing our understanding of mountain belt formation, primarily driven by the collision of continental plates (Argand, 1924; Dewey and Bird 1970; Powell and Conaghan, 1973; Le Fort, 1996; Kohn, 2014). Rugged mountain regions serve as critical components of the global hydrological system and are often described as “natural water towers” due to their capacity to capture, store, and release freshwater (Viviroli and Weingartner, 2008). Tectonic convergence in many of these regions has created high-relief, steep terrains that offer ideal topographic conditions for harnessing water’s kinetic energy. Although mountain regions cover only about 32% of global river basin areas, they contribute more than 60% of total discharge, emphasizing their disproportionate role in water supply (Viviroli et al., 2007).

Globally, several countries have effectively utilized the topographic advantages of rugged terrain to generate substantial amounts of renewable energy. China’s Three Gorges Dam, the world’s largest hydropower facility (22,500 MW) (USGS, 2018; Kumar, 2022; NS Energy, 2025) is situated in a steep gorge along the Yangtze River. In South America, the Itaipu Dam (14,000 MW), jointly operated by Brazil and Paraguay, exploits the Paraná River’s gradient and rugged terrain to supply a substantial share of regional electricity. Similarly, Europe’s Glendoe Hydroelectric Scheme in the Scottish Highlands utilizes a 600-meter head across steep mountainous terrain to generate 100 MW of electricity (SSE, 2009). In South Asia, India’s Bhakra-Nangal Dam, situated in the lower Himalayas along the Sutlej River, utilizes the natural valley topography to generate 1,325 MW (CWC, 2017). Likewise, the Upper Tamakoshi Hydroelectric Project (456 MW), located in the highlands of Dolakha District, capitalizes over 800 meters of hydraulic head from glacial rivers descending steep Himalayan slopes (NEA, 2020).

Nepal presents a textbook example of how mountainous topography facilitates hydropower development. Nepal’s rugged terrain is intersected by approximately 6,000 rivers draining a total area of

194,471 km^2. Of these, 33 rivers have drainage basins exceeding 1,000 km^2, offering a theoretical hydropower potential of 83,000 MW, of which only about 2% has been developed (Sharma and Awal, 2013; Alam et al. 2017), where 43000 MW is technically and economically achievable (WECS, 2019). Nepal's hydropower potential varies across its provinces due to differences in topography. Nepal is divided into seven provinces, among which Province 1 (Koshi) and Province 6 (Karnali) have the highest potential, with capacities of 22,820 MW and 17,799 MW, respectively. In contrast, Province 2 (Madesh) has the lowest potential, totaling only 341 MW). Nepal's energy capacity surpluses to 3602 MW as of 2025, March (economic survey 2025/2026), with the continued expansion of electricity generation capacity, Nepal is prioritizing the implementation of smart grid technologies to decarbonize the energy sector, enhance grid efficiency, and facilitate the integration of renewable energy sources. As a part of this broader shift toward sustainable and resilient clean energy, new projects are being proposed on high terrain having high gross head for a peaking run of river (PROR), which is supported by geophysical investigations, including 2D electrical resistivity imaging, to assess terrain suitability for infrastructure development and this study will help understand the feasibility of this hydropower project in rocky topography.

Several geophysical techniques could potentially be applied to investigate geological structures near the surface (Epting et al., 2009). Subsurface geological investigations are carried out for a range of purposes including engineering construction, groundwater exploration, seismic activity monitoring (Acworth, 1987; Burger and Burger, 1992; Mukhopadhyay et al., 2006; Satyabala and Bilham 2006; Hassan Imam et al., 2013), geotechnical investigations (Suzuki et al. 2000; Kneisel, 2006; Chambers et al., 2006; Cardarelli et al., 2007; Thompson et al., 2017; Lin et al., 2018), karst features (McGrath et al., 2002; Khalil 2006), landslide slope stability assessment (Jhinkwan et al. 2023; Sigdel et al. 2025) and few investigation focused on case studies of dam inspections (e.g, Wise'n et al. 2000; Karastathi et al., 2002; Al-Fares, 2011). Geophysical data have been widely used in hydrology to find and map underground geological structures such as fault zones (Rehfeldt et al., 1992; Rubin et al., 1992; Hubbard and Rubin, 2000; Lapenna et al., 2005; Singha et al., 2015; Soupois et al., 2007; Colangelo et al. 2008; Gélis et al. 2010; Binley et al., 2015). The adoption of modern geophysical techniques in mountain geomorphology has accelerated due to their efficiency, minimally invasive nature, and capacity to deliver high-resolution subsurface information relative to conventional drilling (Demanet et al., 2001). Advances in acquisition and processing now permit precise characterization of near-surface lithology in structurally complex terrains (Kneisel, 2006), substantially expanding the analytical and applied potential of geophysical investigations (Huayllazo et al., 2023; Nassim et al., 2024). Different geophysical tools have been adopted for studying the hydropower potential in Nepal Himalaya, among them 2D ERT is highly applied techniques in identifying the feasible location for the hydropower components. Pant (2005), Ghimire et al. (2017), Lamsal et al. (2020) Takamte et al. (2022) used the 2D ERT method to delineate subsurface geological structures for hydropower studies. Silwal and Paudyal (2018) also used this method to identify the subsurface lithology of Dotigad hydropower project with different hydraulic components. Adhikari et al. (2019), Mebrahtu (2019), Srivastava et al. (2022), and Acharya et al. (2023) also used this technique for investigating the subsurface geology for hydropower dam site suitability and rehabilitation.

Despite considerable advancements in hydropower exploration across Nepal, the remote Karnali province remains largely under-investigated, and its subsurface characteristics pertinent to energy development are poorly constrained. While hydropower feasibility studies have proliferated in more accessible regions, detailed geophysical assessments in Karnali are sparse, and no systematic Electrical Resistivity Tomography (ERT) investigations have been conducted along key river segments. In this study, ERT has been applied to selected sites along the Mugu Karnali River to characterize subsurface lithologies, identify fractured or weathered bedrock, and assess geotechnical stability. The resulting high-resolution subsurface models not only inform local hydropower feasibility but also provide insights into broader geological and hydrogeological conditions of the region, offering a framework for future energy development and geotechnical investigations in similar underexplored segments of Karnali.

Study Area

Geology of the Area

The Mugu Karnali valley (Figure 1) extends approximately E–W and offers about 30–40 km of almost uninterrupted exposure of the primary tectono-metamorphic units (Montomoli et al. 2013). The project area is located within the Higher Himalayan Sequence (HHS) and is near the Main Central Thrust (MCT) zone. The Galwa Tectonic Window is surrounded by a geological formation dominated by two-mica gneiss, quarzitic gneiss, quartzite, garnet–kyanite–mica schist or gneisse, amphibolite, and calc-gneiss of the Higher Himalaya. Above this sequence lies a thick layer, extending several thousand meters, consisting of granite–gneiss, migmatite, paragneiss, and carbonate rocks. Kyanite, typically found in the lower parts of this sequence, transitions to sillimanite in the higher elevations (Fuchs, 1974). In the northern part of the Higher Himalayan crystalline region, there is an intrusion by Mugu Granite (Hagen, 1969).

The Mugu Granite exhibits a medium-grained texture characterized by hypidiomorphic crystals. Notably, it contains twinned and zoned microcline phenocrysts,

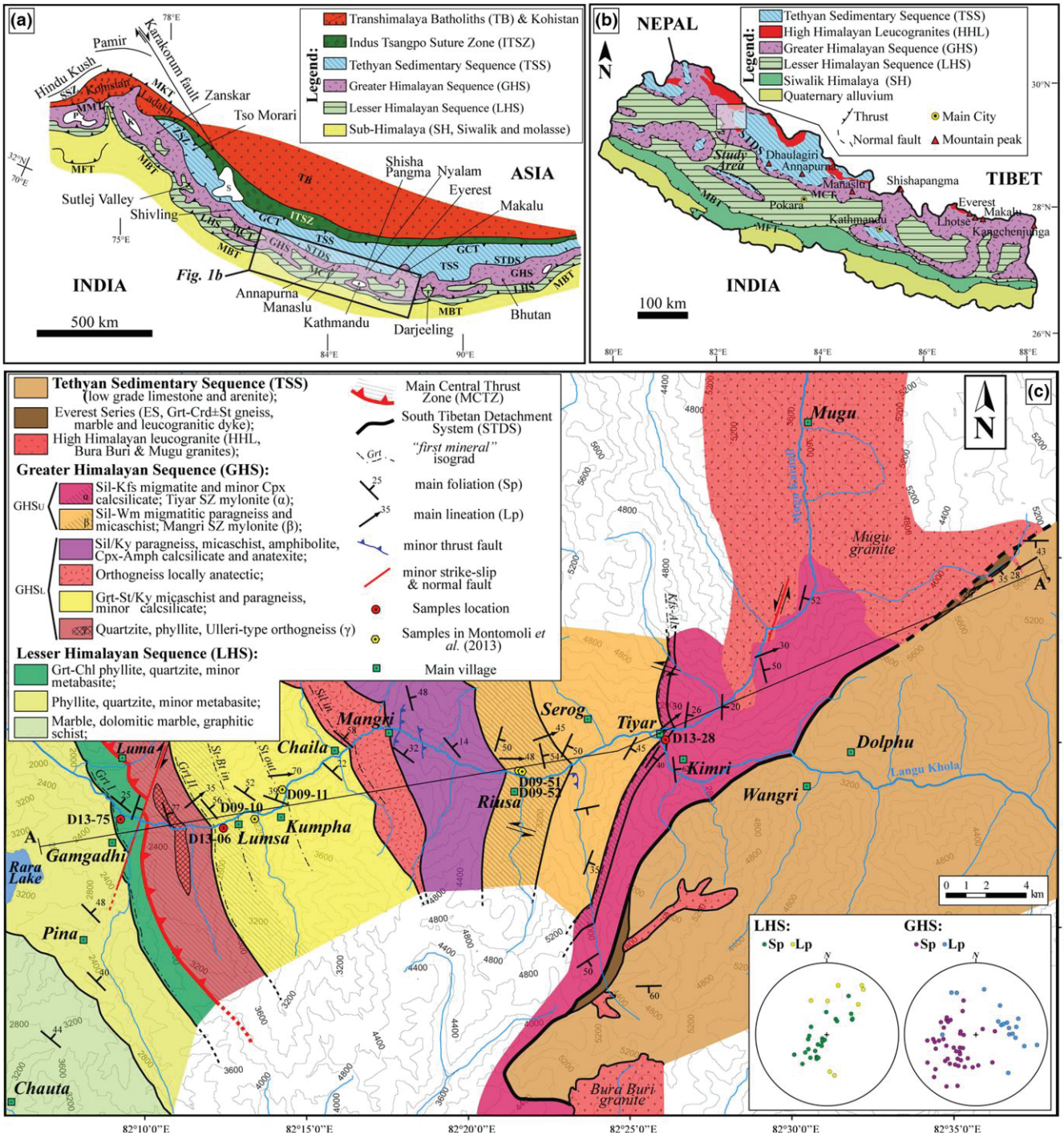

Figure 1, (a) Geological map of the Himalayan range (after Law et al. 2004). The approximate location of (b) is reported; (b) geological map of the Nepalese Himalaya (after Montomoli et al. 2013 and references therein). The Mugu Karnali valley (study area) is shown; (c) Tectono-metamorphic map of the Mugu Karnali valley (Western Nepal). For simplicity, only samples cited in the text or in Montomoli et al. (2013) are indicated. Cross-section trace (A–A') of Fig. 2 is shown. In the inset, stereo plots of the main structural elements of LHS and GHS are reported (Wulff net – lower hemisphere). SSZ, Shyok suture zone; ZSZ, Zanskar shear zone; MKT, Main Karakoram Thrust; MMT, Main Mantle Thrust; TB, Tibetan Block; ITSZ, Indus Tsangpo Suture Zone; GCT, Great Counter Thrust; TSS, Tethyan Sedimentary Sequence; GHS, Greater Himalayan Sequence; STDS, South Tibetan Detachment System; MCT, Main Central Thrust; MBT, Main Boundary Thrust; MFT, Main Frontal Thrust; K, Kashmir basin; P, Peshawar basin; S, Sutlej basin.

some reaching lengths of up to 1 cm, which encapsulate plagioclase, biotite, muscovite, and sporadic occurrences of sillimanite oriented parallel to the zoned peripheries of potassium feldspar (K-feldspar) (Fuchs, 1977). The boundary between the Mugu Granite and the migmatite complex is gradual rather than distinct. Migmatization processes were partially influenced by the intrusion of the Mugu Granite, evidenced by migmatites hosting older augen gneisses and some paragneisses intersected by folded veins of granite. Conversely, the granite itself contains numerous xenoliths of augen gneiss (Fuchs, 1977).

The Higher Himalayan Sequence (GHS) is positioned above the Lesser Himalayan Sequence (LHS) and serves as the metamorphic core of the Himalayan mountain-building process. The LHS is bordered to the south by the Main Boundary Thrust (MBT) and to the north by the Main Central Thrust (MCT), both of which trend approximately northwest-southeast and dip towards the northeast, roughly perpendicular to the mountain range's orientation (Colchen and Le Fort, 1986; Le Fort, 1975). The uppermost layer of the granite is composed of a sequence including calc-gneiss, marble, calcschist, and calc-phyllite. These rocks belong to the lower section of the Dhaulagiri Limestone, with a decrease in metamorphic grade observed as one move upwards in the stratigraphy. The Higher Himalayan crystalline in this region exceeds a thickness of 10 km (Fuchs, 1974).

The proposed site lies in Mugu District of Karnali Province (Figure 2). The project layout consists of a 27 m high gated barrage, 16497.26 m, and a 7 m diameter in horseshoe shaped tunnel on the right bank of the river, a 20 m Dia and 66.49 m high surge shaft (circular concrete-restricted orifice type) and surface powerhouse: housing four generating units of 70.59 each. The proposed run-of-river project is a high head project with an installed capacity of 306 MW, which is in Mugum Karmarong Rural Municipality and Chhayanath Rara Municipality shown in Figure 2. The headworks area is located at Mugum Karmarong Rural Municipality ward number 3 and powerhouse area is located at Chhayanath Rara Municipality ward number 12. The proposed project lies between 82° 13' 45" E to 29° 32' 46" N and 82° 25' 55" E to 29° 35' 50" N.

Stratigraphy

Stratigraphically, the project area is divided into the following units (Figure 3).

Lumsa Unit

This unit is exposed around Lumsa Village and falls into Lesser Himalayan Sequence separated from Higher Himalayan Crystalline by the MCT. The lithology of the unit consists of thinly foliated, fine-to medium-grained, slightly to moderately weathered grey schist with intercalated thin-bedded, medium-grained, moderately weathered light grey micaceous quartzite containing quartz veins. The mineral assemblage includes quartz, feldspar, mica, and garnet. The thickness of this unit exceeds 3 km.

Chhaila Unit

This unit falls under Higher Himalayan Crystallines above the MCT. The rock types include schist and quartzite with occasional concordant intrusion of amphibolite. The schist contains abundant garnets of size up to 1 cm. Kyanite flakes are also developed on quartz veins. Malachite mineralization is also present on quartzite at some localities. The thickness of this unit is 4.5 km.

Mangri Unit

This unit is widely distributed around Mangri Village. The lithology consists of thin-to medium-foliated, thin-to thick-banded, coarse-grained, slightly weathered, medium strong to strong light grey granitic gneiss with partings of weak grey mica schist. The mineral assemblage consists of quartz, feldspar, mica, and tourmaline in granitic gneiss. Schist contains quartz, feldspar, and mica. The thickness of this unit is 5.5 km.

Darima Unit

This unit is well exposed around Darima Village at road-cut sections, river-cut sections and hills and ridges. The rock types include medium-to massive-bedded, coarse-grained, jointed, moderately to slightly weathered, grey and pink quartzite with coarse-grained, moderately weathered weak grey schist partings. Steep cliffs are developed due to the presence of strong quartzites at this unit. The thickness of this unit is 1.5 km.

Pulu Unit

This unit is well exposed around Pulu Village. The lithology consists of thin- to medium-foliated, coarse-grained, thick to massive-banded, slightly to faintly weathered grey banded gneiss with migmatite, granitic gneiss and occasional thin-bedded grey quartzites. The strata are generally north dipping. Quartz boudins and M-type folds are abundant on quartz veins which are both parallel and oblique to foliation planes. The thickness of this unit is more than 1.2 km.

Methodology

ERT survey

Electrical resistivity methods have wide advantage of efficiency and adaptability to topography and become a mature tool for subsurface study (Wu et al. 2023).

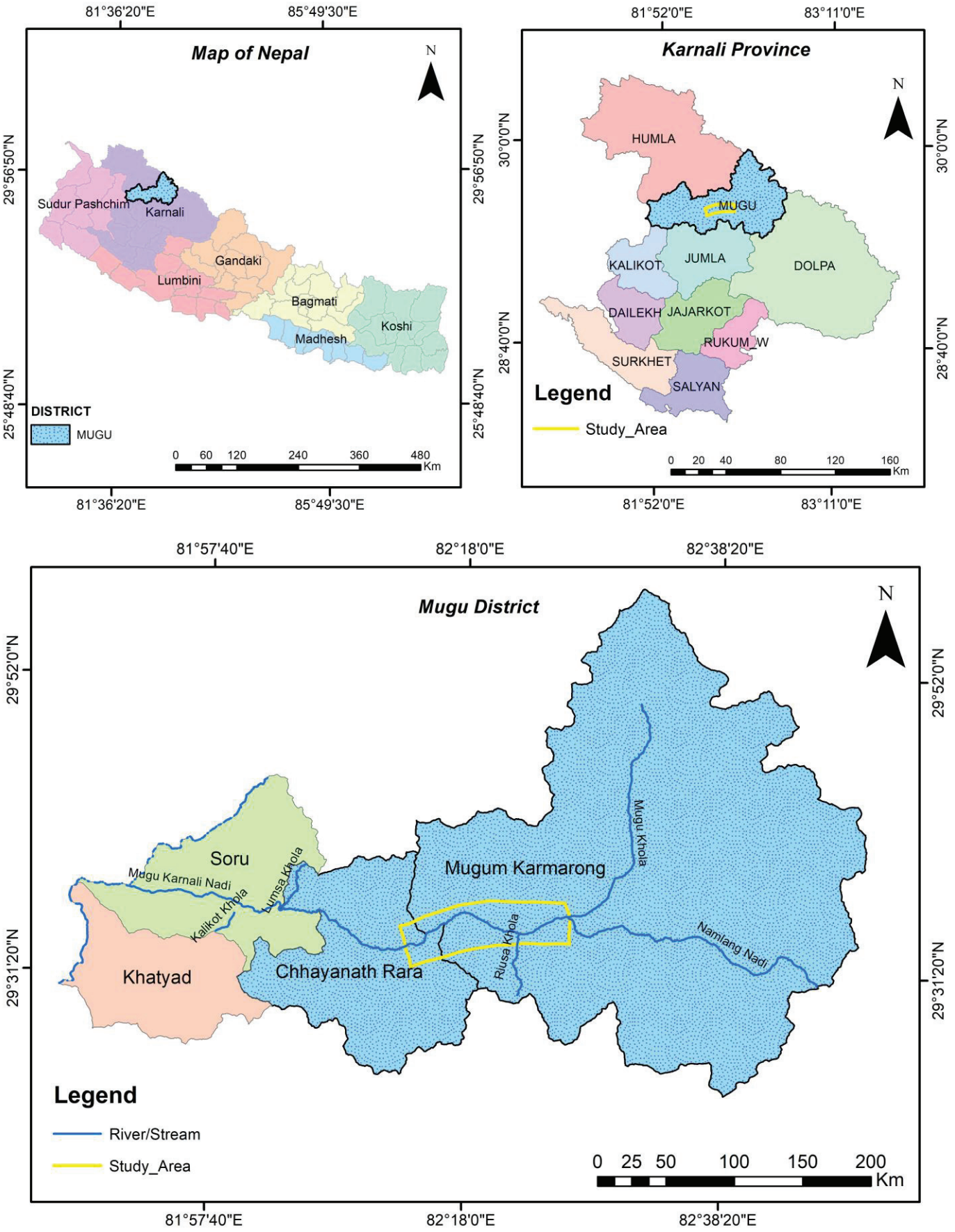

Figure 2, Location map of study area.

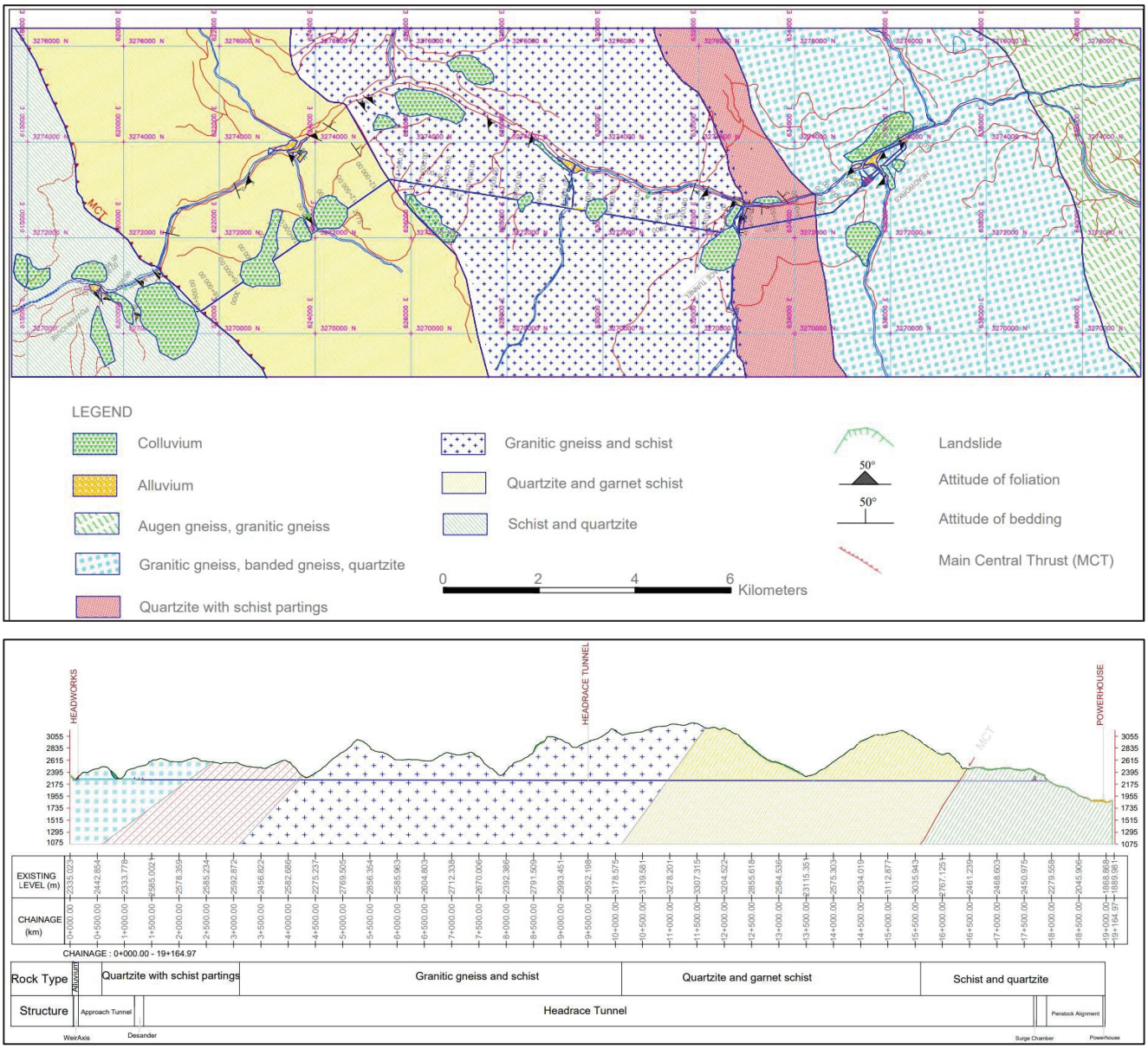

Figure 3, Engineering geological maps and geological cross-section along the project area.

Geophysical methods have a wide range of applications in locating or tracing an object of interest as suggested by the geophysical response to the object. In ERI surveys, electrical resistivity is recorded (measured in Ω m), representing the reciprocal of electrical conductivity. Resistivity Imaging is a geo-electrical method utilized for acquiring detailed 2D and 3D images of intricate subsurface geology (Griffiths and Barker, 1993). This technique involves deploying various electrode configurations such as Wenner, Schlumberger, dipole-dipole, pole-dipole, pole - pole (Dobrin, 1982). In surface ERT applications, electrodes are often installed in a straight-line arrangement using multicore cables. The Wenner array method was selected because of its strong resistance to noise and reliability in outlining horizontal subsurface features (Falae et al., 2019). According to Dobrin (1982), the method detects changes in subsurface geology by evaluating the apparent resistivity, which indicates variations in electrical resistivity. Samouëlian et al. (2005) offer an in-depth explanation of the theory and fundamental principles underlying ERT.

The fundamental principle of ERT relies on the varying electrical conductivity of subsurface materials, which is influenced by numerous factors. These factors include rock type, porosity, permeability, pore connectivity, temperature, salinity, cation exchange capacity, clay content, the nature of fluids or water present, degree of weathering, presence of fractures or faults, discontinuities (Hao et al., 2002; Tejero et al., 2002; Kim et al., 2007; García-Moreno and Mateos 2011; Cardarelli et al., 2010; Ha et al., 2010; Lech et al., 2020), rock associations, deformation, and water-rock interactions or alterations. (Aizebeokhai et al., 2010, Hasan et al., 2018, Hung et al., 2020). In hard rock terrains, electrical resistivity can vary over a large range

depending on weathering degree, water saturation, etc. (Hasan et al., 2020). ERT generates an image of subsurface resistivity, which can be interpreted to infer different lithologies or rock types based on their resistivity contrasts (Hasan et al. 2020). The outline of the methodology for subsurface characterization is given in the flow chart (Figure 4).

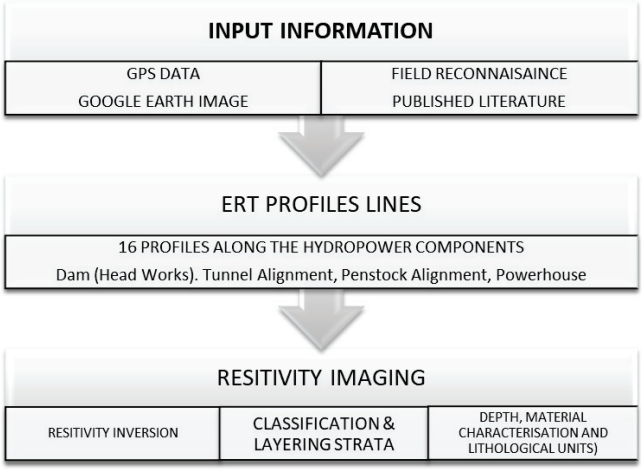

Figure 4, Methodology flow chart for subsurface characterization.

Data acquisition and processing

Data acquisition was carried out by using equipment known under the brand name GEOMATIVE GD10 SUPREME 2D PLUS MULTI-ELECTRODE RES/IP IMAGING SYSTEM manufactured by GEOMATIVE CO., LTD., China. The ERT imaging setup is depicted in Figure 5. During the investigation, 60 electrodes were linked by two cables, spaced at 5 m distances arranged in straight lines (Cubbage et al., 2017) giving maximum of 300 m length following the guideline set by Loke and Barker (1996). A total of sixteen ERT profiles were used for site characterization, denoted as ERT-1 to ERT-16. To reduce electrode spacing errors, two technicians verified electrode placement before each survey, and salt water was applied to improve ground contact. A reconnaissance survey ensured equipment and configuration reliability. In noisy areas, measurements were repeated 2–3 times for accuracy. Topographic elevations and geographic coordinates were recorded by total station at each electrode for spatial referencing and model correction (Table 1).

The instrument is fully automatic and designed to measure apparent resistivity as well as induced polarization of the subsurface materials. In a noisy area, the signal is significantly enhanced by stacking data measured in many cycles (4-10 stacks). It consists of three main units all housed in a single casing: the transmitter, the receiver, and the microprocessor. The electrically isolated transmitter sends out well-defined and regulated signal currents.

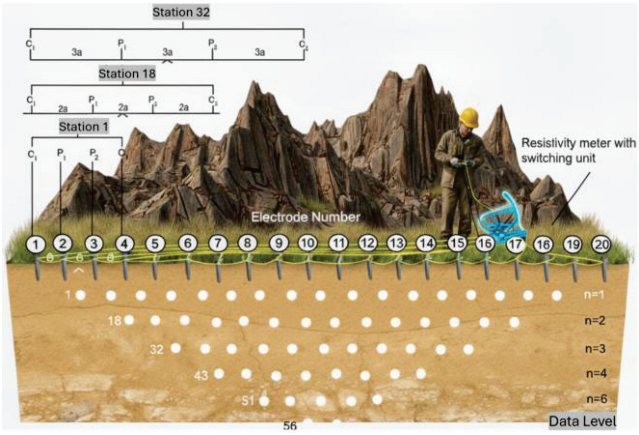

Figure 5, Schematic diagram of a multi-electrode system, and a possible sequence of measurements to create a 2-D pseudo section. (modified after Loke et al., 2013).

The receiver discriminates against noise and measures voltages correlated with transmitted signal current. The microprocessor monitors and controls operations and calculates results. The apparent resistivity is calculated automatically and displayed in digital form. Stainless steel electrodes (30 cm long) were used for both current transmission and voltage receiving. These electrodes were grounded in each profile and related to the Geomative GD-10 by specially designed CA30 ERT cables.

The inversion routine employed by the RES2DINV program relies on the smoothness-constrained least squares method (De Groot-Hedlin and Constable, 1990; Saski, 1992). Pre-processing of data to obtain a high-quality data set is followed by tomographic inversion. Data inversion code is another main component of the 2D-ERT method. A popular inversion algorithm, RES2Dinv, created by Loke and Barker (1996) and improved by Loke et al., 2003, works using a least-squares method with smoothness constraints. Geological interpretation of the resistivity tomogram is based on geometry along with resistivity values of such layers and/or patches. Surface geological, hydrogeological, geomorphological information play key roles during the interpretation of the resistivity tomograms and are interpreted with reference to established resistivity (Figure 6).

To improve the clarity and resolution of the resulting models, RMS error statistical analysis was utilized to filter out noise and data artifacts prior to processing (Miller et al., 2008). Post-inversion datasets with high RMS error values were discarded, most likely due to poor electrode-ground contact. Rucker et al. (2011) define absolute error as the absolute deviation between two repeated measurements. Each inversion included at least seven iterations, and only those with RMS errors below 10.0 were retained for interpretation.

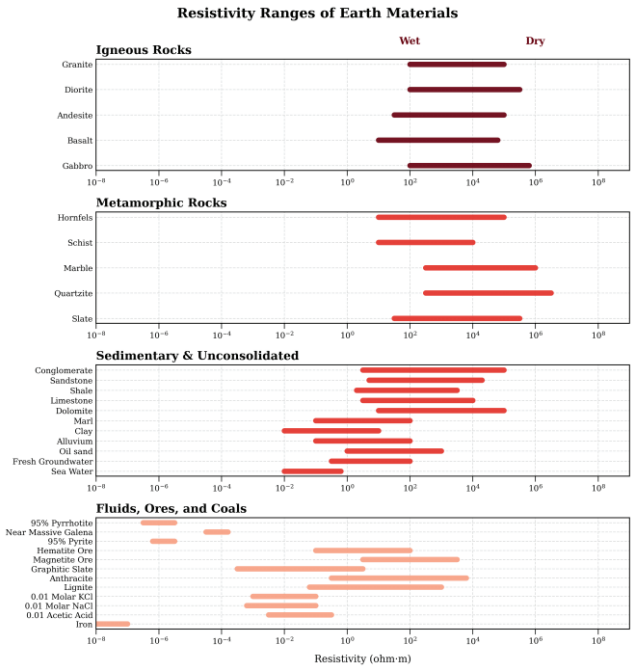

Figure 6, Electrical conductivity and resistivity of various rocks, soils and minerals (modified after Telford et al., 1990).

Table 1, ERT surveys with RMS error lower than 10%.

Profile	Length (m)	Data Points	RMS Error (%)	Profile	Length (m)	Data Points	RMS Error (%)
ERT-1	300	371	8.3	ERT-9	300	533	4.4
ERT-2	300	548	2.5	ERT10	300	554	4.3
ERT-3	300	510	6.1	ERT11	300	410	8
ERT-4	300	527	6.2	ERT12	300	518	8.1
ERT-5	300	521	4	ERT13	300	379	7.7
ERT-6	300	527	4	ERT14	150	119	7.2
ERT-7	300	545	2.4	ERT15	150	99	9
ERT-8	150	117	6.2	ERT16	150	135	6.2

Results and Discussion

ERT Profiles

The 2D data was inverted into resistivity models, showing both lateral and vertical subsurface resistivity distribution. The models revealed a wide variation of subsurface information. A total of 16 profiles, covering a combined length of 4,100 meters, were surveyed during the investigation. The electrical resistivity survey was carried out along different profile lines in various hydropower components including the reservoir area, adit tunnels, headworks area, intake site, powerhouse, penstock, and tunnel axis (Figure 7). The models reveal a spectrum of resistivity zones, ranging from low to relatively high. Geological materials are categorized based on their resistivity values, with fresh bedrocks, fresh to moderately weathered bedrocks, and weathered bedrocks with minimal fractures.

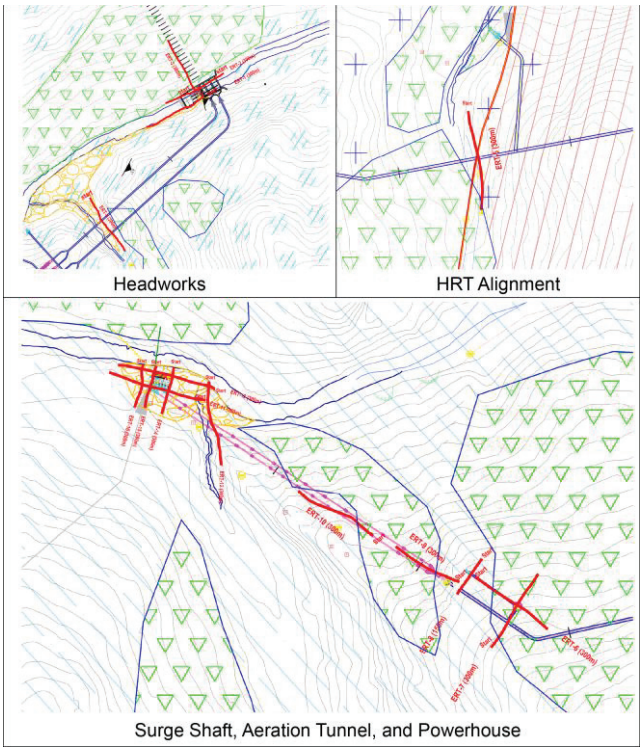

Figure 7, Drawings showing ERT alignments in the surveyed area.

The four ERT profiles conducted in the headworks area reveal consistent subsurface patterns with notable local variations. All profiles show a clear distinction between an overburden layer and underlying fractured bedrock, with varying degrees of saturation and resistivity (Figure 8). ERT-1, conducted along the left bank of the Mugu Karnali River, displays four layers, including thin colluvium and alluvium overlying saturated fractured bedrock with resistivity variations likely reflecting differences in lithology and groundwater presence; field observations support this, with alternating granitic gneiss, banded gneiss, and quartzite. In contrast, ERT-2 and ERT-3, both on the right bank, depict simpler two-layered structures with a moderately thick overburden (3–10 m in ERT-2 and 7–46 m in ERT-3) and low-resistivity, saturated fractured bedrock below, suggesting more uniform subsurface conditions in these locations. ERT-4, carried out along the right bank of Puwa Khola, shows greater lateral variation in the overburden; saturated alluvium dominates the left side (2–8 m thick), while colluvium with mixed resistivity occupies the right (2–12 m thick). Like the others, ERT-4 reveals a fractured, saturated bedrock beneath the overburden. Overall, the profiles consistently identify fractured bedrock as the foundational layer, while variability in overburden thickness, resistivity, and saturation reflect changes in topography, lithology, and proximity to the river.

The ERT profiles ERT-5 through ERT-8, conducted along the right bank of the Riusa Khola and surrounding tunnel zones, consistently delineate a three-layered subsurface structure, albeit with noticeable lateral variations in resistivity and lithology (Figure 9).

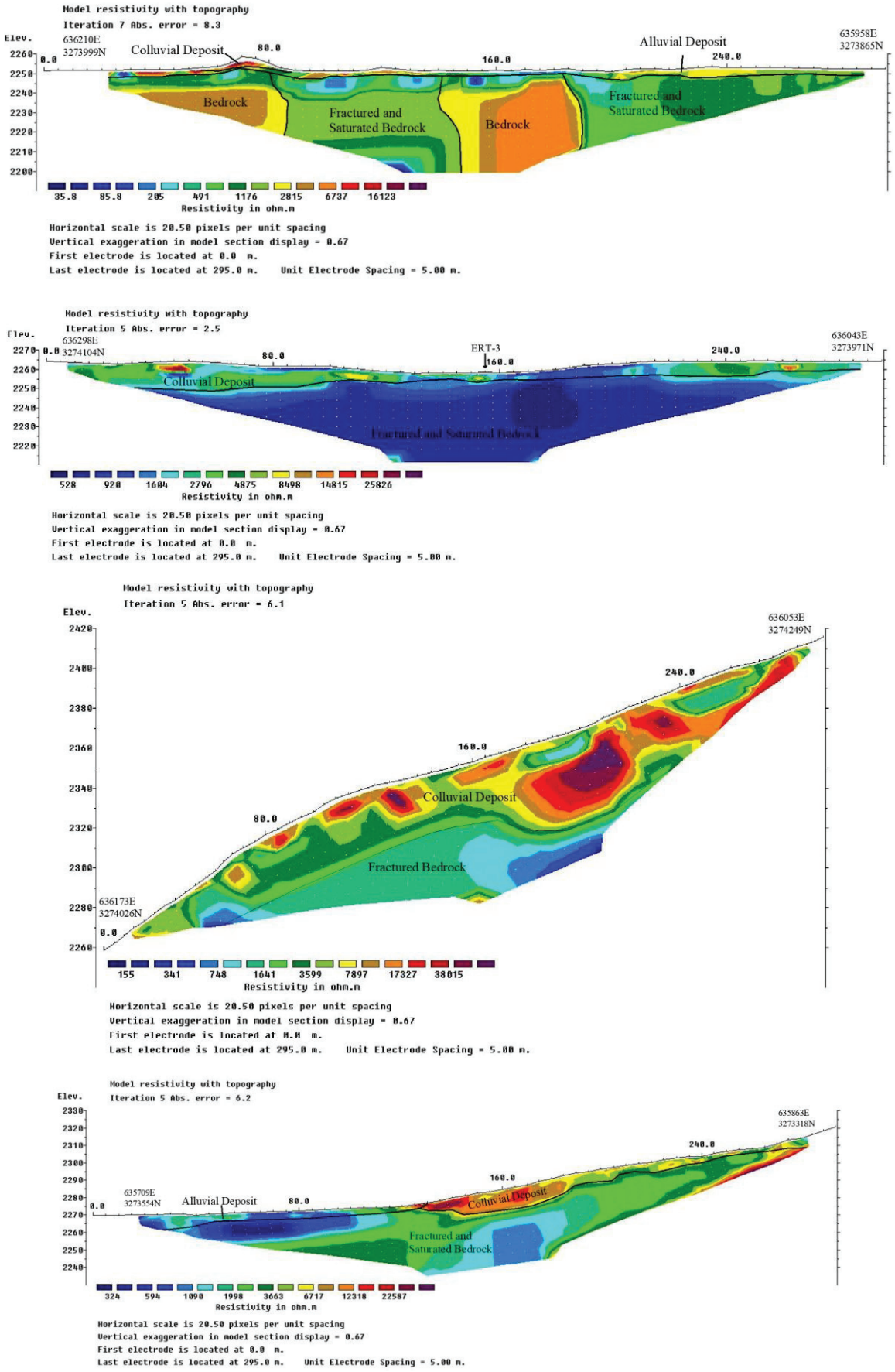

Figure 8, 2D resistivity models for lines 1-4 at the proposed powerhouse, showing lateral and vertical subsurface resistivity variations (5 m inter-profile spacing).

ERT-5, aligned with the headrace tunnel, reveals a 4–11 m thick, dry colluvial overburden, characterized by relatively high resistivity. This layer is underlain by massive granitic gneiss with schist partings, displaying high resistivity values indicative of intact rock conditions. Toward the end of the profile (chainage 182–278 m), the resistivity markedly decreases, suggesting a transition to fractured and weathered bedrock, potentially influenced by seepage or structural weaknesses.

ERT-6 and ERT-7, obtained along the surge shaft hillslope, exhibit a broadly similar subsurface configuration. Both profiles show a thin -to moderately - thick colluvial cover of approximately 2-8 m in ERT-6 and 2.5-6 m in ERT-7, overlying moderately weathered bedrock of 11–17 m and 6–16 m thick, respectively. The lowermost layers in both profiles correspond to alternating schist and quartzite horizons, inferred from contrasting resistivity patterns. The deeper section of ERT-6 (chainage 68–255 m) shows relatively low resistivity, reflecting a predominance of schistose material, whereas ERT-7 exhibits higher resistivity, suggesting a greater quartzite content.

ERT-8, located along the aeration tunnel portal, though shorter in length (150 m), also reveals a clear three-layer structure. The uppermost overburden is very thin (~1 m), followed by a moderately weathered bedrock layer (5–11 m thick), and a deeper low-resistivity zone interpreted as interbedded schist and quartzite.

Overall, the ERT-5 to ERT-8 profiles depict a consistent stratigraphic framework—an upper colluvial cover underlain by weathered rock and then more competent bedrock. However, the resistivity variations across the profiles reflect local lithological heterogeneity with quartzite-dominated zones exhibiting higher resistivity, while schist-rich sections are associated with lower values, implying differences in permeability and degree of fracturing.

ERT-9, ERT-11, and ERT-12, each 300 m long and conducted along the penstock alignment near Lumsa Village on the left bank of the Mugu Karnali River, reveal layered but variable subsurface configurations with differing degrees of complexity (Figure 10).

ERT-9 displays a typical three-layer sequence comprising of (i) a heterogeneous colluvial layer (2–7 m thick) with variable but generally high resistivity; (ii) a moderately weathered bedrock zone (5–27 m thick); and (iii) a deeper unit characterized by alternating quartzite and garnet schist, inferred from contrasting resistivity values.

ERT-11 shows a two-layer section, consisting of a thick, variable overburden (2–25 m) composed of loose, unconsolidated materials with sporadic boulders, underlain by a fractured and saturated bedrock composed of schist and quartzite. A sharp drop in resistivity from chainage 83 m onward marks highly fractured zones, possibly linked to faulting or increased water content.

ERT-12, the most geoelectrically complex of the three, delineates four distinct layers: (i) an upper heterogeneous alluvial layer (up to 27 m thick); (ii) a thin colluvium (<4 m); (iii) a moderately weathered bedrock (3–14 m thick); and (iv) a deep, saturated bedrock layer with low resistivity (<4300 Ω·m), interpreted as interbedded schist and quartzite.

Collectively, these profiles confirm the presence of colluvial and weathered/fractured bedrock sequences along the penstock alignment. However, ERT-12 is unique in capturing a deeply saturated bedrock zone beneath thick alluvium, in contrast to the relatively simpler two-layer configuration of ERT-11 and the resistive, quartzite-rich bedrock in ERT-9.

ERT-13 through ERT-16, carried out across the turbine foundation zones near the powerhouse area on the left bank of the Mugu Karnali River, predominantly indicate a two-layered subsurface system (Figure 11). This structure comprises an upper alluvial overburden and an underlying fractured, saturated bedrock.

ERT-13 (300 m) and ERT-14 (150 m), both aligned along the upstream turbine foundations, reveal thick alluvial overburden dominated by boulder- and gravel-rich sediments, ranging from 8–30 m and 4–12 m, respectively. Beneath this layer lies a fractured schist–quartzite bedrock, interpreted from moderate to low resistivity values. ERT-14 demonstrates a relatively uniform overburden distribution with localized resistive anomalies, likely indicating embedded boulders or compact gravel zones.

Similarly, ERT-15 and ERT-16 (each 150 m long) exhibit comparable subsurface conditions, characterized by an upper alluvium layer with heterogeneous resistivity reflecting variable grain size and moisture content. The underlying moderately to highly fractured bedrock shows variable resistivity patterns consistent with alternating schist and quartzite layers.

Across all four profiles, the overburden thickness varies from 2 to 16 m, while bedrock occurs at shallow to moderate depths (approximately 4–26 m). Despite localized resistivity contrasts, the overall interpretation indicates a consistent geological framework within the powerhouse site, comprising of a coarse-grained, thick alluvial cover resting upon fractured and partially saturated bedrock, with spatial variations controlled primarily by lithology and degree of fracturing.

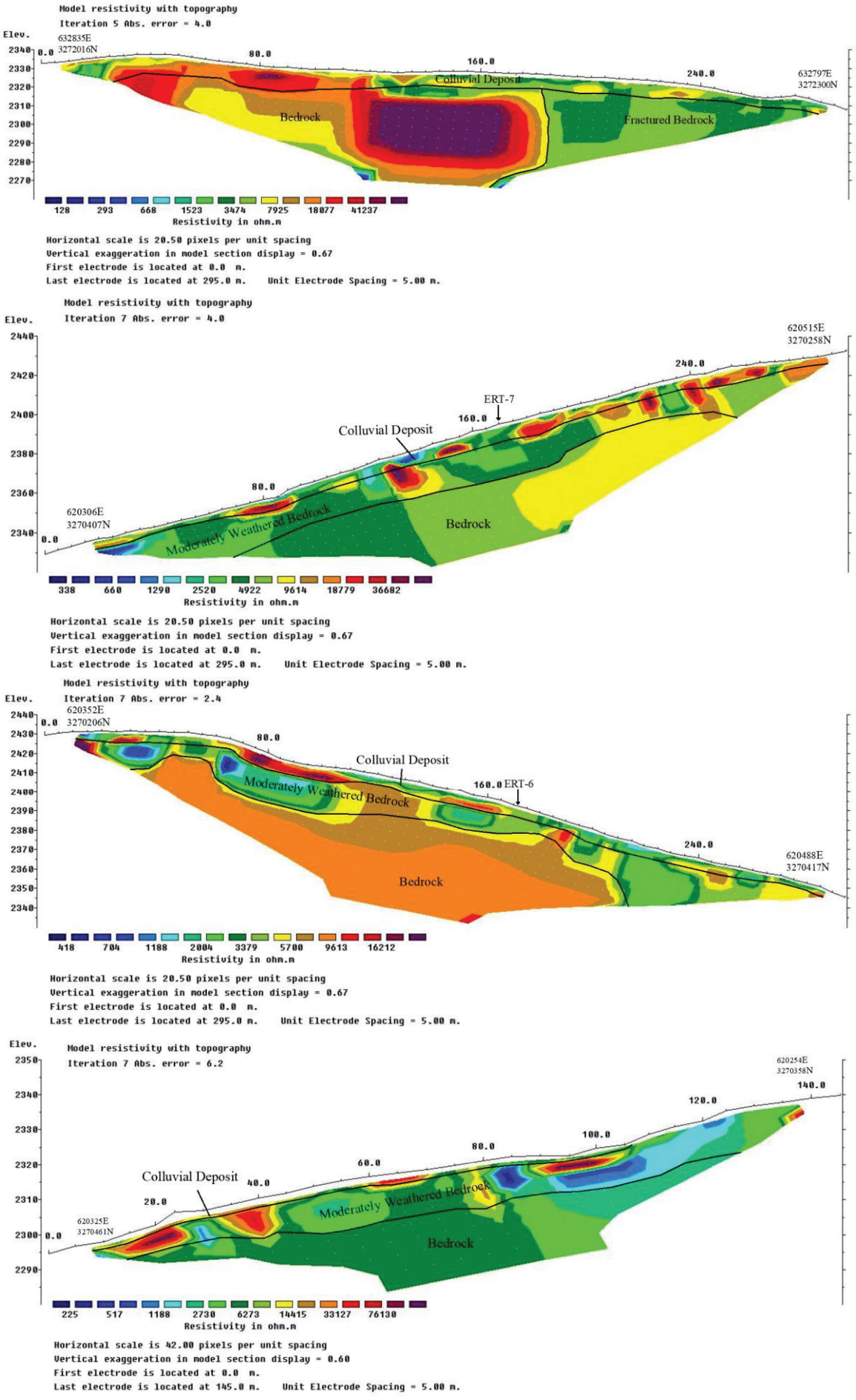

Figure 9, 2D resistivity models for lines 5 - 8 at the proposed powerhouse, showing lateral and vertical subsurface resistivity variations (5 m inter-profile spacing).

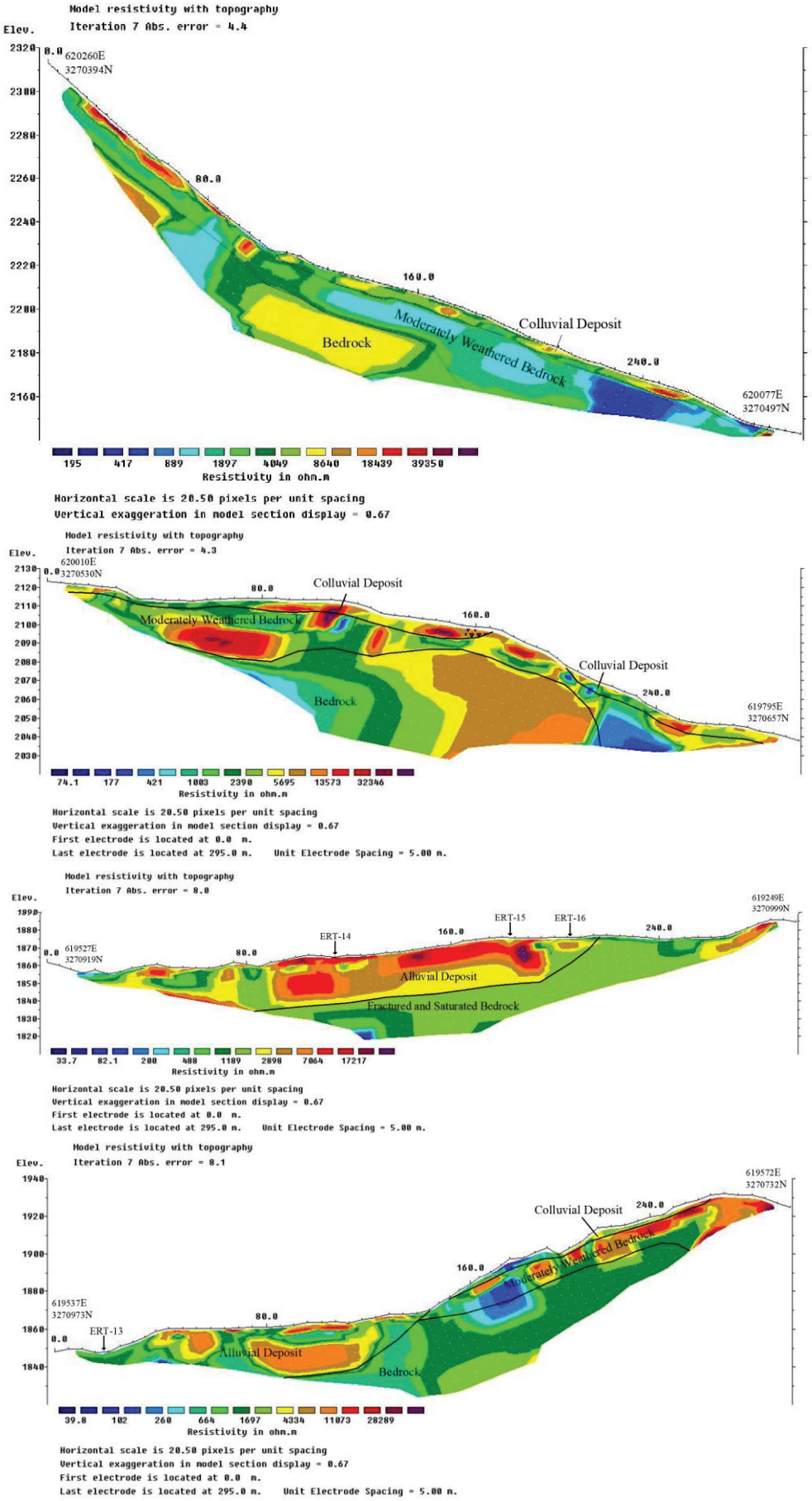

Figure 10, 2D resistivity models for lines 9–12 at the proposed powerhouse, showing lateral and vertical subsurface resistivity variations (5 m inter-profile spacing).

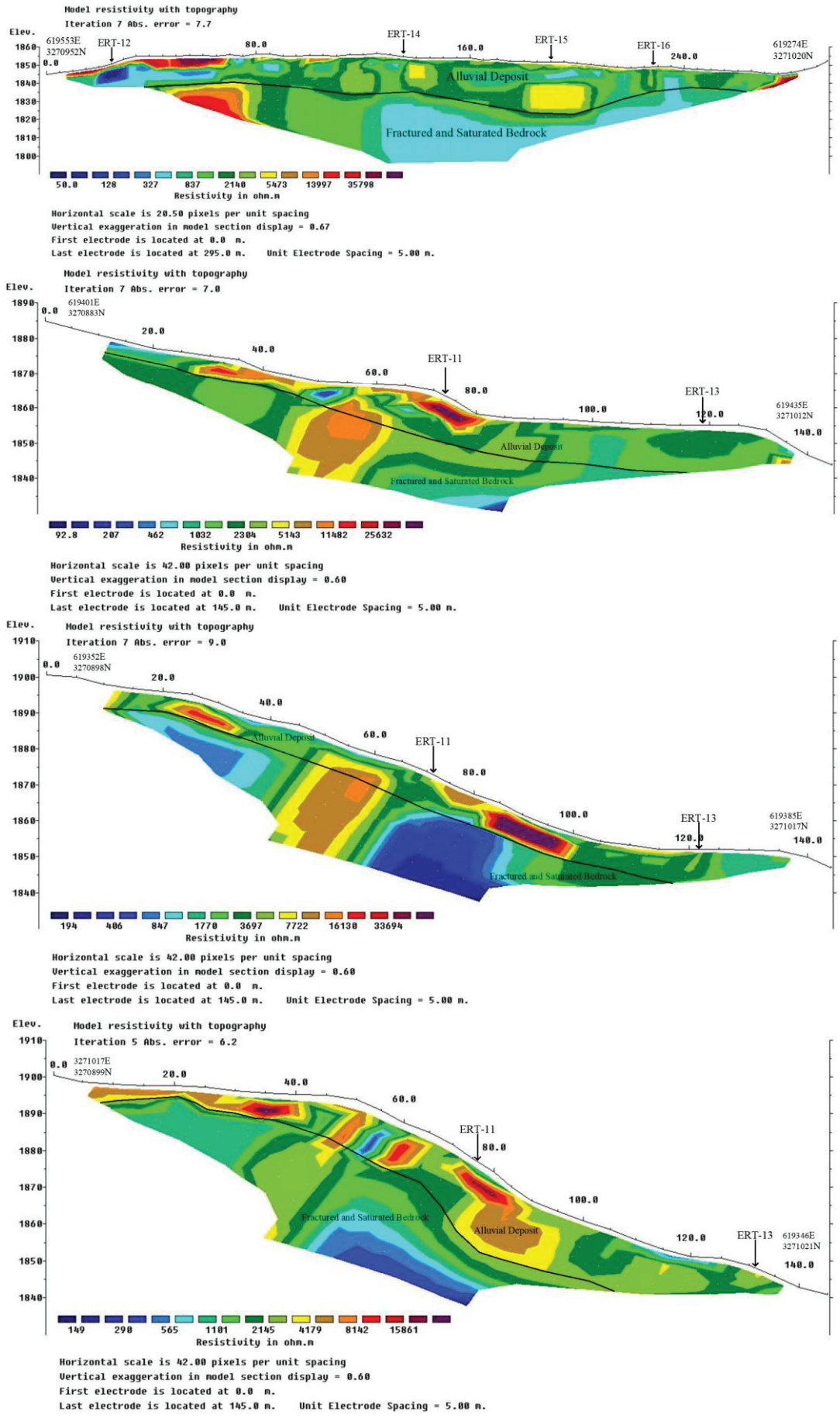

Figure 11, 2D resistivity models for lines 13–16 at the proposed powerhouse, showing lateral and vertical subsurface resistivity variations (5 m inter-profile spacing).

Conclusions

The results of ERT survey demonstrate its effectiveness as a reliable geophysical method for resolving upper crustal heterogeneities and delineating subsurface geological features in rugged terrain. The field instrumentation, designed to support synchronous voltage measurements across extensive multi-electrode arrays, enabled resistivity profiling over distances exceeding 4 km. The rocks around the project area have three local lithological units such as the schist, quartzite and gneiss.

Based on the resistivity values, the uppermost layer is characterized by relatively low to moderate resistivity (20–400 Ω·m), corresponding to unconsolidated colluvial and alluvial sediments with thicknesses ranging from 1 to 46 m. Beneath this, an intermediate resistivity zone (1,000–4,500 Ω·m) represents moderately weathered to fresh bedrock, typically 3 to 27 m thick, composed predominantly of schist, quartzite, and granitic gneiss. The basal layer exhibits variable resistivity signatures (<1,000 Ω·m) associated with fractured and saturated competent bedrock, occurring at depths between 4 and 30 m, and reflecting local lithological heterogeneity and groundwater presence.

Moreover, the surveyed area is generally suitable for the proposed hydropower components; however, additional ground-truth investigations such as borehole drilling, in-situ testing, and detailed geotechnical mapping would further validate the ERT interpretations and provide greater assurance for long-term structural stability.

Acknowledgments

The authors thank the anonymous reviewers for their critical comments, corrections, and thoughtful suggestions, which greatly improved the quality and comprehensiveness of this paper.

Author Contributions

Kapil, Gyanendra, and Dilendra contributed to the conceptualization and methodology of the study. Kapil, Gyanendra, and Rishi were responsible for data collection and site investigation. Kapil and Gyanendra contributed to data processing, interpretation, and prepared the original draft of the manuscript. Dilendra contributed to data curation and validation of result. Kapil, Dilendra, Gyanendra, Rishi, Praveen, Fahim, and Faraz were involved in review and editing. All authors reviewed and approved the final version of the article before submission.

Data Availability

The data generated and analyzed during the current study are available from the corresponding author upon reasonable request. Additional data will be made available as part of ongoing collaborative research efforts.

Declarations

The authors declare no competing interests. The authors declare that they have no known competing financial interests or personal relationships that could have appeared to influence the work reported in this article.

References

Acworth, R. I. (1987). The development of crystalline basement aquifers in a tropical environment. Quarterly Journal of Engineering Geology, 20, 265–272. https://doi.org/10.1144/GSL.QJEG.1987.020.04.02

Acharya, M., Shrestha, K. K., Bhandari, K., and Timilsina, A. (2023). Comparative study of two geophysical methods to investigate the depth of weak zone: A case study of Kulekhani-I Hydroelectric Project Dam, Makwanpur, Nepal. Journal of Earth Science and Climatic Change, 14(737), 2.

Adhikari, B., Acharya, U., Acharya, K., and Ghimire, S. (2019). Engineering geological investigation of dam site of proposed Sunkoshi-2 Hydropower Project, Khurkot area, eastern Nepal. Journal of Nepal Geological Society, 58, 181–188. https://doi.org/10.3126/jngs.v58i0.24603

Aizebeokhai, A. P., Olayinka, A. I., and Singh, V. S. (2010). Application of 2D and 3D geoelectrical resistivity imaging for engineering site investigation in a crystalline basement terrain, southwestern Nigeria. Environmental Earth Sciences, 61(7), 1481–1492. https://doi.org/10.1007/s12665-010-0464-z

Alam, F., Alam, Q., Reza, S., Khurshid-ul-Alam, S. M., Saleque, K., and Chowdhury, H. (2017). A review of hydropower projects in Nepal. Energy Procedia, 110, 581–585. https://doi.org/10.1016/j.egypro.2017.03.188

Al-Fares, W. (2011). Contribution of the geophysical methods in characterizing the water leakage in Afamia B Dam, Syria. Journal of Applied Geophysics, 75(3), 464–471. https://doi.org/10.1016/j.jappgeo.2011.07.014

Argand, E. (1924). La tectonique de l'Asie. In Congrès Géologique International, Belgique, Comptes Rendus de la 13ème Session, en Belgique 1922 (pp. 171–372). Liège: H. Vaillant-Carmanne.

Binley, A., Hubbard, S. S., Huisman, J. A., Revil, A., Robinson, D. A., Singha, K., and Slater, L. D. (2015). The emergence of hydrogeophysics for improved understanding of subsurface processes over multiple scales. Water Resources Research, 51(6), 3837–3866. https://doi.org/10.1002/2015WR017016

Burger, H. R., and Burger, D. C. (1992). Exploration geophysics of the shallow subsurface. New Jersey: Prentice-Hall.

Cardarelli, E., Cercato, M., and Di Filippo, G. (2007). Assessing foundation stability and soil–structure interaction through integrated geophysical techniques: A case history in Rome (Italy). Near Surface Geophysics, 59(3), 244–259. https://doi:10.3997/1873-0604.2006026

Cardarelli, E., Cercato, M., Cerreto, A., and Di Filippo, G. (2010). Electrical resistivity and seismic refraction tomography to detect buried cavities. Geophysical Prospecting, 58, 685–695. https://doi.org/10.1111/j.1365-2478.2009.00854.x

Central Water Commission (CWC). (2017). Bhakra Beas Management Board Report. Government of India.

Chambers, J. C., Kuras, O., Meldrum, P. I., Ogilvy, R. D., and Hollands, J. (2006). Electrical resistivity tomography applied to geologic, hydrologic, and engineering investigations at a former waste disposal site. Geophysics, 71(6), B231–B239. https://doi.org/10.1190/1.2360184

Colangelo, G., Lapenna, V., Loperte, A., Perrone, A., and Telesca, L. (2008). 2D electrical resistivity tomographies for investigating recent activation landslides in Basilicata region (southern Italy). Annals of Geophysics, 51(1), 12. https://doi.org/10.4401/ag-3048

Colchen, M., and Le Fort, A. (1986). Annapurna–Manaslu–Ganesh Himal: Notice de la carte géologique au 1/200,000e (Bilingual ed.). Paris: Centre National de la Recherche Scientifique.

Cubbage, B., Noonan, G. E., and Rucker, D. F. (2017). A modified Wenner array for efficient use of eight-channel resistivity meters. Pure and Applied Geophysics, 174(7), 2705–2718. https://doi.org/10.1007/s00024-017-1535-9

De Groot-Hedlin, C., and Constable, S. (1990). Occam's inversion to generate smooth, two-dimensional models from magnetotelluric data. Geophysics, 55, 1613–1624. https://doi.org/10.1190/1.1442813

Demanet, D., Renardy, F., Vanneste, K., Jongmans, D., Camelbeeck, T. and Meghraoui, M. (2001). The use of geophysical prospecting for imaging active faults in the Roer Graben, Belgium. Geophysics, 66, 78–89. https://doi.org/10.1190/1.1444925

Dewey, J. F., and Bird, J. M. (1970). Mountain belts and new global tectonics. Journal of Geophysical Research, 75, 2625–2685. https://doi.org/10.1029/jb075i014p02625

Dobrin, M. B. (1982). Introduction to geophysical prospecting (3rd ed.). New Delhi: McGraw–Hill.

Epting, J., Huggenberger, P., and Glur, L. (2009). A concept for integrated investigations of karst phenomena in urban environments. Engineering Geology, 109(3–4), 273–285. https://doi.org/10.1016/j.enggeo.2009.08.013

Falae, P. O., Kanungo, D. P., Chauhan, P. K. S., et al. (2019). Electrical resistivity tomography (ERT) based subsurface characterisation of Pakhi landslide, Garhwal Himalayas, India. Environmental Earth Sciences, 78, 430. https://doi.org/10.1007/s12665-019-8430-x

Fuchs, G. (1974). On the geology of the Karnali and Dolpo regions, west Nepal. Mitteilungen der Geologischen Gesellschaft in Wien, 66–67, 21–35.

Fuchs, G. (1977). The geology of the Karnali and Dolpo regions, western Nepal. Jahrbuch der Geologischen Bundesanstalt, Wien, 120(2), 1–103.

Ghimire, H., Bhusal, U. C., Khatiwada, B., and Pandey, D. (2017). Geophysical investigation using two-dimensional electrical resistivity tomography method to delineate subsurface geological structures at Dudhkoshi-II (230 MW) Hydroelectric Project, Solukhumbu District, Eastern Nepal. Journal of Nepal Geological Society, 55, 45–56.

Griffiths, D. H., and Barker, R. D. (1993). Two-dimensional resistivity imaging and modeling in areas of complex geology. Journal of Applied Geophysics, 29, 21–26. https://doi.org/10.1016/0926-9851(93)90005-J

Ha, H. S., Kim, D. S., and Park, I. J. (2010). Application of electrical resistivity techniques to detect weak and fracture zones during underground construction. Environmental Earth Sciences, 60, 723–731. https://doi.org/10.1007/s12665-009-0210-6

Hagen, T. (1969). Report on the Geological Survey of Nepal. Vol. 1: Preliminary Reconnaissance. Mémoires de la Société Helvétique des Sciences Naturelles, 86(1), 185 pp.

Hasan, M., Shang, Y., and Jin, W. J. (2018). Delineation of weathered/fracture zones for aquifer potential using an integrated geophysical approach: A case study from South China. Journal of Applied Geophysics, 157, 47–60. https://doi.org/10.1016/j.jappgeo.2018.06.017

Hasan, M., Shang, Y., Jin, W. J., and Akhter, G. (2020). An engineering site investigation using a non-invasive geophysical approach. Environmental Earth Sciences, 79, 265. https://doi.org/10.1007/S12665-020-09013-3

Hassan Imam, M. D., Hossain, D., and Woobaid Ullah. (2013). Geoelectrical resistivity survey for the evaluation of hydrogeological condition of Bagerhat Sadar and the adjacent areas, Bangladesh. Journal of the Geological Society of India, 82, 290–294. https://doi.org/10.1007/s12594-013-0152-1

Huayllazo, Y., Infa, R., Soto, J., Lazarte, K., Huanca, J., Alvarez, Y., and Teixidó, T. (2023). Using electrical resistivity tomography method to determine the inner 3D geometry and the main runoff directions of the large active landslide of Pie de Cuesta in the Vítor Valley (Peru). Geosciences, 13, 342. https://doi.org/10.3390/geosciences13110342

Hubbard, S. S., and Rubin, Y. (2000). Hydrogeological parameter estimation using geophysical data: A review of selected techniques. Journal of Contaminant Hydrology, 45(1–2), 3–34. https://doi.org/10.1016/S0169-7722(00)00117-0

Hung, Y.-C., Chou, H.-S., and Lin, C.-P. (2020). Appraisal of the spatial resolution of 2D electrical resistivity tomography for geotechnical investigation. Applied Sciences, 10, 4394. https://doi.org/10.3390/app10124394

Jhinkwan, V. S., Chore, H. S., and Agnihotri, A. K. (2025, October). Application of electrical resistivity tomography (ERT) for the evaluation of slope susceptibility: A review. In International Conference on Environmental Geotechnology, Recycled Waste Materials and Sustainable Engineering (pp. 215–224). Singapore: Springer Nature Singapore. https://doi.org/10.1007/978-981-97-8393-9_20

Khalil, M. H. (2006). Geoelectric resistivity sounding for delineating saltwater intrusion in the Abu Zanima area, West Sinai, Egypt. Journal of Geophysics and Engineering, 3, 243–251. https://doi.org/10.1088/1742-2132/3/3/006

Kim, J. H., Yi, M. J., Song, Y., Seol, S. J., and Kim, K. S. (2007). Application of geophysical methods to the safety analysis of an earth dam. Journal of Environmental and Engineering Geophysics, 12, 221–235. https://doi.org/10.2113/JEEG12.2.221

Kneisel, C. (2006). Assessment of subsurface lithology in mountain environments using 2D resistivity imaging. Geomorphology, 80(1–2), 32–44. https://doi.org/10.1016/j.geomorph.2005.09.012

Kohn, M. J. (2014). Himalayan metamorphism and its tectonic implications. Annual Review of Earth and Planetary Sciences, 42, 381–419. https://doi.org/10.1146/annurev-earth-060313-055005

Kumar, R. (2022). Case 16: Three Gorges Dam—The world's largest hydroelectric plant. In Sustainable Hydropower in Developing Countries (pp. 423–439). Springer. https://doi.org/10.1007/978-3-030-96725-3_20

Law, R. D., Searle, M. P., and Simpson, R. L. (2004). Strain, deformation temperatures, and vorticity of flow at the top of the Greater Himalayan slab, Everest Massif, Tibet. Journal of the Geological Society, 161, 305–320. https://doi.org/10.1144/0016-764903-047

Lapenna, V., Lorenzo, P., Perrone, A., Piscitelli, S., Rizzo, E., and Sdao, F. (2005). 2D electrical resistivity imaging of some complex landslides in the Lucania Apennine chain, southern Italy. Geophysics, 70(3), G27–G36. https://doi.org/10.1190/1.1926571

Lamsal, I., Ghimire, S., and Acharya, K. (2020). Geological and geophysical study in Udheri Khola area, Nalgad Hydroelectric Project, Jajarkot District, Lesser Himalaya, Western Nepal. Bulletin of the Department of Geology, 22, 11–16. https://doi.org/10.3126/bdg.v22i0.33409

Lech, M., Skutnik, Z., Bajda, M., and Markowska-Lech, K. (2020). Applications of electrical resistivity surveys in solving selected geotechnical and environmental problems. Applied Sciences, 10(17), 2263. https://doi.org/10.3390/app10072263

Le Fort, P. (1975a). Himalaya: The collided range. Present knowledge of the continental arc. American Journal of Science, 275A, 1–44.

Le Fort, P. (1996). Evolution of the Himalaya. In A. Yin and T. M. Harrison (Eds.), The tectonics of Asia (pp. 95–106). Cambridge University Press.

Lin, C.-H., Lin, C.-P., Hung, Y.-C., Chung, C.-C., Wu, P.-L., and Liu, H.-C. (2018). Application of geophysical methods in a dam project: Life cycle perspective and Taiwan experience. Journal of Applied Geophysics, 158, 1–12. https://doi.org/10.1016/j.jappgeo.2018.07.012

Loke, M. H., Chambers, J. E., Rucker, D. F., Kuras, O., and Wilkinson, P. B. (2013). Recent developments in the direct-current geoelectrical imaging method. Journal of Applied Geophysics, 95, 135–156. https://doi.org/10.1016/j.jappgeo.2013.02.017

Loke, M. H., and Barker, R. D. (1996). Rapid least-squares inversion of apparent resistivity pseudosections by a quasi-Newton method. Geophysical Prospecting, 44(1), 131–152. https://doi.org/10.1111/j.1365-2478.1996.tb00142.x

Loke, M. H., Acworth, I., and Dahlin, T. (2003). A comparison of smooth and blocky inversion methods in 2-D electrical imaging surveys. Exploration Geophysics, 34(3), 182–187. https://doi.org/10.1071/EG03182

Loperte, A., Soldovieri, F., Palombo, A., Santini, F., and Lapenna, V. (2016). An integrated geophysical approach for water infiltration detection and characterization at Monte Cotugno rock-fall dam (southern Italy). Engineering Geology, 211, 162–170. https://doi.org/10.1016/j.enggeo.2016.07.018

Magnekou Takamte, C. R., Ntomba, S. M., Okomo Atouba, L. C., et al. (2022). Geophysical and geological considerations for characterizing the dam foundation during the Memve'ele dam construction (southern Cameroon): Influence on the dam type

retained. Environmental Earth Sciences, 81, 343. https://doi.org/10.1007/s12665-022-10463-0

Marescot, L., Monnet, R., and Chapellier, D. (2008). Resistivity and induced polarization surveys for slope instability studies in the Swiss Alps. Engineering Geology, 98(1–2), 18–28. https://doi.org/10.1016/j.enggeo.2008.01.010

McGrath, R. J., Styles, P., Thomas, E., and Neale, S. (2002). Integrated high-resolution geophysical investigations as potential tools for water resource investigations in karst terrain. Environmental Geology, 42, 552–557. https://doi.org/10.1007/s00254-001-0519-2

Miller, C. R., Routh, P. S., Brosten, T. R., and McNamara, J. P. (2008). Application of time-lapse ERT imaging to watershed characterization. Geophysics, 73(3), G7–G17. https://doi.org/10.1190/1.2907156

Montomoli, C., Carosi, R., and Iaccarino, S. (2015). Tectonometamorphic discontinuities in the Greater Himalayan Sequence: A local or a regional feature? Geological Society, London, Special Publications, 412, 25–41. https://doi.org/10.1144/SP412.3

Mukhopadhyay, S., Tyagi, C., and Rai, S. S. (2006). The attenuation mechanism of seismic waves in Northwestern Himalayas. International Geophysical Journal, 167, 354–360. https://doi.org/10.1111/j.1365-246X.2006.03117.x

Nassim, H., Atmane, L., Lamine, H., Mouloud, H., and Anes, M. (2024). Integrated geotechnical and electrical resistivity tomography to map the lithological variability involved and breaking surface evolution in landslide context: A case study of the Targa Ouzemour (Béjaia). Water, 16(4), 682. https://doi.org/10.3390/w16050682

Nepal Electricity Authority (NEA). (2020). Annual report 2019/20.

NS Energy. (2025). Three Gorges Dam Hydropower Station. Retrieved June 19, 2025, from https://www.nsenergybusiness.com/projects/three-gorges-dam-hydropower-station

Pant, R. S. (2005). Application of 2D-ERT in feasibility study of hydropower projects in Nepal. In Symposium on the Application of Geophysics to Engineering and Environmental Problems 2005 (pp. 344–357). https://doi.org/10.4133/1.2923480

Powell, C. M., and Conaghan, P. J. (1973). Plate tectonics and the Himalayas. Earth and Planetary Science Letters, 20(1), 1–12. https://doi.org/10.1016/0012-821X(73)90134-9

Rehfeldt, K. R., Boggs, J. M., and Gelhar, L. W. (1992). Field study of dispersion in a heterogeneous aquifer: 3. Geostatistical analysis of hydraulic conductivity. Water Resources Research, 28(12), 3309–3324. https://doi.org/10.1029/92WR01758

Rubin, Y., Mavko, G., and Harris, J. (1992). Mapping permeability in heterogeneous aquifers using hydrologic and seismic data. Water Resources Research, 28(7), 1809–1816. https://doi.org/10.1029/92WR00154

Rucker, D. F., Noonan, G. E., and Greenwood, W. J. (2011). Electrical resistivity in support of geological mapping along the Panama Canal. Engineering Geology, 117(1–2), 121–133. https://doi.org/10.1016/j.enggeo.2010.10.012

Samouëlian, I., Cousin, A., Tabbagh, A., Bruand, G., and Richard, G. (2005). Electrical resistivity survey in soil science: A review. Soil and Tillage Research, 83(2), 173–193. https://doi.org/10.1016/j.still.2004.10.004

Satyabala, S. P., and Bilham, R. (2006). Surface deformation and subsurface slip of the 28 March 1999 Mw = 6.4 West Himalaya Chamoli earthquake, from InSAR analysis. Geophysical Research Letters, 33(23), L23305. https://doi.org/10.1029/2006gl027422

Sharma, R. H., and Awal, R. (2013). Hydropower development in Nepal. Renewable and Sustainable Energy Reviews, 21, 684–693. https://doi.org/10.1016/j.rser.2013.01.013

Singha, K., Day-Lewis, F. D., Johnson, T., and Slater, L. D. (2015). Advances in interpretation of subsurface processes with time-lapse electrical imaging. Hydrological Processes, 29(6), 1549–1576. https://doi.org/10.1002/hyp.10280

Sigdel, A., Dhakal, P., Silwal, C. B., and Acharya, S. (2025). Slope stability assessment of Ramche and Dhaibung landslides in Central Nepal using geological, geophysical, and geotechnical approaches. Contributions to Geophysics and Geodesy, 55(3), 265–296. https://doi.org/10.31577/congeo.2025.55.3.1

Srivastava, H., Tiwari, R., Vijay, and Singh, D. (2022). A review on various geotechnical and geophysical investigations for a dam rehabilitation project. In Dam Engineering for the Future (pp. xxx–xxx). Springer. https://doi.org/10.1007/978-981-19-4739-1_8

Suzuki, K., Toda, S., Kusunoki, K., Fujimitsu, Y., Mogi, T., and Jomori, A. (2000). Case studies of electrical and electromagnetic methods applied to mapping active faults beneath thick Quaternary sediments. Engineering Geology, 56(1–2), 29–45. https://doi.org/10.1016/S0013-7952(99)00132-5

Soupois, P. M., Georgakopoulos, P., Papadopoulos, N., Saltos, V., Andreadakis, A., Vallianatos, F., Sanis, A., and Makris, J. P. (2007). Use of engineering geophysics to investigate a site for a building foundation. Journal of Geophysics and Engineering, 4(2), 94–103. https://doi.org/10.1088/1742-2132/4/1/011

SSE (Scottish and Southern Energy). (2009). Glendoe Hydro Scheme Overview.

Telford, W. M., Geldart, L. P., and Sheriff, R. E. (1990). Applied geophysics (2nd ed.). Cambridge University Press.

Tejero, A., Chávez, R. E., Urbieta, J., and Flores-Márquez, E. L. (2002). Cavity detection in the southwestern hilly portion of Mexico City by resistivity imaging. Journal of Environmental and Engineering Geophysics, 7(3), 130–139. https://doi.org/10.4133/jeeg7.3.130

Thompson, S., Kulessa, B., Benn, D., et al. (2017). Anatomy of terminal moraine segments and implied lake stability on Ngozumpa Glacier, Nepal, from electrical resistivity tomography (ERT). Scientific Reports, 7, 46766. https://doi.org/10.1038/srep46766

U.S. Geological Survey (USGS). (2018). Three Gorges Dam: The world's largest hydroelectric plant. Retrieved June 19, 2025, from https://www.usgs.gov/special-topics/water-science-school/science/three-gorges-dam-worlds-largest-hydroelectric-plant

Viviroli, D., Dürr, H. H., Messerli, B., Meybeck, M., and Weingartner, R. (2007). Mountains of the world, water towers for humanity: Typology, mapping, and global significance. Water Resources Research, 43, W07447. https://doi.org/10.1029/2006WR005653

Viviroli, D., and Weingartner, R. (2008). "Water towers"—A global view of the hydrological importance of mountains. In E. Wiegandt (Ed.), Mountains: Sources of water, sources of knowledge (pp. 15–30). Springer. https://doi.org/10.1007/978-1-4020-6748-8_2

Water and Energy Commission Secretariat (WECS). (2019). Assessment of hydropower potential of Nepal.

Wise'n, R., Bjelm, L., and Dahlin, T. (2000). Resistivity imaging as a pre-investigation method in urban environments. In Proceedings EEGS-ES 6th Meeting (CH05). https://doi.org/10.3997/2214-4609.201406221

Wu, J., Dai, F., Liu, P., et al. (2023). Application of electrical resistivity tomography in groundwater detection on the Loess Plateau. Scientific Reports, 13, 4821. https://doi.org/10.1038/s41598-023-31952-7

Asian Journal of Engineering Geology

Volume 2, No. 1

Table of Content

Official Journal of Nepal Society of Engineering Geology (NSEG)
Dhobighat, Lalitpur, Nepal
For Online Submission: https://ajeg.nseg.org.np